**SANDIA REPORT**

SAND2008-5736
Unlimited Release
Printed September 2008

# An Analysis of the Pull Strength Behaviors of Fine-Pitch, Flip Chip Solder Interconnections Using a Au-Pt-Pd Thick Film Conductor on Low-Temperature, Co-Fired Ceramic (LTCC) Substrates

Paul T. Vianco, Jerome A. Rejent, J. Mark Grazier, Alice C. Kilgo, Gary L. Zender, Paul F. Hlava, and Fernando R. Uribe

Approved for public release; further dissemination unlimited.

**Sandia National Laboratories**

# An Analysis of the Pull Strength Behaviors of Fine-Pitch, Flip Chip Solder Interconnections Using a Au-Pt-Pd Thick Film Conductor on Low-Temperature, Co-Fired Ceramic (LTCC) Substrates

Paul T. Vianco, Jerome A. Rejent, J. Mark Grazier, Alice C. Kilgo,
Gary L. Zender, Paul F. Hlava and Fernando R. Uribe

Sandia National Laboratories
P.O. Box 5800
Albuquerque, New Mexico 87185

## Abstract

The assembly of the BDYE detector requires the attachment of sixteen silicon (Si) processor dice (eight on the top side; eight on the bottom side) onto a low-temperature, co-fired ceramic (LTCC) substrate using 63Sn-37Pb (wt.%, Sn-Pb) in a double-reflow soldering process (nitrogen).  There are 132 solder joints per die.  The bond pads were gold-platinum-palladium (71Au-26Pt-3Pd, wt.%) thick film layers fired onto the LTCC in a post-process sequence.  The pull strength and failure modes provided the quality metrics for the Sn-Pb solder joints. Pull strengths were measured in both the as-fabricated condition and after exposure to thermal cycling (-55/125°C; 15 min hold times; 20 cycles). Extremely low pull strengths – referred to as the *low pull strength phenomenon* – were observed intermittently throughout the product build, resulting in added program costs, schedule delays, and a long-term reliability concern for the

detector.  There was no statistically significant correlation between the low pull strength phenomenon and (1) the LTCC "sub-floor" lot; (2) grit blasting the LTCC surfaces prior to the post-process steps; (3) the post-process parameters; (4) the conductor pad height (thickness); (5) the dice soldering assembly sequence; or (5) the dice pull test sequence.  Formation of an intermetallic compound (IMC)/LTCC interface caused by thick film consumption during either the soldering process or by solid-state IMC formation was not directly responsible for the low-strength phenomenon.  Metallographic cross sections of solder joints from dice that exhibited the low pull strength behavior, revealed the presence of a reaction layer resulting from an interaction between Sn from the *molten* Sn-Pb and the glassy phase at the TKN/LTCC interface. The thick film porosity did not contribute, explicitly, to the occurrence of reaction layer.  Rather, the process of printing the very thin conductor pads was too sensitive to minor thixotropic changes to ink, which resulted in inconsistent proportions of metal and glassy phase particles present during the subsequent firing process.  The consequences were subtle, intermittent changes to the thick film microstructure that gave rise to the reaction layer and, thusly, the low pull strength phenomenon.  A mitigation strategy would be the use of physical vapor deposition (PVD) techniques to create *thin* film bond pads; this is multi-chip module, deposited (MCM-D) technology.

## Acknowledgements

# Contents

**Page**

# List of Figures

application has been highlighted in yellow.  The error bars are based upon a 95% confidence interval for the mean.

**Figure 8**                                                                                      **37**
Failure mode analysis of DuPont™ pull tests in Reference 1 based upon the scanning electron micrographs of the cross sections of four test sites.

**Figure 9**                                                                                      **38**
Flip chip solder bump on die U12, SF1168 showing the microstructure of the interconnection.

**Figure 10**                                                                                     **39**
SEM photographs showing the single print, thick film structures from **(a)** the BDYE die flip chip and **(b)** the DuPont™ pull test specimen (Reference 1).

**Figure 11**                                                                                     **41**
**(a)** Stereo photograph showing the locations of the pad height measurements made on the sub-floors. **(b)** Example of the raw, height data that was analyzed to determine actual pad thickness.

**Figure 12**                                                                                     **43**
Plots of mean pad heights (blue, top row; red, bottom row; green, left row; and yellow, right row) and pull strength (white) as a function of sub-floor lot: (a) as-fabricated condition and (b) post-20 thermal cycles (-55°C/125°C).  The dotted lines represented the acceptance criteria limits for the individual die pull strengths.

**Figure 13**                                                                                     **44**
Plots of minimum pad heights (blue, top row; red, bottom row; green, left row; and yellow, right row) and pull strength (white) as a function of sub-floor lot: (a) as-fabricated condition and (b) post-20 thermal cycles (-55°C/125°C).

**Figure 14**                                                                                     **46**
(a) Schematic diagram showing the location of the pad height measurements made on the lot #21 sub-floors prior to die flip chip assembly.  The selected locations were of dice to be tested in the as-fabricated condition. The remaining sites used the same pattern, but had the assembled dice pull tested after thermal cycling. (b) The method used to calculate the height of the pads on each row.

spectroscopy: (a) surface analysis and (b) at a near-surface depth where C < 3 at.%. The "half" error bars indicated one standard deviation.

were data from sub-modules that were exposed to the healing treatment (250°C, 260 hours, air). The blue symbols ("Rev 0") were the strength values of sub-modules that were not subjected to the healing treatment. The one-half error bars were one standard deviation.

**Figure 33**                                                                 89
(a) TKN/LTCC failure mode percentage and (b) pull strength as a function of sub-floor LTCC lot numbers. The respective data were averaged between the top side and bottom side dices. The sub-modules were in the *thermal cycled condition*. The red symbols ("Rev 1") were data from sub-modules that were exposed to the healing treatment (250°C, 260 hours, air). The open triangles were the as-fabricated pull strength values. The blue symbols ("Rev 0") were the strength values of sub-modules that were not subjected to the healing treatment. The one-half error bars were one standard deviation.

**Figure 34**                                                                 92
(a) Pull strength as a function of sub-module number (lot number in italics). All of the sub-floors were exposed to the healing treatment (250°C, 260 hours, in air) prior to assembly into the sub-modules. The error bars were one standard deviation. (b) Pull strength lower acceptance limit (mean – 95% confidence interval) as a function of sub-module number. The strength data are the average of top side and bottom side. The turquoise and orange lines note the acceptance limit for the as-fabricated and post-thermal cycled cases.

**Figure 35**                                                                 98
Illustration of the location of the Au-Pt-Pd thick film flip chip pad relative to the dielectric layers in the initial sub-floor manufacturing step with lot #29 material. The illustration shows the configuration of the two sub-floors, S-Lot29-1 and -2, which were made with the higher viscosity, thick film paste while the sub-floors, S-Lot29-3 and -4, were made with for the TKN paste having the correct viscosity.

**Figure 36**                                                                 99
Pull strength as a function of sub-floor number of the four sub-module units assembled with lot #29 LTCC material designated S-Lot29-X (X = 1, 2, 3, and 4). The half-error bars are one standard deviation.

**Figure 37**                                                                 101
Pull strength as a function of sub-module number of the four sub-module units assembled with lot #29 LTCC material: SF-Lot29-3, S-Lot29-4, SF1594, and SF1599. The data were separated into top side and bottom side strengths for the as-fabricated or thermal cycled conditions. The half-error bars are one standard deviation.

**Figure 44** (a) Pull strength as a function of sub-module designation for the Flight 12 process monitor, SF1660 (sub-floor lot #30). The pull strength data from the Flight 11 process monitors, SF1591 and SF1608 were also included. The as-fabricated and thermal cycle conditions were represented by the blue and red symbols, respectively; top side data were designated by the solid symbols while open symbols indicated the bottom side data. The error bars are one standard deviation. (b) Pull strength acceptance data as a function of the process monitor sub-module. The minimum strength criteria (which are averages of the top side and bottom side results) are 6.75 lb and 4.5 lb for the as-fabricated and post-thermal cycled conditions, respectively.

**Figure 45** Failure mode analysis of sub-modules SF1591 and SF1608 (both Flight 11) as well as SF1660 (Flight 12) assembled from lot #30 LTCC material: (a) as-fabricated and (b) post-thermal cycle conditions. Per the legends, the lighter shade of colors are the TKN/LTCC failure mode and darker shades are the TKN/LTCC+divots mode. Top side and bottom side data were distinguished in each plot.

**Figure 46** (a) Pull strength as a function of sub-module designation for the Flight 13 process monitors, SF1659 and SF1662 (both lot #30). The pull strength data from the process monitors of Flight 11 (SF1591 and SF1608, lot #29)) and Flight 12 (SF1660, lot #30) were also included. The as-fabricated condition was represented by the blue symbol color; top side data used the solid symbols while open symbols designated the bottom side data. The error bars are one standard deviation. (b) Pull strength acceptance data as a function of the process monitor sub-module. The minimum strength criteria (which are averages of the top side and bottom side results) are 6.75 lb and 4.5 lb for the as-fabricated and post-thermal cycled conditions.

**Figure 47** (a) Pull strength as a function of process monitor sub-module designations as follows: Flight 14, SF1731 and SF1751; Flight 15, SF1726 and SF1742; Flight 16, SF1802; and Flight 17, SF1815. The data were distinguished according to top side and bottom side as well as as-fabricated and post-thermal cycled. The error bars are one standard deviation. (b) Pull strength acceptance data as a function of the process monitor sub-module. The minimum strength criteria (which are averages of the top side and bottom side results) are 6.75 lb and 4.5 lb for the as-fabricated

and post-thermal cycled conditions. The strengths are an average between the top side and bottom side.

**Figure 62** 140

Graph of pull strength as a function of die site for the sub-module SF512. The data were divided into segments representing the as-fabricated and post-thermal cycled conditions. The minimum individual die pull strength limit is shown. Sites U01 – U08 are on the top side of the sub-module while sites U09 – U16 are on the bottom side.

**Figure 63** 141

Graphs of the failure mode results from sub-module SF512 for: (a) as-fabricated condition and (b) post thermal cycled condition. Each of the four failure modes is designated by color on the bar graphs.

**Figure 64** 142

SEM/EDXA elemental maps of selected flip chip solder joints from die on the sub-module SF512 having the TKN/LTCC failure mode after pull testing: (a) U09, joint L15, as-fabricated condition, high strength of 11.2 lb and (b) U05, joint R15, post-thermal cycled condition, having a low strength of 0.99lb. The elements of Au, Pt, and Pd were combined into a single color, yellow, to represent the thick film metal. The elements Si and Al were combined as red, representing the LTCC material. Pink is the Sn element and blue is Pb, the latter corresponding primarily to the TKN glassy phase.

**Figure 65** 144

Stereo photographs of the SF523 show tests performed on each of the die sites located on the top side (a) and the bottom side (b) of the unit. These maps represented, as well, the tests performed on the duplicate sub-module, SF541.

**Figure 66** 146

(a – d) SEM micrographs showing the microstructure of a representative solder joint, in this case, taken from the die U10 (post-thermal cycle; no underfill) from SF523. Both high magnification images (b, d) confirmed good integrity of the (Au, Pt, Pd)Sn$_4$ IMC/LTCC and TKN/LTCC interfaces.

**Figure 67** 147

SEM micrographs showing the microstructure of a representative solder joint of the die U02 (post-thermal cycle with underfill from sub-module SF541. There were no indications of cracking along the interface between the (Au, Pt, Pd)Sn$_4$ IMC and LTCC substrate.

**Figure 68** 149

Pull strength of dice on SF088 that was subjected to an air burn-in at 125°C for 282 hours. Comparable data were included from four other sub-

modules, SF023, SF029, SF035, and SF045, that were not subjected to a burn-in treatment.

treatment.  The same locations were evaluated for sub-module SF264, which was exposed to the burn-in conditions of 125°C, 240 hours.

U04, joint 3; Trace 2) of SCA075 was exposed to 10800 thermal cycles (0°C/100°C).  The TKN was fully consumed by solid-state IMC growth.

## Nomenclature

AES          Auger electron spectroscopy

BDYE       Burst detection yield enhancement

BSE          Backscattered electron (image)

LTCC       Low-temperature, co-fired ceramic

SE            Secondary electron (image)

SEM        Scanning electron microscope

SNL         Sandia National Laboratories

TFN         Thin film

TKN        Thick film

# 1.0 BACKGROUND INFORMATION AND PRELIMINARY ANALYSES

*1.1 Low Pull Strength Phenomenon*

The BDYE sub-module assembly is categorized as a multi-chip module – ceramic (MCM-C) technology.  The silicon (Si) dice are attached to the low-temperature co-fired ceramic (LTCC) sub-module floor using 63Sn-37Pb (wt.%, abbreviated Sn-Pb) flip chip solder joints.  The Sn-Pb solder bumps are received already attached to the die under-bump metallurgy (UBM).  The UBM solderable coating is an electroless Ni-P layer.

The solder bond pads on the LTCC surface are a single layer of the DuPont™4596 thick film (TKN) conductor.  The metal component, which has the 71Au-26Pt-3Pd alloy composition (wt.%), is accompanied by the glass phase that bonds the metal component to the LTCC substrate.  The conductor is fired on the LTCC substrate as a "post-process" step, that is, after the layers of LTCC tape have been pressed, dried, and fired to form the sub-floor.

There is no additional solder added to joints at the time that the sub-floor (LTCC substrate, alone) is assembled into the sub-module (LTCC plus the dice).  The assembly process uses a tacky flux to support the wetting-and-spreading action of the die solder bumps upon melting.  A total of sixteen (16) dice are placed on the LTCC sub-floor.  Eight dice are attached to each of the top side (positions U01 – U08) and eight are soldered to the bottom side (positions U09 – U16).  The top side dice are placed and soldered into place first, using a Sikama conduction soldering furnace (in nitrogen).  Then, the remaining dice are placed on the bottom side and the unit passed a second time through the furnace.  Therefore, the top side solder joints are reflowed twice.

Acceptance of the material quality and flip chip assembly process for the subsequent building of flight hardware, is determined by the as-fabricated, pull strength and failure modes of the Sn-Pb solder joints observed on a module referred to as the *process*

*monitor.* After assembly of the process monitor, the dice on the process monitor are subjected to a tension test as illustrated in Fig. 1a. A scanning electron microscope (SEM) photograph of the pull-tested die appears below the photograph. The maximum tensile load was recorded for each die, together with the failure mode count for all 132 solder joints. There were four failures modes, which are shown by the SEM photographs in Fig. 1a and schematic diagrams in Fig. 1b. The "Si (Ni-P)/solder" mode refers to failure at the interface between the solder and the Ni-P UBM. The "Si (Ni-P + UBM)/Solder" mode describes fracture within the UBM layers of the die. The "TKN/LTCC" mode occurs when the thick film layer separates from the LTCC substrate material along their mutual interface. The last failure mode, "TKN/LTCC + divot," refers to the case when a piece of the LTCC substrate accompanies fracture along the TKN/LTCC interface. Interestingly, it was extremely rare to observe a failure within the solder volume of the bump. When observed, it was typically near the Si UBM interface and, as such, was counted as the "Si (Ni-P)/solder" failure mode. More importantly, however, the absence of fracture directly in the solder indicated that it was exceptionally strong when compared to the two interface above and below it. Contributing factors to the high strength of the Sn-Pb solder included its intrinsically high strain hardening rate and Au, Pt, and Pd additions resulting from the thick film dissolution.

The pull tests were performed on the process monitor in the *as-fabricated* condition and after it was exposed to *thermal cycling.* The as-fabricated condition was evaluated by pull testing the dice at alternating positions designate as U01, U03, U06, and U08 on the top side and dice U09, U11, U14, and U16 on the bottom side. The pull tests preformed specifically on the as-fabricated sub-module, were used to establish a pass/fail decision for continuing to build flight units, based upon the acceptance criteria below:

*As-fabricated:*      [Mean – 95%CI] > 6.75 lbs

                         Minimum load of any one die > 4.5 lbs

                         [TKN/LTCC + divot] < 25% of *all* joints.
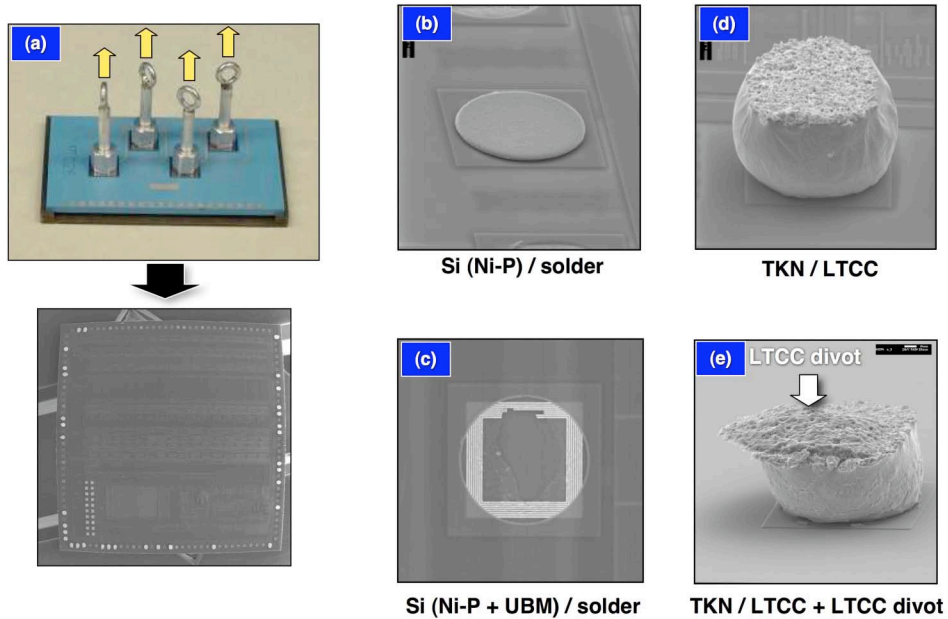
(a)
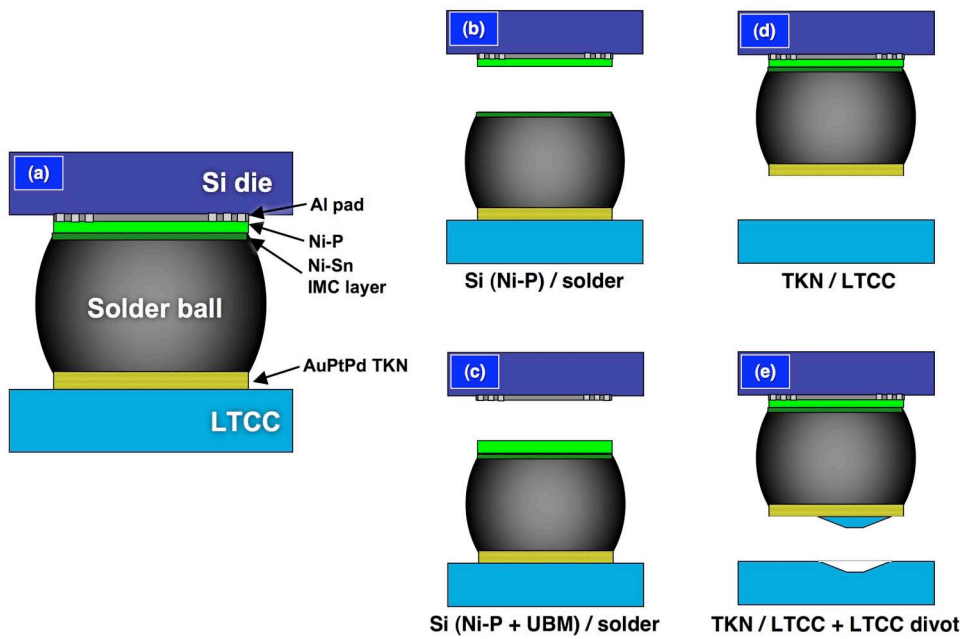


(b)

**Fig. 1** (a) Pull test and failure modes of the die solder joints: (a) Stereo photograph of the BDYE process monitor having the aluminum nuts and eyelets in place for the pull test. The SEM photographs of the four failure modes: (b) Si (Ni-

**27**

P)/solder interface; (c) Si (Ni-P + UBM)/solder interface; (d) TKN/LTCC interface; and (e) TKN/LTCC + divot. (b) Schematic diagrams of the four failure modes. The letter (b-e) correspond to the SEM photograph letters in (a).

The 95% confidence interval (CI) was used to address the data scatter. After the dice were pull tested in the as-fabricated condition, the sub-module was exposed to 20 thermal cycles between -55°C and 125°C in an air furnace. Then, the remaining dice (top: U02, U04, U05, and U07; bottom: U10, U12, U13, and U15) were pull tested. The acceptance conditions for those samples are:

*Post-20 TC:* [Mean – 95%CI] > 4.5 lbs

Minimum strength of any one die > 4.5 lbs

[TKN/LTCC + divot] < 40% of *all* joints

The post-thermal cycled data were used "for information, only" to assess possible deviations in material quality and/or manufacturing processes. (Recall from above that the "go/no-go" decision to continue with the assembly of flight sub-modules was determined by the as-fabricated test results.) The post-thermal cycle strength and failure mode data contributed to the decision to actually *use* of subsequently-built "flight" sub-modules for next-assembly or to withdraw them from such, pending a further assessment of the "failed" process monitor data. Using this approach, in the event that flight units are to be scrapped because the post-thermal cycle, process monitor test results (pull strength and failure mode), the loss is limited to only those completed lot units and not the higher valued, next-assemblies. This approach is a compromise between providing sub-modules that meet project schedule and assuring the manufacturing quality and long-term reliability of the final flight hardware.

The thermal cycling test methodology also had a basis in the materials engineering of the interconnections. The maximum number of cycles was determined to be twenty (20). Experiments indicated that, above twenty cycles, *additional* defects were

introduced into the interconnections, as indicated by a significant drop in pull strength. These supplemental defects would obscure the detection of defects caused by material deficiencies or poor assembly process using the pull strength metric. Therefore, twenty thermal cycles would activate, what were surmised to be, pre-existing manufacturing and/or latent defects in the interconnections.

An attribute of the twenty thermal cycle test was because, in fact, there was the nominal strength loss (which, incidentally, is the reason for the different acceptance criteria vis-à-vis the as-fabricated condition). Thus, the post-thermal cycle pull strength can be sensitive to *changes* in those defect levels, which in turn, provides the means to reveal changes in material quality or assembly process control. (In colloquial terms, the "edge-of-the-cliff" is now known.)

The lower pull strengths were accompanied by an increased frequency of the TKN/LTCC and TKN/LTCC + LTCC divots failure modes. Therefore, the defects that were activated by the thermal cycling regiment, were associated with the TKN/LTCC interface and underlying LTCC material, respectively. (In fact, LTCC divots were observed almost exclusively after thermal cycling; they were rarely detected in the as-fabricated condition.)

It appeared that, in the case of acceptable pull strengths (> 4.5 lb) that were realized at the start of the program (lots #4 – 20), all of the interfaces and material layers had approximately the same intrinsic strength. This conclusion was drawn from the data in Fig. 2, where the frequency of the TKN/LTCC failure mode was plotted as a function of pull strength (load). There was a wide range of frequencies to this failure mode (and conversely, as similar case for the other failure modes) when pull strengths were above 4.5 lb. However, the introduction of significant degradation into the solder joints, as indicated by a drop in the pull strength metric below 4.5 lb, was primarily through a weakening of the TKN/LTCC interface indicated by the high propensity for this failure

mode. Incidentally, the data in Fig. 2 illustrate the basis for 4.5 lb as the lower limit of the acceptance criteria.



**Fig. 2** TKN/LTCC failure mode frequency as a function of pull strength (load) for as-fabricated and post thermal cycle process monitor data combined from the sub-floor lots #4 – 20.

It has been observed throughout this program that, frequently, a process monitor would experience low die pull strengths.  This event was referred to as the *low pull strength phenomenon.*  Sometimes, the strength loss was observed only in the post-thermal cycled condition.  In other instances, low pull strengths were observed in the as-fabricated condition. When the low pull strength phenomenon was observed in the as-fabricated condition, there was subsequently a very sharp loss of pull strength after exposure to thermal cycling.  These trends are illustrated in Fig. 3, which shows a compilation of as-fabricated and post-thermal cycle pull strengths as a function of sub-floor lot numbers for the process monitors.  In general, the low pull strength phenomenon appeared after lot #11; however, it is clear in Fig. 3 that the degradation did not occur in a consistent manner, based upon the sub-floor lot sequence.

**Fig. 3** Graph of as-fabricated (blue) and post-thermal cycle (red) die pull strengths as a function of sub-floor lot # 4 – 20 per the associated process monitor.

The low pull strength phenomenon data in Fig. 3 were further analyzed by comparing the resulting pull strength acceptance parameter, [Mean – 95%CI], against the acceptance criteria of 6.75 lb and 4.5 lb for the as-fabricated and post-thermal cycled conditions, respectively.  The data are represented by the bar chart in Fig. 4 and clearly demonstrate that low pull strength phenomenon prevents the associated process monitors from meeting the acceptance criteria.

A second trend, which was observed through the course of the early process monitor pull testing activities, was the difference of pull strengths between dice on the top side of the module versus those on the bottom side.  Specifically, the top side dice had slightly higher pull strengths than the bottom side dice.  Moreover, the lower the pull strength, the greater was the magnitude of that difference between the two sides.
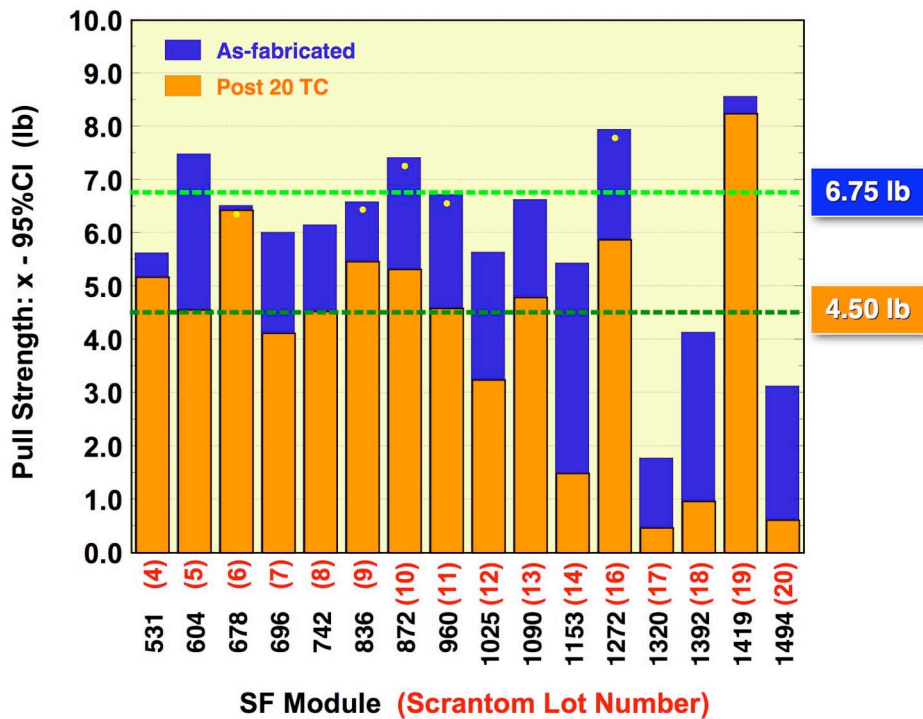
**Fig. 4** Bar graph showing the [Mean – 95%CI] acceptance parameter as a function of sub-floor lot number 4 to 20 of the process monitors. Both the as-fabricated and post thermal cycle data were included in the plot, along with the acceptance criteria, 6.75 lb and 4.5 lb, respectively.

Thus, the difference was particularly large for a sub-module having the low pull strength phenomenon, as illustrated in Fig. 5 for process monitors taken from sub-floor lot #20. In fact, the thermal cycling exposure appeared to further accentuate this difference of pull strength, albeit, not consistently so. Lastly, the error bars indicated very little dependence upon the strength magnitudes; top side versus bottom side; or as-fabricated versus thermal cycled condition.

At this juncture, it was clear that the low pull strength phenomenon could impact the long-term reliability of the flip chip solder joints on the BDYE sensor assembly. Therefore, it became necessary to determine the source of the low pull strength phenomenon.
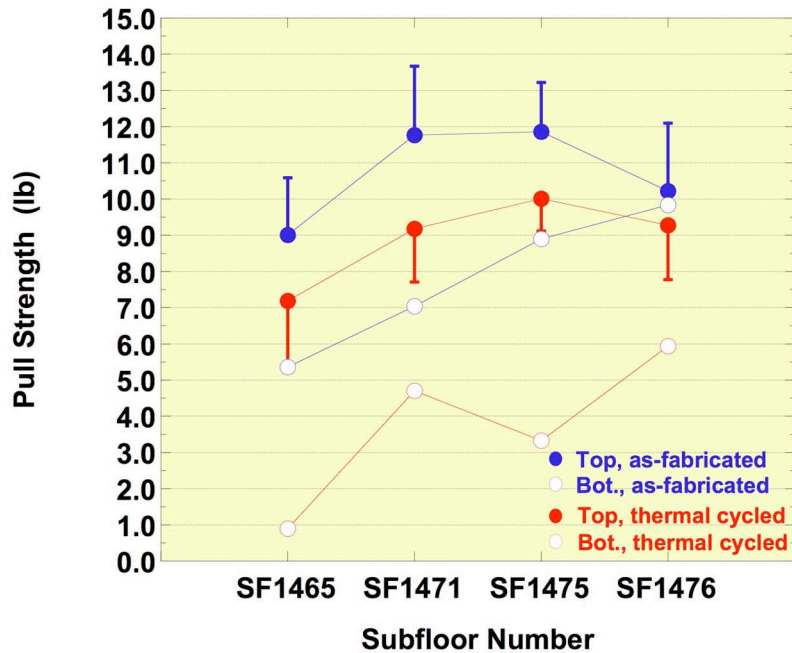
**Fig. 5** Plot of pull strength (load) versus four sub-modules built from sub-floors of lot #20. The pull strengths data were separated into top side and bottom side values. The data included the as-fabricated condition as well as after thermal cycling. The error bars were one standard deviation.

Two generalized approaches were taken in this effort. The first approach was to examine the material set and assembly processes from the manufacturing perspective. The objective was to quickly identify a probable source of the low strengths – not necessarily the root cause at this point – in order to quickly correct any deficiency to meet program schedule. Factors that were considered included the thickness of the bond pads on the LTCC as well as the furnace atmosphere used to attach the braze pins to the sub-floors.

The second effort was to perform a more exacting materials analysis on the solder interconnections. The objective of this task was to identify, expressly, the root cause of the low pull strength. Optical metallography, SEM imaging, electron microprobe analysis (EPMA), as well as Auger electron spectroscopy (AES) provided the analytical tools used in this part of the investigation. The microstructural analysis was conducted

in parallel with the processing investigation due to the limited availability of test units. Therefore, the sequence of events may, at times, appear to be out-of-sequence.

Before describing in detail the results of the aforementioned studies, it is necessary to understand the nominal microstructure of the flip chip solder joints. Therefore, background information is provided in the next section that describes this interconnection technology.

*1.2 Interconnection Mechanical Properties and Microstructure*

It was noted above that the low pull strength phenomenon coincided with an increased occurrence of failures at the TKN/LTCC interface; in most cases, all 132 interconnections on a die exhibited this failure mode. Also under these circumstances, the frequency of LTCC divots that accompanied the TKN/LTCC separation, which was always very small, diminished to zero in most instances. These observations clearly indicated that the source of the reduced pull strengths rested specifically with the TKN/LTCC interface.

A recent study examined the mechanical strength of Sn-Pb solder joints made to the Au-Pt-Pd thick film layer, using the DuPont™ pull test (also called the "shepherd's hook" test) [1]. The test specimen is shown in Fig. 6a. There were nine bond pads that were post-processed on each sample (print-dry-fire sequence). The pull tests were performed on the six sites of columns "1" and "3". Three samples were tested per each of the matrix conditions; therefore, there were a total of 18 measurements per each such condition. Shown in Fig. 6b are the wires ("shepherd's hooks") soldered to the pads. A sample that was subjected to pull testing is shown in Fig. 6c.

The test geometry of the DuPont™ pull test is different from that of the flip chip solder bumps. However, both test regiments are based upon the maximum tensile strength. In the case of the DuPont™ pull test, the maximum tensile strength occurred at the onset of the test. Both tests used the same displacement rate. Therefore, the strength results
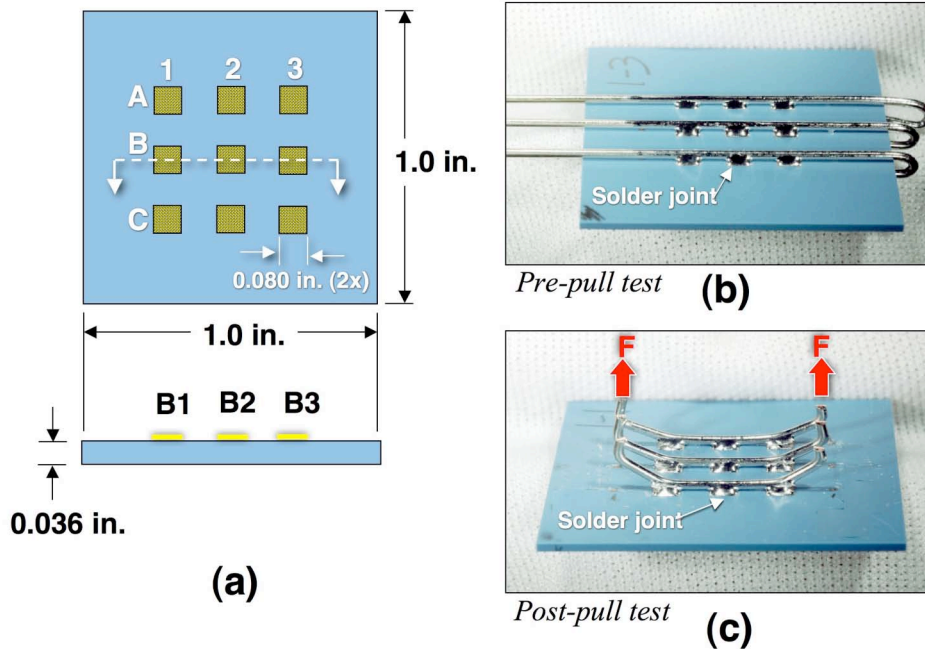
**Fig. 6** (a) Schematic diagram of the DuPont™ pull test sample in Reference [1]. (b) Stereo photograph of the test sample with the wires ("shepherd's hooks") soldered to the pads. (c) Stereo photograph showing the test sample after the pull test, which was performed on sites having column designators "1" and "3" per (a) [1].

should be comparable between the two data sets. In fact, like the flip chip case, the inherent strengths of the interfaces and materials in the shepherd's hook solder joint configuration were also comparable to one-another. Of the several different sample configurations evaluated in Reference 1, there were two cases that were pertinent to the BDYE experiments: (a) a single print, Au-Pt-Pd thick film layer (no via) and (b) a triple printed, Au-Pt-Pd layer. These two cited cases serve as pseudo-baseline data against which can be compared the BDYE data.

Shown in Fig. 7 are the pull strength data from Reference 1. The data having relevance to the BDYE tests are highlighted in yellow. The single print Au-Pt-Pd layer had a slightly lower mean strength value compared to the more robust, triple thick layer next to it, but certainly within the statistical significance of the 95% confidence interval represented by the error bars. From these results, it can be concluded that the single

layer of Au-Pt-Pd TKN on LTCC, which replicates the BDYE interconnection technology, is not prone to having an intrinsically low pull strength.
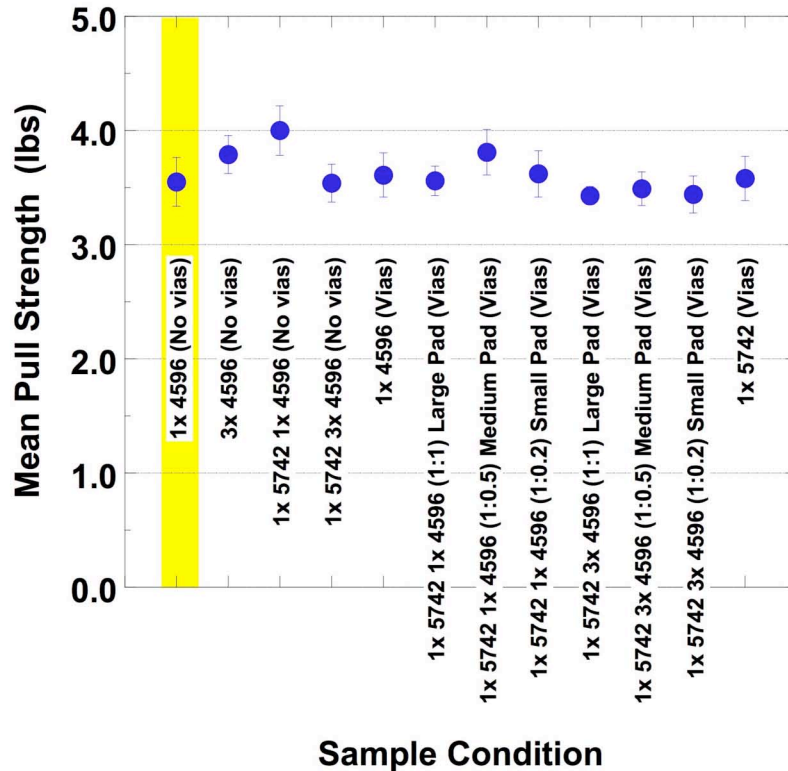


**Fig. 7** Pull strength as a function of thick film configuration from the testing in Reference 1. The test configuration that was pertinent to the BDYE application has been highlighted in yellow. The error bars are based upon a 95% confidence interval for the mean.

The test results in Reference 1 were further examined for the failure modes, using metallographic cross sections. The potential failure sites included: (1) the solder/TKN interface; (2) the TKN/LTCC interface; (3) the bulk solder; (4) the bulk LTCC substrate ("divot"); and (5) the bulk thick film layer. Mode (5) was not relevant to the BDYE test data because bulk TKN failures did not take place in single thick film layers. The results are presented in Fig. 8 with, again, the data relevant to the BDYE case study highlighted in yellow. In the case of the single TKN layer, the solder/TKN and TKN/LTCC failure

modes occurred nearly equally.  Therefore, the single Au-Pt-Pd thick film layer was not predisposed to fail at the TKN/LTCC interface.
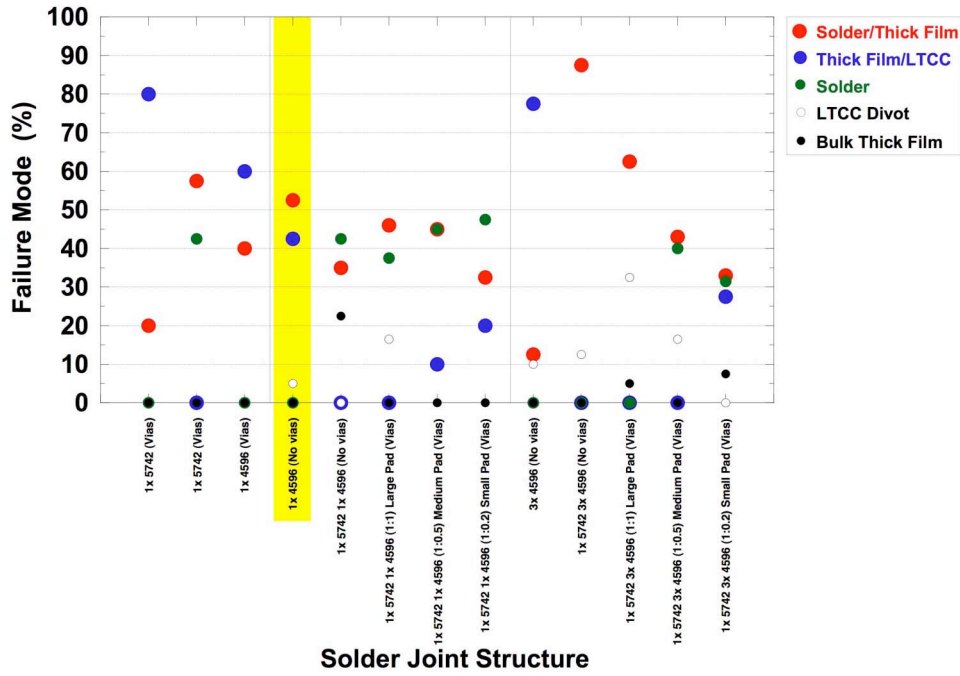


**Fig. 8** Failure mode analysis of DuPont™ pull tests in Reference 1 based upon the scanning electron micrographs of the cross sections of four test sites.

In summary, the study cited as Reference 1 provided baseline data of the mechanical behavior of the single print, Au-Pt-Pd thick film layer.  Those data indicated that the single print layer can have satisfactory pull strengths.  Moreover, there is no indication that the single print layer is not necessarily predisposed to the TKN/LTCC failure mode.

However, in order to establish a stronger correlation between the results cited in Reference 1 and the behavior of the BDYE flip chip joints, a direct comparison was made between the corresponding interconnection microstructures, in particular, the thick film layers.  Shown in Fig. 9, is a representative solder bump from die U12 (bottom side) of SF1168.  There was not a continuous TKN/LTCC interface due to voids, which are a natural consequence of the firing process for Au-Pt-Pd thick films.  Because of the

limited quantity of metal powder particles that were deposited to achieve a thin pad layer, those voids had dimensions that were comparable to the overall layer thickness. Yet, where there was a TKN/LTCC interface, it showed good integrity with no indications of cracks or delamination.
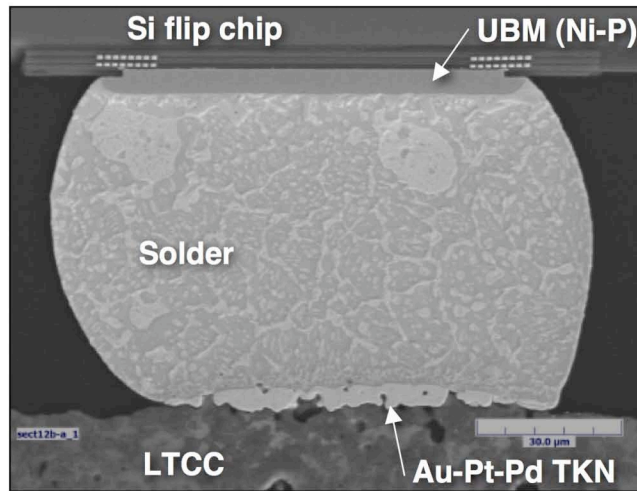


**Fig. 9** Flip chip solder bump on die U12, SF1168 showing the microstructure of the interconnection.

The solder joint in Fig. 9 was also shown in Fig. 10, along side a similar SEM photograph of the single thick film layer from Reference 1, using a higher magnification that targeted the thick film layer and its interface with the LTCC substrate. The yellow dashed lines in Fig. 10(b) are a superposition of the thickness of the BDYE thick film layer in Fig. 10(a). The BDYE layer was approximately one-third as thick as the single print layer of the Reference 1 test specimen, indicating that a smaller quantity of thick film ink was used to make the single print, BDYE flip chip pads.  The fact that the flip chip pad originated from a reduced quantity of paste is also evidenced the lesser presence of glassy phase observed in the near-interface LTCC material.
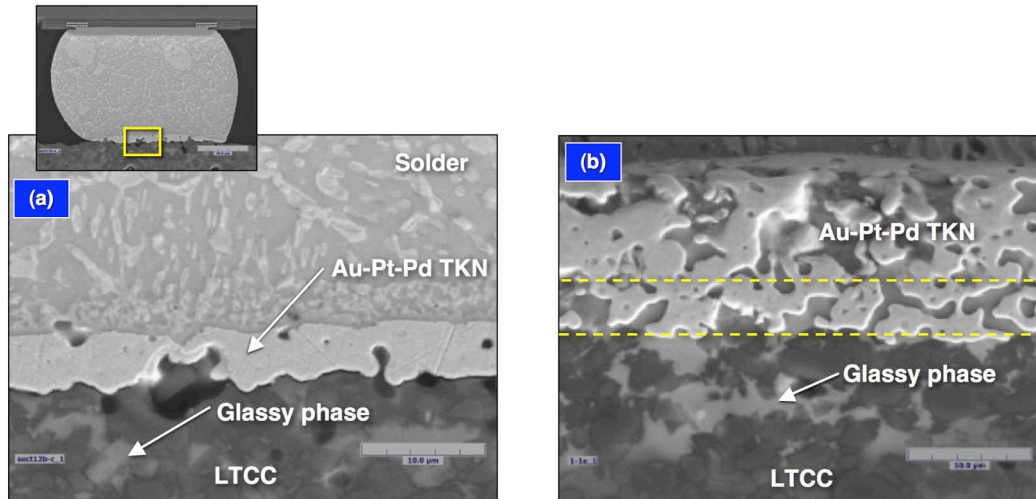
**Fig. 10** SEM photographs showing the single print, thick film structures from (a) the BDYE die flip chip and (b) the DuPont™ pull test specimen (Reference 1).

The comparison of Fig. 10(a)] to [Fig. 10(b)] resulted in the following summation: There was a difference between the thickness of the BDYE flip chip thick film pads and those on the Reference 1 pull test specimen. Although the soldering processability of the two thicknesses (e.g., dissolution) were similar, there could potentially be difference of mechanical properties due to the different microstructures. Therefore, the data from Reference 1 provides the bounding case of a relatively thick, *single print* layer (hence, single print-dry-fire sequence) against which to compare the behavior of the thinner, single print BDYE layer.

There are two primary consequences to the solder joints that can arise from the microstructure of thinner bond pads:

1. The limited thickness provides an increased accessibility of the Sn-Pb solder to the glassy phase at the TKN/LTCC interface. Previous studies have shown that Sn can degrade that glassy phase interfacial bond [2 – 7].
2. The thinner print of the thick film can result in there being less glassy phase with which to bond the Au-Pt-Pd conductor to the LTCC surface. Potentially, the

TKN/LTCC interface bond could be less robust against mechanical stresses, flaws, and environmental degradation than those of the joins evaluated in Reference 1 [2, 8].

In summary, the data in the Reference 1 study established an upper bounds in terms of the pull strength and failure mode behavior to be expected from the BDYE Sn-Pb interconnection made to the single print, Au-Pt-Pd thick film.  The low pull strength phenomenon established a *lower bound* that may be associated with the considerably thinner, BDYE flip chip bond pads.

Therefore, the analyses described in Section 1.0 are described below in sub-sections 1.3 – 1.5.  The objective of these efforts was to determine the sensitivity of the mechanical properties of the BDYE solder interconnection to the thick film pad geometry, flip chip soldering process, and pull test steps and, moreover, whether any such sensitivities are sufficiently strong to cause the low pull strength phenomenon. The specific sub-section topics are: (a) the effects of pad height (conductor thickness), flip chip assembly sequence, and mechanical (pull) test sequence described in sub-section 1.3; (b) the possible roll of the LTCC firing process that is outlined in section 1.4; and (c) the effects of down-stream processes that were inadvertently performed in hydrogen-nitrogen environments, which are described in section 1.5.

*1.3 Pad Height (Thickness), Flip Chip Assembly Sequence, and Mechanical (Pull) Test Sequence Effects*

The size and pitch of the flip chip solder joints resulted in, correspondingly, very limited aperture dimension – length, width, and thickness – of the screen used to print the Au-Pt-Pd paste that formed the conductive solder bond pad.  Moreover, the technique of multiple print-dry-fire sequences, which can be used to build up a thick film layer, could *not* be used in this application, because the required placement repeatability could not be realized between each print-dry-firing sequence.   Therefore, the formation of the Au-Pt-Pd thick film pads was limited to a single print process that resulted in pad heights

**40**

(thickness) that varied between 3.0 – 8.0 μm. This range can be compared to values of 13 – 21 μm that can be achieved routinely with double and triple (3x) print-dry-fire sequences.

A study was performed to determine whether the low pull strengths could be correlated with thickness of the flip chip bond pad conductor layer. A sub-floor was obtained from each of the lots #4 – #20. The thickness or "height" of the Au-Pt-Pd bond pads was measured by profilometry, using the sample pattern shown in Fig. 11 (a). The top trace (blue) and bottom trace (red) spanned the four dice; the left trace (green) and right trace (yellow) each spanned two dice.
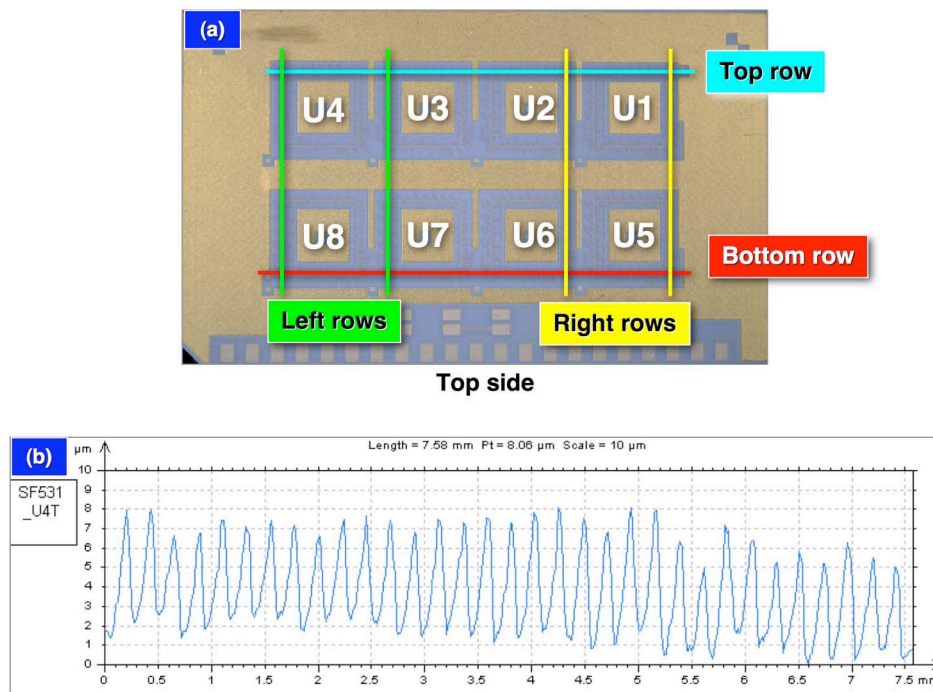


**Fig. 11** (a) Stereo photograph showing the locations of the pad height measurements made on the sub-floors. (b) Example of the raw, height data that was analyzed to determine actual pad thickness.

Only those pads on the top surface were measured. Although it was recognized that there had developed a difference of pull strength values between top and bottom sides

of the sub-module, the bottom surface was not similarly measured for the following reasons: (1) Previous measurements had indicated no repeatable, significantly different pad heights between the two sides. (2) The overall effect of the low pull strength phenomenon applied to both sides. (3) And, the amount of data requiring analysis would have become unmanageable, especially in the absence of compelling technical reasons to pursue those measurements per points (1) and (2).

The pad height analysis began with the obtaining the pad height raw data, a sample of which is provided in Fig. 11 (b). Each peak represents one of each of the 33 pads intercepted by the scanner trace. The actual bump heights were determined by the difference between absolute peak height and the baseline datum taken on the sub-floor surface. The data analysis routine broke down the results into individual die and was required to address a changing baseline (i.e., sub-floor surface) height between traces. After the pad height measurements had been completed, the top side was assembled with eight dice, using the flip chip assembly process. Four of the dice were tested in the as-fabricated condition. Then, the partially-built sub-modules were exposed to the process monitor, thermal cycling condition (20 cycles, -55°C/125°C) and the remaining four dice, subsequently pull tested.

The mean pad height and mean pull strength were plotted as a function of sub-modules' sub-floor lot numbers in Fig. 12: (a) as-fabricated and (b) post-thermal cycled. The colored circles - red, blue, green and yellow – represented the four pad height traces (Fig. 11a), which were average values computed from both the as-fabricated and thermal cycled dice sites prior to assembly of the dice. The corresponding pull strengths (white circles) of those same dice were added to the plots. A qualitative inspection of the two plots in Fig. 12 did not indicate as correlation between the pull strength (white circles) and pad height measurements (colored circles).
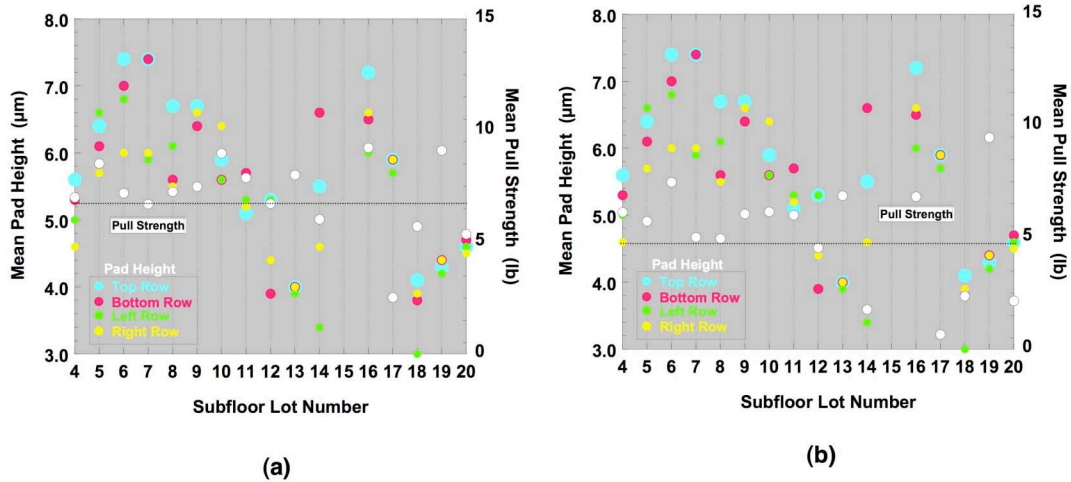
**Fig. 12** Plots of mean pad heights (blue, top row; red, bottom row; green, left row; and yellow, right row) and pull strength (white) as a function of sub-floor lot: (a) as-fabricated condition and (b) post-20 thermal cycles (-55°C/125°C). The dotted lines represented the acceptance criteria limits for the individual die pull strengths.

This analysis was extended to look for correlations between pull strength and (1) standard deviation, which represented pad height variability, as well as (2) minimum pad height. Slightly different plots were used, as illustrated in Fig. 13 for the case of minimum pad height. All attempts to correlate standard deviation and minimum pad height to pull strength *failed*, as determined by both qualitatively observations as well as quantitatively by regression analyses. The regression analyses returned the square of the correlation coefficient, $R^2$, with values of less than 0.1 for both as-fabricated and thermal cycled conditions.

A second phase of the pad height study was performed because of concerns that the sub-floors from lots #4 – 20 represented a "heritage technology". There were improvements of both processes and materials quality that occurred *after* the fabrication of lot #20. Therefore, the same study was performed on lot #21 sub-floors, which were deemed to represent the "best" technology at the time. The following four sub-floors were used in the experiment: SF1525, SF1545, SF1571, and SF1577. The scope of
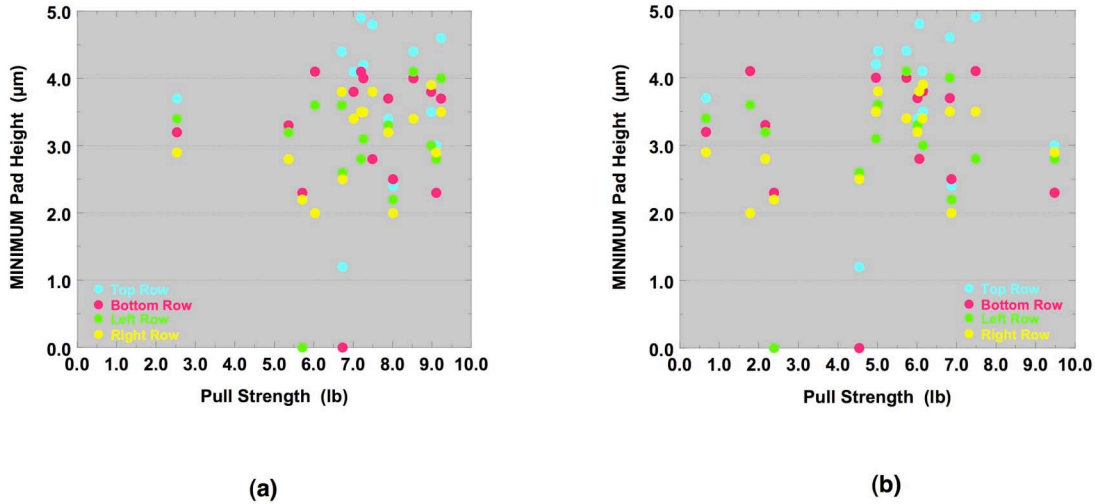
**Fig. 13** Plots of minimum pad heights (blue, top row; red, bottom row; green, left row; and yellow, right row) and pull strength (white) as a function of sub-floor lot: (a) as-fabricated condition and (b) post-20 thermal cycles (-55°C/125°C).

this study was expanded vis-à-vis the previous investigation in order to evaluate different sequences of soldering assembly processes and mechanical testing performed on the two sides and any correlation to the trends observed in the first factor. In the case of the soldering assembly processes, the top side of the sub-floor is assembled first so that those solder joints will be exposed to a *second* reflow cycle during the assembly of the bottom side solder joints. The potentially degrading mechanisms particular to the top side were a greater dissolution of the TKN material and increased infiltration of molten solder into the thick film, towards the TKN/LTCC interface. A consideration was included for the mechanical testing sequence in order to rule out any procedural or equipment performance bias associated with the pull test sequence of top side dice tested first *followed by* the bottom side dice.

The sub-floors were assembled with dice using one of the following scenarios:

- **SF1525 ("normal)**: Top side assembled first; top side pull tested first.
- **SF1545**: Top side assembled first; bottom side pull tested first.

- **SF1571**: Bottom side assembled first; bottom side pull tested first.
- **SF1577**: Bottom side assembled first; top side tested first.

Dice pull tests were performed on the sub-modules in the as-fabricated condition as well as after exposure to the process monitor, thermal cycling regiment (20 cycles, -55°C/125°C).

The pad height data were taken at those sites that would then be populated with dice that, in turn, would be pull tested. The diagram in Fig. 14a shows the locations of the pad height measurements that were made on the top, bottom, left, or right rows of thick film pads for dice to be tested in the as-fabricated condition. The term "F" designated the front (top) side; "B" designated the back (bottom) side. The even numbers were the horizontal row of pads; the odd numbers were the vertical row of pads as oriented in Fig. 14a. A similar pattern was used on the other dice sites that had the solder joints exposed to the thermal cycling environment prior to pull testing. The objective for examining the orientation effect was the fact that the printing of the thick film pads occurred by the movement of the squeegee in one direction. There can be potential anisotropies in the quantity of paste deposited per pad due to the this effect.

At each designated row, the measurements were made at eight (8) pads in the manner shown in Fig. 14b. As previously, the height of the pad was referenced to the surface of the LTCC sub-floor. The pad heights were combined together according to orientation and the side of the sub-floor. Thus, this approach allowed for investigating possible correlations between the following metrics: (a) pad height; (b) pad orientation; (c) top side, as-fabricated pull strength; (d) bottom side, as-fabricated pull strength; (e) top side, post-thermal cycle pull strength; and (f) bottom side, post-thermal cycle pull strength.
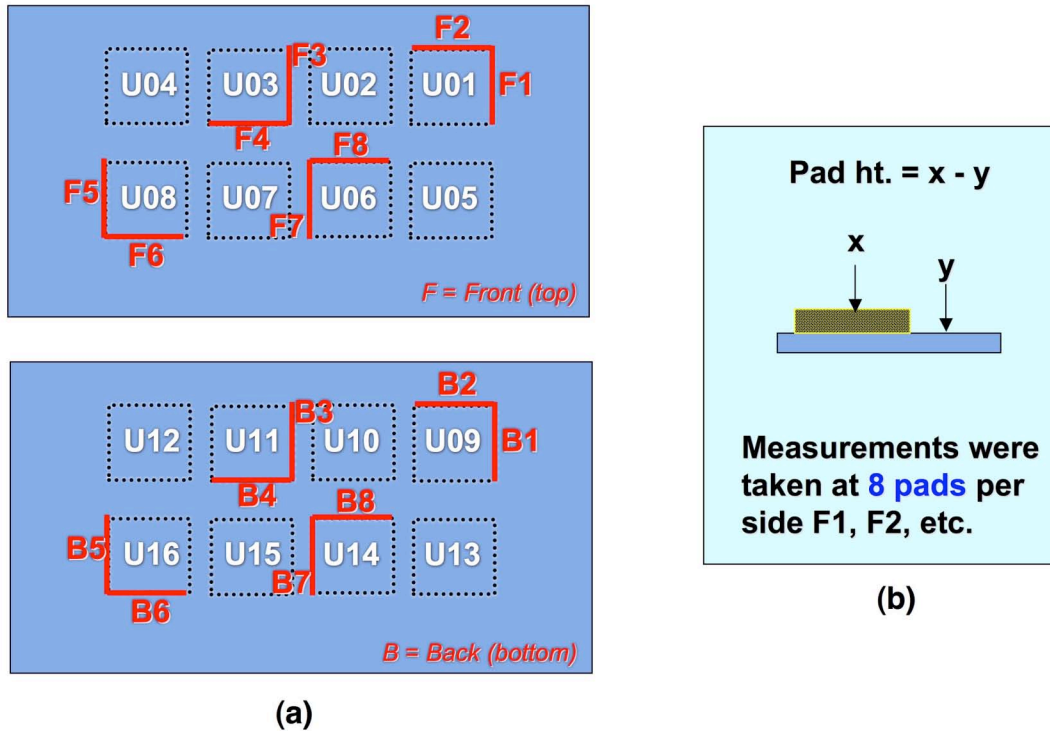
**Fig. 14** (a) Schematic diagram showing the location of the pad height measurements made on the lot #21 sub-floors prior to die flip chip assembly.  The selected locations were of dice to be tested in the as-fabricated condition. The remaining sites used the same pattern, but had the assembled dice pull tested after thermal cycling. (b) The method used to calculate the height of the pads on each row.

After the pad height measurements were completed, the sub-floors were assembled with the flip chip dice.  The top side dice U01, U03, U05, and U07 as well as bottom side dice U09, U11, U13, and U15 were pull tested in the as-fabricated condition.  The remaining dice on either side were pull tested following thermal cycling.

Shown in Fig. 15a is a graph of the mean pad height (white circles with error bars representing ± one standard deviation) as well as maximum and minimum pad heights (black circles) as a function of trace designator for the sub-floor, SF1525.  These data were representative of the other three sub-floors, as well.  In all four cases, there were no consistent trends that distinguished the pad height parameters as a function of pad

orientation – vertical (odd) versus horizontal (even) – of either the top or bottom sides for any of the test vehicles.



<p style="text-align:center">(a)</p>
<p style="text-align:center">(b)</p>
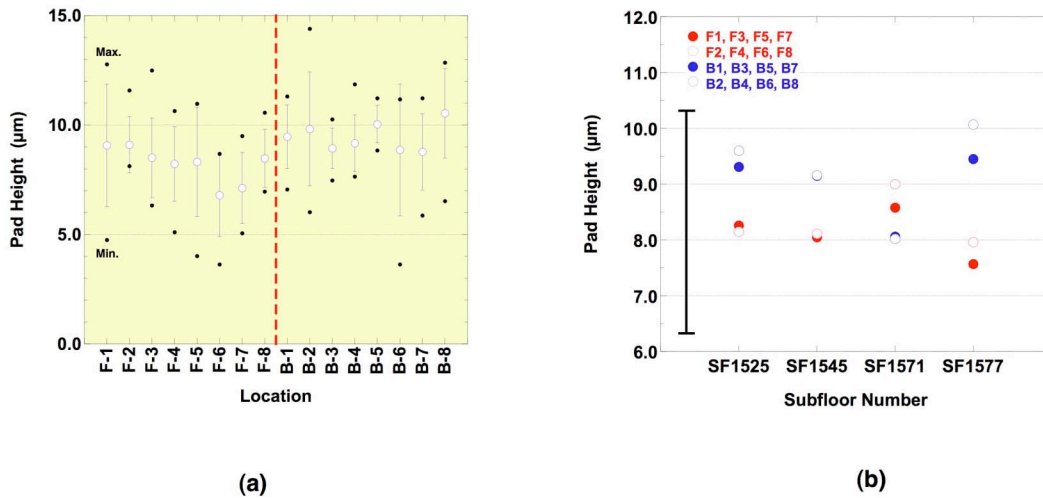
**Fig. 15** (a) Plot of the mean pad height (white circles, ±one standard deviation error bars) as well as maximum and minimum pad height on the SF1525 sub-floor from lot #21 (as-fabricated pull test dice sites). The error bars are ±one standard deviation. (b) Mean pad heights of the four sub-floors from lot #21. Symbols distinguish top and bottom sides (red and blue) and orientation (solid versus open symbols). The single error bar is representative of the ±one standard deviation of the means.

Next, *average pad heights* (as-fabricated pull test dice sites) were compared between orientations as well as top side versus bottom side as a function of each sub-floor sample; those data appear in Fig. 15b. The error bars were left off of the individual data points for clarity; rather, a single error, which represented the data spread between sets (±one standard deviation), was used. It appeared that, in three-of-four cases, the bottom side had a greater, mean pad height than did the top side. However, the sub-floor SF1571 was the exception to this trend. Also, there did not appear to be an effect of orientation, which would have reflected an effect of the thick film printing direction. Therefore the results shown in Fig. 15, which were also representative of sites on which dice were pull tested after thermal cycling, did not indicate consistent trends of pad height versus orientation or the particular side of the sub-floor substrate.

The pull test strength data were plotted in Fig. 16 as a function of sub-module number. The symbol shape and color identified top side and bottom side as well as as-fabricated and post-thermal cycled conditions. Recall that these units were assembled and tested in different sequences to determine if those steps had a role on the strength trends (bulleted list, above). The consistent trends were: (1) that the bottom side strength values were consistently lower than were the topside strengths and (2) the post-thermal cycled strengths were lower than the as-fabricated strengths. There was no dependence upon the pull test sequence, that is, whether the top side or the bottom side was tested first, thus allaying fears that the second side (usually, the bottom side) was damaged by the preceding pull test of the top side. Also, mean pull strengths of units SF1571 and SF1577 were less than those of the other two modules, particularly in the as-fabricated condition. At first glance, that trend would suggests that the side solder assembled first – in the case of these two sub-modules, the bottom side – had a low pull strength. If true, then the sub-modules SF1525 and SF1545 should have had lower top side pull strengths than those of SF1571 and SF1577 because the top side dice were assembled first in those two former pair. However, that trend was not observed in Fig. 16. Therefore, the sequence of the assembly process did not have a significant effect on the pull strengths. More importantly, the difference in pull strengths between the top and bottom sides of the sub-modules must be a consequence of the thick film properties and, in particular, the response of the thick film to the presence of the solder joint above it.

The relatively wide range of pull strength values in Fig. 16, per the different sub-modules, provided an opportunity to find a correlation, if any, between pad height and pull strength. Shown in Fig. 17 are plots of pull strength as a function of pad height for (a) top sides of the sub-modules and (b) the bottom sides of the sub-modules; both cases are the as-fabricated condition. The two pad orientations were represented by different symbols types; nevertheless, the same die pull strength value was assigned to

48
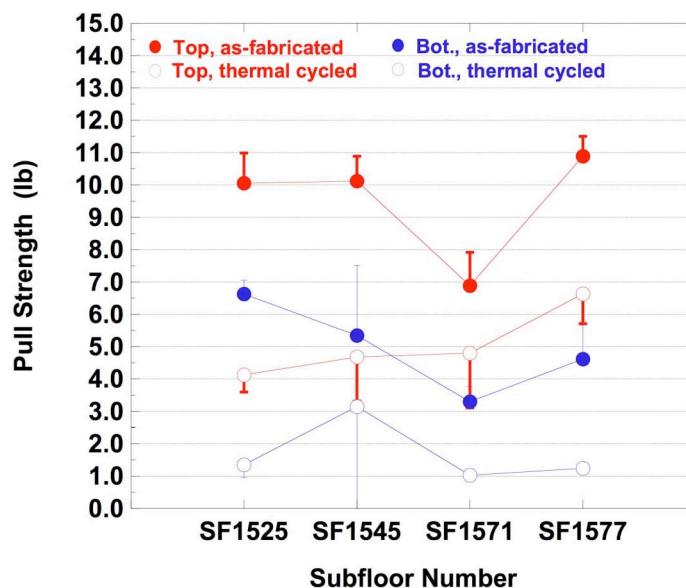
**Fig. 16** Plot of the mean strengths of the four sub-modules built from lot #21 sub-floors. The data were identified as top side (closed symbols) and bottom side (open symbols) as well as as-fabricated (blue-colored symbols) and thermal cycled (red-colored symbols).

both orientations for each sub-module. The individual error bars (±one standard deviation) were placed on the data point that pertained to the pull strength; a single, representative error bar for the pad height data was included on the bottom of the plot. A linear regression analysis was performed on the two orientations with pull strength as the dependent variable and pad height as the independent variable.

Shown in Fig. 17a is the case of the top side pull strengths and pad heights. The trend was for the pull strength to decrease with increasing pad height, which was opposite to the expected behavior. The regression trend was not significant because the variation in pad height was relatively narrow, particularly in relationship to the error bars of the data. The regression analyses appeared to confirm that there was no significant correlation between pull strength and the observed range of pad heights.
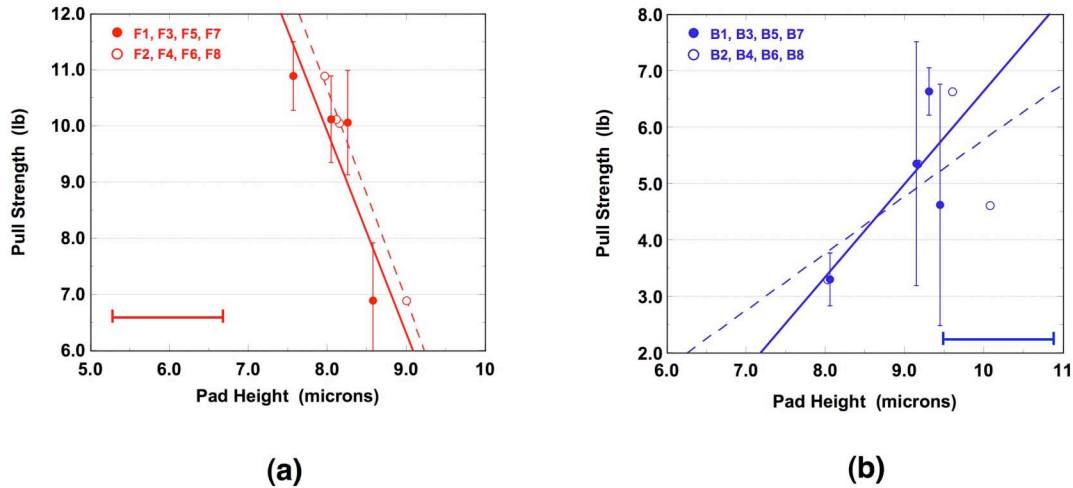
**Fig. 17** Plots of pull strength versus pad height as determined from the four sub-modules representing lot #21. These data were for the *as-fabricated* condition: (a) top side and (b) bottom side. Solid lines were the linear regression to the solid symbols; dashed line pertained to the open symbols. The error bars were ±one standard deviation.

The same regression analysis was performed on the bottom side interconnections; those results are plotted in Fig. 17b. Here, there was a greater variation in the pad height and the expected trend was observed, that is, the pull strength increased with increasing pad height. However, the correlation (as indicated by the $R^2$ value) was extremely poor for either of the two pad orientations. Therefore, it could not be concluded from the data in Fig.17 that there was a significant correlation between pad height and pull strength for either the top side or bottom side sites.

A similar analysis was made of the post-thermal cycle pull strength data. Those results appear in Fig. 18 for the two sides of the sub-modules. Interestingly, the same general trends were observed for the top side results (Fig. 18a) and bottom side results (Fig. 18b), as were recorded for the corresponding as-fabricated data in Figs. 17a and 17b, respectively. But, as was the case with the as-fabricated analysis, the trends lacked the statistical significance needed to establish a correlation between the observed range of pad heights and die pull strength.
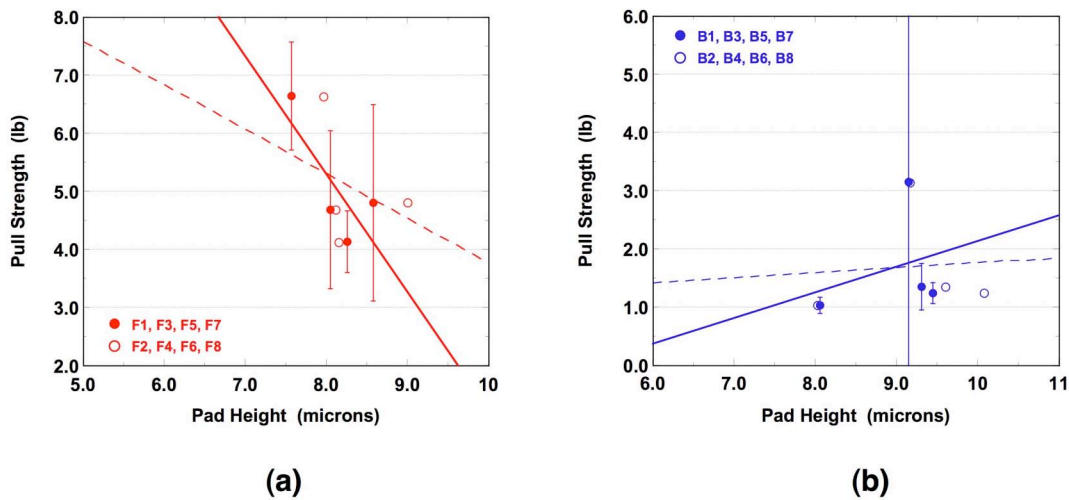
**Fig. 18** Plots of pull strength versus pad height as determined from the four sub-modules representing lot #21. These data were for the *thermal cycled* condition: (a) top side and (b) bottom side. Solid lines were the linear regression to the solid symbols; dashed line pertained to the open symbols. The error bars were ±one standard deviation.

In the cases of date in both Figs. 17 and 18, the trends did not reflect the different assembly and test sequences represented by the four sub-modules nor the differences in pull strengths as recorded in Fig. 16.

In summary, two investigations were performed to determine whether the observed range in the Au-Pt-Pd bond pad heights (thicknesses) affected the die pull strengths and, furthermore, in the event of such an effect, that the latter was responsible for the low pull strength phenomenon. The independent variables were the solder assembly sequence between top side and bottom side, as well as the pull test sequence between the two sides. The dependent variable was pull strength. Ancillary factors for correlation analysis included pad height and as-fabricated versus post thermal cycled conditions. The following conclusions were drawn from these studies:

1. There was no statistically significant correlation between pull strength and either the dice assembly sequence or pull test sequence.

2. A correlation could not be established between pad height and the pull strength values for either the as-fabricated or post-thermal cycled conditions. Therefore, the range of pad heights (thicknesses) recorded for these sub-modules, which were equally representative of other sub-modules assembled from sub-floor lots #4 – 20, would not be a root-cause for the low pull strength phenomenon.

3. It could be concluded that the difference in pull strengths between the top and bottom sides of the sub-modules was a consequence of one or more properties of the thick film *other than* expressly, pad height. Those yet, undetermined properties, become significant when the solder joint was made to the layer and may be associated with the low pull strength phenomenon.

*1.4 LTCC Firing Process*

The thick film pads used for the flip chip solder joints, were fired on to the LTCC base material as post-processing steps. The top side pads were applied first, followed by the bottom side pads so that the top side thick film pad structures were exposed to an extra firing step[1]. On the other hand, the bottom side LTCC surface was exposed to the furnace environment of the top side process prior to having the thick film pads printed and fired onto it. Therefore, there were two possible scenarios affecting the respective TKN/LTCC interfaces: (a) *top side*, the TKN/LTCC interface was impacted, directly*,* by being exposed to an extra firing step and (b) *bottom side*, the TKN/LTCC interface may have been affected, indirectly, because the LTCC surface was exposed to the furnace conditions used for the top side, post-process.

Each of these scenarios was further regarded in terms of an impact on the pull strength of the TKN/LTCC interface and, more critically, providing evidence as to the root-cause of the lower pull strength phenomenon. Specific mechanisms were hypothesized. The

---

[1] In the fabrication of actual sub-floors, the bottom side is post-processed prior to the top side. However, for the objective of this experiment, that difference is not important.

top side TKN/LTCC interface could have experienced additional interdiffusion of thick film and/or LTCC constituents (metals or glass phases) caused by the additional firing environment.  As noted in Reference 1, between 2 and 3 firing steps actually improved the bond pad pull strengths.  Nevertheless, potential damage mechanisms due to excessive interdiffusion must be addressed as well as mechanical damage caused by thermal expansion mismatch residual stresses at the interface.  On the bottom side, exposure to the top side, post-process firing step could have left the LTCC surface with compositional changes by either solid-state diffusion furnace contamination that potentially degraded adhesion between it and the subsequently applied thick film layer.

It should be noted that, in the overall process sequence used to make the sub-floors from the LTCC substrate, the extra firing step on the top side may actually have a limited effect when compared to the bottom side.  Although the study cited in Reference 1 indicated that the TKN/LTCC interface is sensitive to the number of firing steps, this effect was observed when there were only a few such post-processing steps.  In the case of the BDYE sub-floors, the top side experiences fifteen (15) post-process firing sequences after deposition of the flip chip bond pads.  The bottom side bond pads are exposed to a total of fourteen (14) additional firing steps.  In addition, these post-process steps are exercised alternately between the top and bottom side. Therefore, it is not expected that a single, additional exposure would significantly alter the intrinsic properties of either the TKN/LTCC interface or the thick film structure on the top side. On the other hand, the bottom side LTCC surface could be affected by the first post-processing step used to put on the top side bond pads.  If there is degradation to the surface, that damage could be retained throughout the remaining post-process steps, thereby appearing as lower pull strengths of the bottom side dice.

Therefore, an investigation was undertaken with two objectives.  The first goal was to understand the top side and bottom side LTCC surface compositions immediately following substrate manufacturing, but prior to post-processing.  The second goal was to document the response of the LTCC surface compositions to the post-process firing

steps, including any secondary effects caused by the presence of the thick film paste used to form the bond pads.

The analysis technique chosen to quantitatively assess the LTCC surface compositions was Auger electron spectroscopy. This methodology, when used at low voltage (5keV) can detect differences in the alumina and oxide glass concentrations on the surface (which comprise the LTCC material). It is capable of identifying light element contaminants such as C, K, Na, and Ca. However, its sensitivity to the heavier metallic elements such as Fe, Ni, Cu, etc. was significantly reduced at these voltages.

The surface analysis data is important in terms of changes that could directly impact thick film pad adhesion. It was also desired to understand potential changes to the bulk LTCC material that may have an indirect effect on the TKN/LTCC interface. Therefore, the Auger sputter-depth profile technique was used on these test vehicles. Auger spectroscopy data were obtained after 0.2, 0.4, 0.6, 0.8, and 1.0 min of sputtering. In the absence of a calibrated standard, the actual depth reached after each sputtering interval could only be estimated to be approximately 25, 50, 75, 100, and 125 angstroms.

The study used four samples taken from the sub-floors designated as "pre-lot #29". The "pre-" prefix was used because, strictly speaking, these sub-floors did not complete the entire LTCC build process in order to perform this study. Thus, they were not "officially" from lot #29. One of four sub-floors was exposed to one of the following process cases:

1. *Baseline* unit: No thick film post-processing was performed on either side.
2. *Single side* unit: Only the top side thick film flip chip pads were print-dry-fired on the LTCC surface.
3. *Series sequence* unit: The top side thick film pads were print-dry-fired, followed by the bottom side pads. This is the *normal sequence* used to make the units.

4. *Parallel sequence* unit: The top side pads were printed and dried, followed by the bottom side pads, print and dried. Then, the both the top side and bottom side thick film pads were fired at the same time.

Thus, the number of thick film post-process firing exposures received by the sub-floor of each case were: case 1, zero (0), baseline; case 2, one (1); case 3, two (2); and case 4, one (1).

As noted above, the first goal was to assess both the top side and bottom side of the LTCC sub-floor. Hypothetically, the same data should be obtained from the two sides since the entire sub-floor is exposed to cases 1 – 4. However, both sides were evaluate to confirm that (a) there were no intrinsic differences between the two sides of caused by the LTCC fabrication process or (b) whether the presence of the thick film paste indirectly affected the surface composition of the LTCC material.

It is important to reiterate that *only* the thick film, flip chip pad post-processing steps were performed on the sub-floors. These sub-floors were not exposed to the other high temperature post-processing steps (e.g., application of the dielectric layers, etc.). Although this test regiment did not precisely replicate the entire sub-floor manufacturing process, it was surmised that any differences of surface and near-surface compositions that may arise between conditions 1 – 4 would be most accentuated by the fewest number of steps according to the data in Reference 1, thereby providing a worst-case scenario.

The sites are shown in Fig. 19 where the surface analyses were performed on the baseline sub-floor (case 1 above). Two sites were selected on each side. The locations, which were identified by the corresponding die site, were: top side (Fig. 19a), U01 and U07 and bottom side (Fig. 19b), U09 and U15. Only the vias are apparent on the surfaces. The precise locations of the sites were chosen so that they were near to the flip chip bond pads would have been present on a fully-processed assembly.
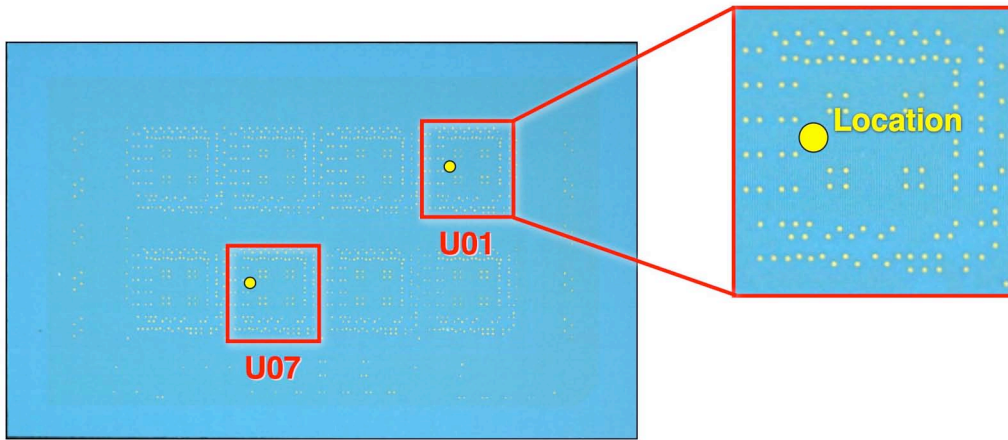
(a)
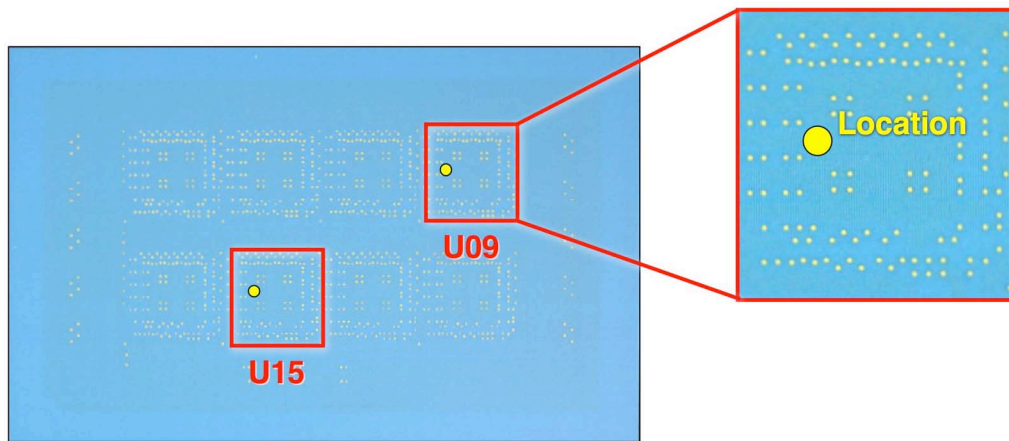


(b)

**Fig. 19** Photographs showing the locations of the Auger electron spectroscopy analyses used to evaluate the surfaces of the *baseline* LTCC sub-floor: (a) top side and (b) bottom side.

The unit representing case 2 had a single side post-processed with the thick film, flip chip pads and traces. The top side is shown in the photograph of Fig. 20; the bottom side had the same appearance as that of Fig.19b.
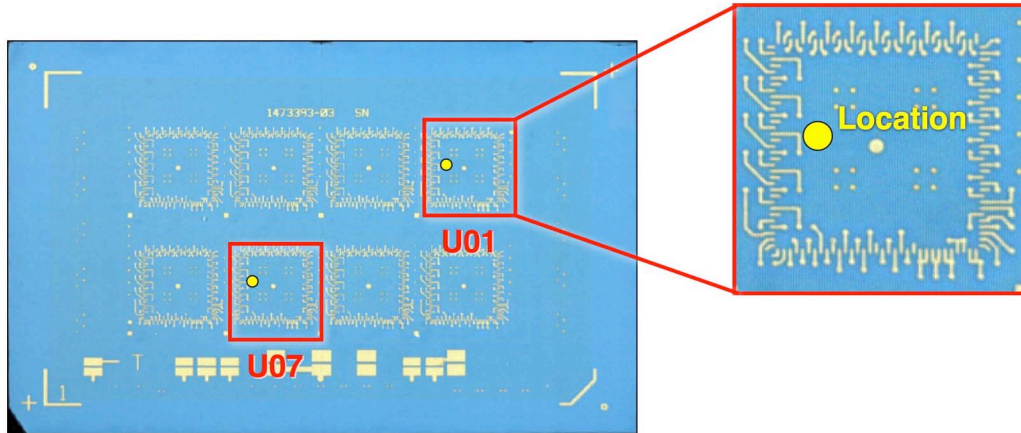
**Fig. 20** Photograph showing the locations of the Auger spectroscopy analyses used to evaluate the top side surface of an LTCC sub-floor (case 2) after top side post-processing with the thick film solder pads and traces. (The bottom side appeared similar to that in Fig. 19b.)

The other two test vehicles, which represented cases 3 and 4, had both sides appear similar to that shown in Fig. 20, with thick flip chip pads and traces at the die sites. The same die sites were evaluated on both sides of these sub-floors, as well.

Shown in Fig. 21 is a plot of the concentration (at.%) of carbon (C) and oxygen (O) as a function of the sub-floor type (case 1, case 2, etc.). The graph in Fig. 21a shows the C and O concentrations on the LTCC surface. (The O signal represents the oxides of Al, Si, Ca, and K that comprise the LTCC material.) The graph in Fig. 21b shows the same elements just below the LTCC surface after sputtering the location with Ar ions[2]. A similar "depth" was evaluated for each sub-floor, which as established by the criterion that the C concentration drop below 3 at.%. The solid symbols are the top side; the open symbols represent the bottom side.

---

[2] It should be noted that a significant development effort was required to be able to perform the sputtering process and Auger spectroscopy on the non-conductive LTCC surface. The use of an "ion blanket" of the area during the Auger signal detection alleviated charge-up on the surface that could significantly distort the readings.
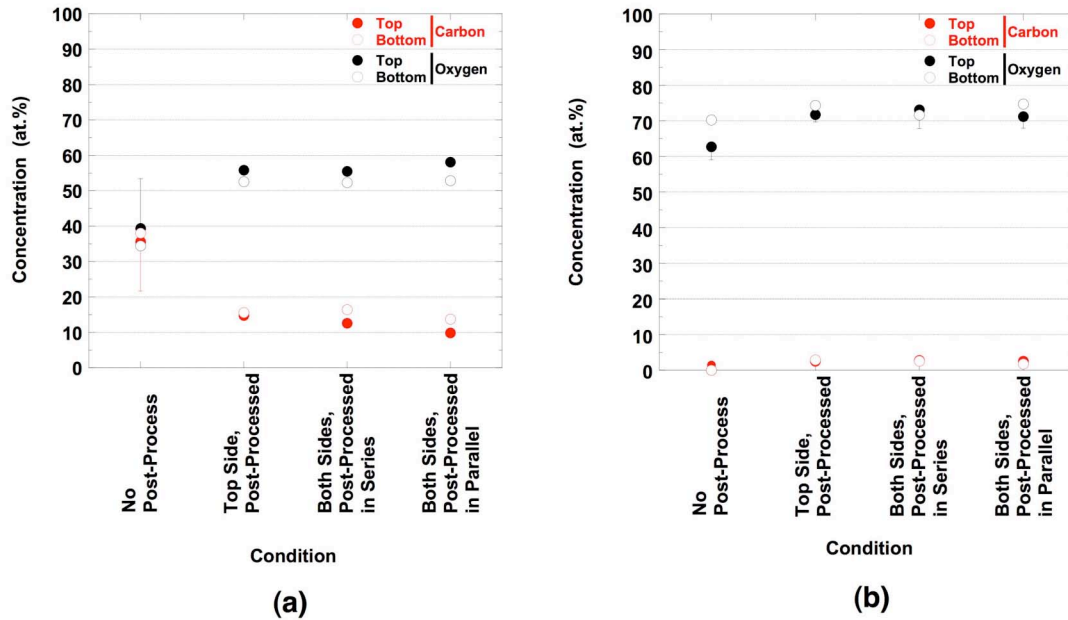
**Fig. 21** Plots of carbon (C) and oxygen (O) atomic concentrations as a function of the thick film (post-process) firing steps determined by Auger electron spectroscopy: (a) surface analysis and (b) at a near-surface depth where C < 3 at.%. The "half" error bars indicated one standard deviation.

The following observations were derived from Fig. 21a. In case 1 for which no thick film post-processing was performed, the C signal was approximately 35 at.% on both the top and bottom sides. The "half" error bars indicated one standard deviation. The scatter on the other data had similar *percent errors*. There was no significant difference between top and bottom sides.

The surface C concentrations of the other three cases 2 – 4 were lower, having values of 10 – 16 at.%. Interestingly there was no dependence upon whether the LTCC substrate was exposed to one post-process firing step (cases 2 and 4) or two such steps (case 3). Also, there continued to be no *statistical* difference between the top and bottom side C or O concentrations although the *mean* values exhibited a consistent behavior of being slightly higher on the bottom side.

The "No Post-Processing" (case 1), C concentration data in Fig. 21a had two potential sources: (1) the surface absorption of carbon compounds from the atmosphere, (2) the LTCC sub-floor manufacturing process (e.g., binder residues), or (3) a combination of the two effects.  If it were assumed that the lower C concentrations observed on the sub-floors of cases 2 – 4 represented only atmospheric absorption, then the nearly three-fold higher surface concentrations for case 1 represented the added contribution from the LTCC fabrication process.  It was surmised that those residues were burned off by the post-process steps used in cases 2 – 4. A comparison between case 3 (two firing steps) versus cases 2 and 4 (a single firing step) would suggest that a single thick film firing step was sufficient to remove that excess C from the LTCC base material.

An important point for consideration in Fig. 21a was whether or not, the 35 – 40 at.% surface C concentration would, in fact, impact the integrity of the TKN/LTCC interface if it were not entirely eliminated during the post-processing step.  Unfortunately, there is no direct data available at this time to state one way or the other, conclusively. However, the data in Fig. 2a provided indirect evidence that the effect was likely minimal. The nearly equivalent C concentrations on both the top and bottom sides does not correlate with the differences in pull strengths between the two sides that was previously documented (e.g., Fig. 16) and, moreover, continued to be observed in lot #29 hardware (to be discussed in detail in a follow-on section).  It is very likely that the residual C contamination is largely burned-away during heat-up to the bonding temperature (850°C) that formed the TKN/LTCC interface.

The surface concentrations of O were also plotted in Fig. 21a.  Higher O concentrations were observed on the post-processed samples (cases 2 – 4) as compared to no post-processing (case 1).  The trend complimented the decrease of C signals, but to a slightly lesser magnitude because of the uncovering of the metal elements that comprise the oxides. The top side had a consistently higher *mean* concentration in all cases; however, again, the differences were not statistically significant.

The C and O concentrations were measured at a depth just below the LTCC surface; those data appear in Fig. 21b.  The plot shows the 3 at.% concentration C concentration criterion; but, the C signals did eventually drop to zero. All cases showed approximately the same increase of the O signal; thus, the O concentrations for cases 2 – 4 remained slightly higher than that of the sub-floor that received no post-processing firing steps (case 1).  Therefore, this trend may represent an intrinsic difference between cases 1 versus 2 – 4 and *may* have contributed to a similar difference at the surface (Fig. 21a). The O concentrations were statistically the same between top and bottom sides in all cases.

The following summary was developed from the data presented in Fig. 21.  The post-processing conditions were effective at removing a significant portion the surface C concentration from the LTCC substrate.  Secondly, the near-surface volume of LTCC exhibited a slightly higher O content after the post-processing thick film deposition steps.  However, the strengths of the C and O signals were not dependent upon the number of the post-processing steps (one or two).  Also, statistically, there was no difference between the top side and bottom side data.

The Auger spectroscopy analysis included the elements Si and Al, which in the form of their respective oxides, are the primary constituents of the LTCC base material. The results of the Auger surface analyses are shown in Fig. 22a.  There were slightly higher *mean* Si and Al concentrations for the post-processing cases 2 – 4 compared to case 1, but within experimental error.  Although opposing trends were observed between the *mean* Si and Al concentrations of top side versus bottom side, the trends lacked statistical significance.  Also, between cases 2 and 4 (single firing step) and case 3 (two firing steps), there were no differences between Si signals or between Al signals, including top side versus bottom side.  Therefore, the Si and Al surface concentration trends were largely anticipated, based upon the C and O data in Fig. 21a, and exhibited no other unusual behavior(s).
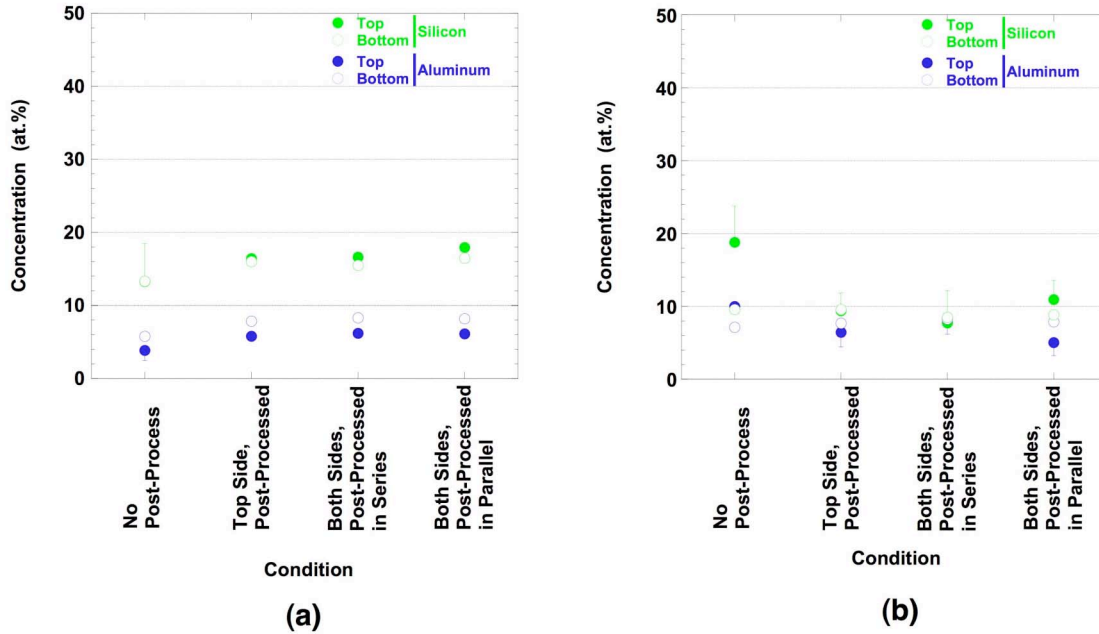
**Fig. 22** Plots of silicon (Si) and aluminum (Al) atomic concentrations as a function of the thick film (post-process) firing steps determined by Auger spectroscopy: (a) surface analysis and (b) at a sub-surface depth where C < 3 at.%. The "half" error bars indicated one standard deviation.

The Auger Si and Al depth profile signals were also analyzed after sputtering. As was the case with the C and O signals, the Si and Al signals were recorded at the point where the C concentration dropped below 3 at.%. Those results appear in Fig. 22b. The Si and Al concentrations were statistically similar to one-another between all cases. The one exception was the relatively high, top side Si signal of the sub-floor that did not receive a post-process firing step. Because the same behavior was not repeated on the bottom side, it was concluded that high Si count was a local anomaly. (A second depth profile, which was not performed, would have provided the needed confirmation.) Also, there was no statistically significant difference between top side and bottom side data of either non-post processed and post-process cases.

Next, a comparison was performed between the surface (Fig. 22a) and near-surface (Fig. 22b) Si and Al data. The only significant trend was a lowering of the Si concentration in the near-surface region. Because this trend did *not* compliment a

decreasing trend of the C signal, it was an actual event. The Si trend was independent of post-processing exposure (0, 1, or 2 exposures).  Also, under all conditions, there was no statistical difference between the top side and bottom side Si concentrations.

The final two elements that were investigated were calcium (Ca) and potassium (K). The Ca and K signals originated from their respective oxide glass modifiers in the LTCC material. The corresponding plots of surface concentration and near-surface region concentration (< 3 at.% C) for the four cases appear in Figs. 23a and 23b, respectively. It is important to recognize that these elements occurred at considerably smaller concentrations than C, O, Al or Si as indicated by the y-axis scales.



(a)                                              (b)
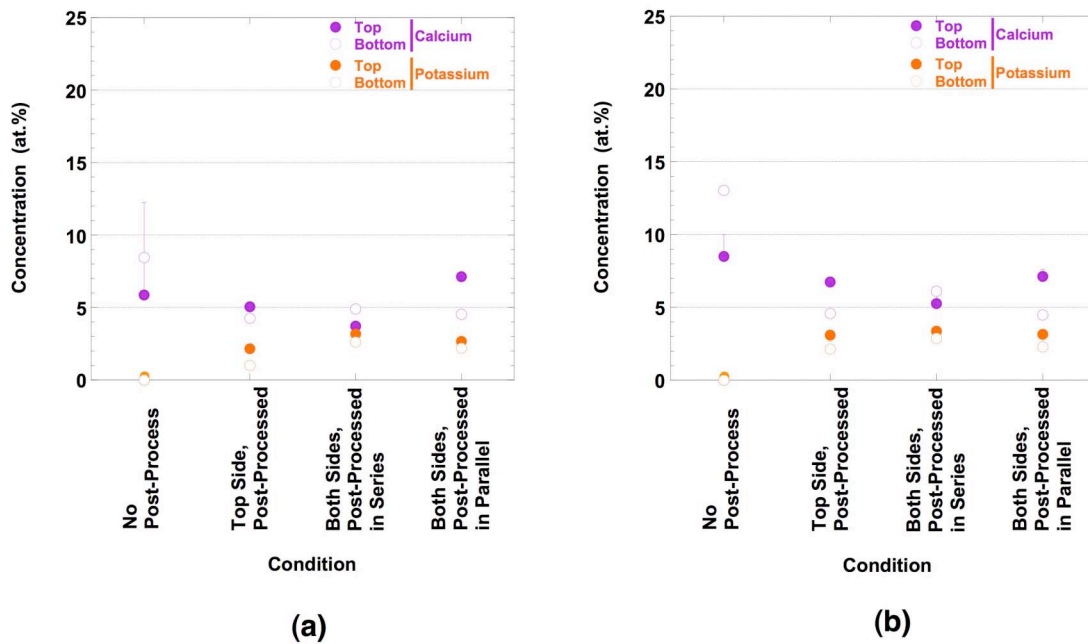
**Fig. 23** Plots of calcium (Ca) and potassium (K) atomic concentrations as a function of the thick film (post-process) firing steps determined by Auger spectroscopy: (a) surface analysis and (b) at a sub-surface depth where C < 3 at.%. The "half" error bars indicated one standard deviation.

A comparison between Figs. 23a and 23b shows very similar trends at the surface and near-surface regions, respectively, for both C and K signals. The K concentration was absent from both the surface and near-surface regions of the sub-floor without any post-

processing step (case 1). The K signal appeared with the sub-floors exposed to one or two post-processing steps to statistically similar levels.  This trend may have been a complimentary effect of the loss of the C with post-processing at the surface; however the appearance of K with post-processing exposures was a "real" effect in the near-surface region.  The top side K concentrations were slightly larger on the top side, but still, within experimental error for both Figs. 23a and 23b.

The Ca signal was present at the surface and near-surface regions of the non-post-processed test article.  The Ca concentration generally decreased with the addition of one post-process step, and then decreased to a minimum value after two post-processing steps (case 3).  This trend, as well as the Ca concentration values, themselves, were similar between the surface and within the near-surface region and exhibited no consistent difference between top and bottom sides.

In summary, the Auger spectroscopy technique was used to determine the distribution of C, O, Al, Si, Ca, and K elements on the surface and near-surface regions of LTCC sub-floors that had been exposed to one of four post-processing conditions.  Two locations were evaluated on each of the top and bottom sides.  First, the specific trends are listed below for each of the major elements:

1.  A higher C surface concentration was observed on the surface of the LTCC sub-floor in the absence of post-processing steps. The reduction in the C surface concentration occurred to the same extent for one or two post-process steps.  There was no statistically significant difference of C concentration between top and bottom sides in any of the four cases.

2.  The surface O content was increased to similar levels after exposure to any of the post-process conditions, presumably due to the loss of C.  The top side concentrations were slightly higher than the bottom side; but the difference was within experimental error.

3. After sputtering to a near-surface depth, the C concentration dropped to nearly zero for all cases.  In the near-surface region, the O concentration was slightly higher for samples exposed to the post-process conditions.  However, there was no dependency on the number of such exposures.  The O concentrations were statistically the same for top and bottom surfaces.

4. The surface Si concentrations were higher than those of Al.  The post-processing steps consistently increased both Si and Al surface concentrations slightly with no dependency on the number of steps.  Some or all of this increase could have been attributed to the loss of C.  In the latter cases, the Si signal showed no difference between top side and bottom side.  The mean Al concentration was slightly lower on the top side; but, the difference was within experimental error.

5. In the near-surface region, the Al concentrations were largely unchanged from those at the surface for all conditions.  On the other hand, the Si concentrations decreased by approximately 10 at. % from the surface to the near-surface location, to levels comparable to Al.  In the sub-surface region, there were no significant differences of Si or Al concentrations between their respective top side and bottom side values.

6. The K signal was absent from both the surface and near-surface regions of the sub-floor without a post-processing step (case 1).  The Ca signal appeared after exposure to one or two post-processing steps.  At the surface, this trend could be explained as an artifact of the loss of surface C; however, the trend was "real" at the near-surface region where C was absent.  The K concentration exhibited a small maximum value for the two post-processing steps at both surface and near-surface locations. There were no consistent differences of K concentrations between top and bottom sides per the experimental error, although, two post-processing steps appeared to reduce those variations.

7. A Ca concentration was present at the surfaces of all samples. The values decreased slightly after the post-process exposures, there being a minimum concentration after two such steps. This trend did not compliment the C surface concentrations and, as such, was "real." Moreover, the same behavior was observed in the near-surface region, although in general, the Ca concentrations were shifted to slightly higher values. There were no consistent differences of Ca concentrations between top and bottom sides due the relatively higher experimental error. However, the two post-processing steps appeared to reduce those variations.

Second, the elemental trends listed above were assessed in terms of potential impact on the TKN/LTCC interface microstructure that underlies the pull strength behavior.

1. The C concentration on the surfaces of LTCC substrates prior to post-processing were reduced by the post-process exposures, although they did not reach zero. A single post-processing step was as effective as two such procedures and there was no significant difference between the top and bottom sides. If it was assumed that the presence of the thick film paste during the top side post-processing does not allow the C to escape from the surface, then the bottom side would have *benefited* from the top side post-processing step by a reduction in the surface C concentration. If C was detrimental to the TKN/LTCC interface strength, then the bottom side would have a higher pull strength, which was *not* the case. Thus, it appeared that the magnitude of C contamination did not affect the TKN/LTCC interface. Or, in the event that the post-process steps were effective at removing the surface C, even with the thick film paste printed on the surface, the residual C contamination would have been similar on both top and bottom sides, and as such, did not correlate with the observed differences in pull strengths.

2. The second significant trend associated with the post-processing was that of Si. On the surface, there was no significant effect of the post-processing steps on the Si concentrations. However, in the near-surface region, the Si concentrations were

lower by nearly one-half ($\Delta$ = -10 at.%). There was no statistically significant difference between one and two post-process steps, or between top side versus bottom side. Therefore, the difference in Si concentrations between the surface and near-surface regions was an intrinsic property of the LTCC material and, being relatively insensitive to the post-processing steps, would have little impact on the TKN/LTCC interface.

3. Potassium was absent from the surface and near-surface regions of the non-post-processed parts. On the surface, the appearance of K with post-process exposure could have been attributed to the reduced C signal. However, the appearance of K in the near-surface region of post-processed parts was a "real" consequence of the latter exposures and, as such, lends some credibility that the same effect could have occurred on the surface. There was a small maximum after two such exposures versus one exposure. There was no consistent trend between top and bottom sides.

4. The Ca signal demonstrated the opposite behavior to that of K concentration, including similar magnitudes. The Ca concentrations decreased between the non-post-processed and post-processed cases at *both* the surface *and* near-surface regions. At the surface, an even greater magnitude of the effect may have occurred; but, the trend was masked by the loss of the C signal. The loss of Ca was accentuated after two post processing steps as indicated by the minimum concentration. The Ca signal showed no consistent dependence on top side versus bottom side locations.

5. The behaviors of the K and Ca concentrations appeared to compliment one-another. But, more importantly, both the K and Ca concentrations were sensitive to the number of post-process steps. Therefore, the fact that the bottom side of the LTCC sub-floor experiences two exposures to post-process conditions could *potentially* lead to TKN/LTCC interface properties differing from those of the top side. Unfortunately, it is not known whether those compositional differences were capable

of altering the TKN/LTCC microstructure – either intrinsically or if a factor, at the observed magnitude of 1 – 2 at. % - to impact the pull strength performance.

In conclusion, Auger electron spectroscopy was used to examine changes to the surface and near-surface chemistries of the LTCC material caused by the post-processing steps.  There were four phenomena that were confirmed consequences of the post-processing steps:

- Removal of C contamination from the surface,
- Higher Si at the surface than in the near-surface region.
- The interchange of Ca and K at the near-surface region.

Only the Ca and K compositions showed a significant dependence on the number of post-processing steps, which could be *potentially* correlated to pull strength differences between top side and bottom side flip chip solder joints.

Lastly, the fact that the C, O, Al, Si, K, and Ca elemental concentrations were not statistically different between the top and bottom sides of the LTCC sub-floors indicated that (1) there was not a significant, intrinsic difference between the compositions of the two surfaces of the LTCC material and (2) the presence of the thick film paste and its firing did not alter the composition of the nearby LTCC material as a secondary effect.

*1.5 Hydrogen-Nitrogen Environments*

1.5.1 Introduction

During the course of assessing the documentation of the sub-floors in lots #4 to #20, it was noted that several sub-floors had the edge or "braze" pins attached to the pads with 80Au-20Sn solder using a nitrogen ($N_2$)-10%hydrogen ($H_2$) atmosphere (approximately 760 torr absolute) rather than strictly a $N_2$ atmosphere. Concern was raised as to whether the $N_2$-$H_2$ atmosphere and, in particular, the $H_2$ content of that atmosphere,

would lead to the reduction of bismuth- (Bi) and lead (Pb)-oxide glasses that bind the thick film layer to the LTCC substrate. Previous tests at Sandia indicated a drop of adhesion between the Au-Pt-Pd thick film and LTCC when exposed to a $H_2$environment (assumedly 100%) at 730°C for 3 min. [9][3].  Unfortunately, it could not be determined from the vendor information those sub-floors that had been exposed to this environment.

The DuPont™ data sheet indicates that a $N_2$ – 3.7%$H_2$ atmosphere can be used when brazing with the 82Au-18In filler metal.  The use of the Au-In filler metal requires a considerably higher process temperature of 580°C versus that required of the Au-Sn solder [10].  Therefore, it can be inferred from the DuPont™ data that there would be a minimal loss of adhesion under a $N_2$ – 3.7%$H_2$ atmosphere and temperatures equal to, or below, 580°C.

It was deemed a "stretch" to assume that the effects of a $N_2$ – 3.7%$H_2$ atmosphere were representative of those of the errant $N_2$ – 10%$H_2$ atmosphere.  Thus, the literature was also evaluated, which considered the reduction of Bi- and Pb-based glasses in a 100% $H_2$ environment as the bounding condition.  Studies performed by Chernogorenko and Lynchak showed that the reduction reaction can occur at 270°C [11].  In a more exacting material analysis investigation using x-ray absorption spectroscopy, Witkowska, et al., showed that a $0.4Bi_2O_3$-$0.6SiO_2$ glass would initially phase separate after 1 hour at 377°C in pure $H_2$ [12].  Approximately 76% of the $Bi_2O_3$ was confirmed to have reduced to elemental Bi after 16 hours.  The remaining 24% was either, still in the glass phase or, in an intermediate state between the glass and elemental states.  Recall that these glasses were fully exposed to a pure $H_2$ environment.  In a follow-on paper by Witkowska, the reduction of composite $Bi_2O_3$ and PbO glass systems to elemental Bi and Pb was also predicted by molecular dynamics simulations [13]. Therefore, in the

[3] The term, "braze" pin, was mis-coined because the alloy, 80Au-20Sn, which is used to attach the pins to the LTCC is actually a solder alloy.  The alloy has a eutectic temperature of 280°C, which below the 450°C demarcation point between solder alloys and brazing filler metals.  Nevertheless, the terminology was retained in this report.  Also, the typical processing temperature for this solder is 300 – 350°C.

presence of pure $H_2$, exposed $Bi_2O_3$ glass and likely, PbO glass, will reduce to elemental Bi and Pb, respectively, to a nominal extent under relatively low temperature conditions. It was warranted to further investigate this issue.

The furnace parameters was confirmed, which was used for the $N_2$-10%$H_2$ exposure. The time-temperature profile of the edge pin attachment process was broken down into the three highest temperature segments: (1) ramp up, 290°C<T<340°C, 1 min; (2) peak, 340°C<T<360°C, 2 min; and (3) ramp down, 340°C>T>250°C, 1 min [14]. These relatively low temperatures, together with a cumulative time period at the highest temperatures of only 4 min, were considerably less severe than those described in the cited works, thereby further minimizing the likelihood that any degradation had take place to the TKN/LTCC bond.

On the other hand, there were two factors that may accelerate the reduction process aside from the lack of experience base that addresses the $N_2$-10%$H_2$ atmosphere composition, explicitly. First, the quantity of glass phases at the interfaces was low so that, even a minor degree of reduction could be detrimental to the interface adhesion. In particular, the rate kinetics of the reduction process(es) were not understood. Secondly, the thick film layer was porous, which increased the extent of TKN/LTCC interface that was exposed to the furnace environment. These unknown factors warranted further analysis of the potential effects of the $N_2$-10%$H_2$ atmosphere on the pull strength behavior of the flip chip die solder joints. The analysis continued by re-evaluating prior data to determine that, given the lot #4 - #20 sub-floors were, in fact, all exposed to the $N_2$-10%$H_2$ atmosphere, then can it be expected that the suspected effect of low pull strength occurred consistently within each lot of such sub-floors.

1.5.2 Passive analyses of sub-floor lots

The approach was taken to further evaluate already-build sub-modules from the lots #4 - #20 to assess the sub-floor-to-sub-floor variation. Lot numbers were identified from which, the sub-floor process monitors showed excellent and marginal pull strengths, by

reviewing Fig. 3 and current materials stores. It was observed that lot #13 (SF1090) provided marginal pull strengths while lots #16 (SF1272) and #19 (SF1419) appeared to exhibit excellent strength performance. Therefore, it was decided to repeat the process monitor pull tests on duplicate sub-modules taken from these lots.

The pull strengths from sub-modules that were determined in the prior process monitor pull tests (SF1090, SF1272, and SF1419) were designated as Rev 0. The duplicate set of pull tests that were performed in the current study, were designated as Rev 1. The sub-modules were: SF1074, SF1204, SF1266, and SF1427 that represented lots #13, #15, #16, and #19, respectively[4]. The Rev 0 and Rev 1 pull strength data are plotted together in Fig. 24, including as-fabricated and post-thermal cycled data. The pull strengths were comparable between Rev 0 and Rev 1 for the sub-modules of lots #13 and #16. The lot #15 sub-module exhibited very low pull strengths in both conditions, as evidence of the lot-to-lot variation of the low pull strength phenomenon. However, of most concern was the significant difference observed between the two sub-modules from lot #19. The pull strengths SF1427 (Rev 1) were considerably lower than the excellent pull strengths observed for SF1419 (Rev 0). These data indicated that there was a significant sub-floor-to-sub-floor variation of pull strengths within a lot. Therefore, it would not be possible to avoid the low pull strength phenomenon, irrespective of the role had by the $N_2$-10%$H_2$ atmosphere, by selecting sub-floors from particular lots.

---

[4] The reason to add the lot #15 module was that the initial database indicated that lots #15 and #16 pedigrees were mixed up. Although it was nearly certain that SF1272 (Rev 0) came from lot #16, it was confirmed that SF1204 and SF1266 originated from lots #15 and #16, respectively.
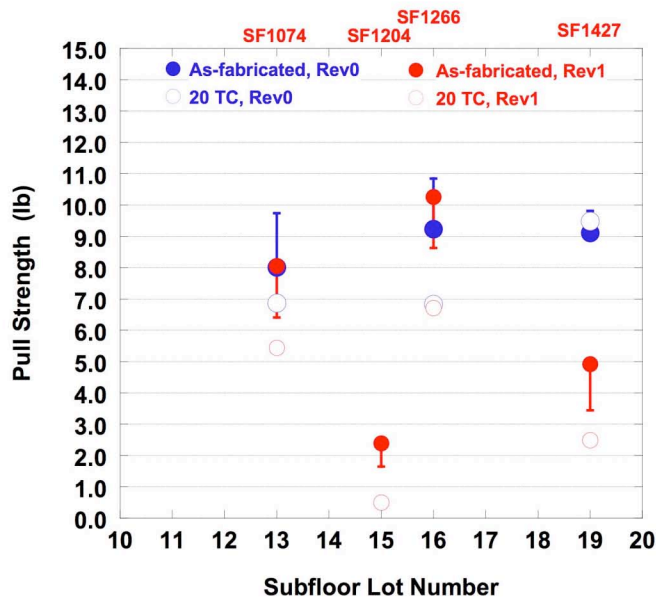
**Fig. 24** Graph of pull strength as a function of sub-floor lot number for the two data sets designated Rev 0 and Rev1. The Rev 1 sub-module numbers, which represented sub-floor lots #13, #15, #16, and #19, are provided at the top. Closed symbols were the as-fabricated results; open symbols designated the post-thermal cycled results. The half error bars are one standard deviation.

1.5.3 Active analyses - double-blind experiment

The previous analysis (1.5.2) indicated that it could not be assured that sub-floors selected from specific lots would have good or poor (low) pull strength performance. Therefore, it was necessary to determine if remedial measures could be taken to restore the pull strength performance of sub-modules made from the sub-floors. However, before remediation could be addressed, it was necessary to confirm that, in fact, exposure to the $N_2$-10%$H_2$ atmosphere was responsible for the low pull strengths, even if the effect was not always reproducible. Therefore, it was decided to expose several sub-floors to the $N_2$-10%$H_2$ furnace in a double-blind study in order to try to reproduce the low pull strength behavior.

At this time, fortunately, the vendor was able to confirm that sub-floors numbered between SF800 and SF1000, which encompassed primarily lots #9 - #11, had *not* been

exposed to the $N_2$-10%$H_2$ atmosphere.  Rather the edge pins were attached in the standard $N_2$ atmosphere.  Eight (8) such sub-floors were set aside.  Four (4) of the sub-floors were exposed to the $N_2$-10%$H_2$ atmosphere.  It was understood that this would be a second exposure to the "braze pin" attachment temperature profile.  The other four units were exposed to a second, standard $N_2$ furnace cycle. The sub-floor pedigrees are listed below:

- 100% $N_2$ (2x):              SF935, SF858, SF827, and SF858

- 100% $N_2$ + $N_2$-10%$H_2$:    SF838, SF846, SF852, and SF973

The sub-floors were assembled with dice, which were then pull tested for the strength data in the traditional process monitor format, which included the as-fabricated and post-thermal cycled conditions.

The graph in Fig. 25a shows the as-fabricated, pull strengths as a function of the sub-floor number.  The sub-module designation was split between those units exposed to the extra, $N_2$-10%$H_2$ environment and those experiencing a second 100% $N_2$ cycle as denoted at the top of the plot.  The data were also separated into top side (red) and bottom side (blue) pull strength performances.  The top side strength values were significantly higher for the sub-modules exposed to the additional 100% $N_2$ atmosphere than those exposed to the $N_2$-10%$H_2$ environment.  This trend implies that exposure to the $H_2$-bearing atmosphere had a detrimental effect on pull strength and, moreover, of a magnitude that was commensurate with the low pull strength phenomenon.  The data spread of the sub-modules SF852 and SF973 were consistently higher than those of the other two units between the two conditions.
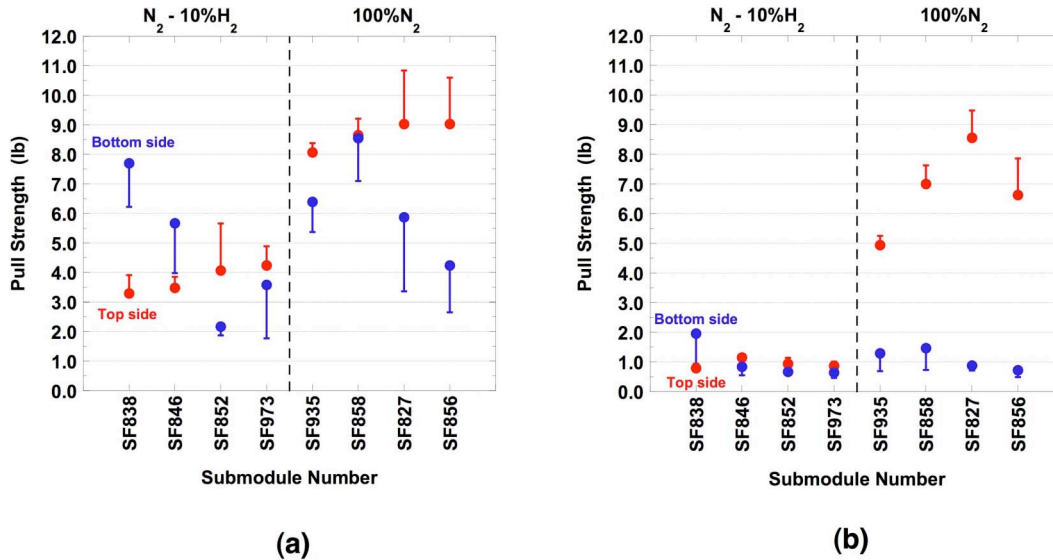
**Fig. 25** Plots of pull strength as a function of sub-module pedigree: (a) as-fabricated and (b) post-20 thermal cycles (-55°C/125°C). All sub-modules were initially exposed to the $N_2$ edge pin soldering cycle. Then, four of the eight were exposed to the $N_2$-10%$H_2$ environment and the other four were exposed to a second $N_2$ environment. The red symbols are the top side data; the blue symbols were the bottom side data. The "single side" error bar is one standard deviation.

The bottom side pull strengths were similarly evaluated. Under either the $N_2$-10%$H_2$ condition or 100% $N_2$ condition, both the mean values and error bars varied considerably between the different sub-modules. There was no consistent trend that discriminated the bottom side pull strengths between the $N_2$-10%$H_2$ or 100% $N_2$ exposures. The data spread of the sub-modules SF852 and SF973 remained consistently higher, but only for the 100% $N_2$ atmosphere. Thus, if the $H_2$-bearing furnace environment was responsible for reducing the top side pull strengths, the effect was not reproduced on the bottom side.

The pull strength values were also obtained from the sub-modules after they had been exposed to 20 thermal cycles (-55°C/125°C); those data were plotted in Fig. 25b. The sub-modules exposed to the $N_2$-10%$H_2$ atmosphere exhibited significant strength losses for both the top side and bottom side interconnections. In the case of those sub-

modules exposes exposed to the 100% $N_2$ atmosphere for a second time, there was a nominal drop in the top side strength and a severe loss of bottom side pull strength. from both environments experienced a general strength loss to the top side and bottom side pull strengths.  In the case of the top side dice, however, that strength decrease was more substantial for the sub-floors, which reached very poor values. The bottom side pull strengths exhibited significant declines in *all* cases, to similar, very low levels.

In summary, the top side pull strengths – both as-fabricated and post-thermal cycled – indicated that exposure to the braze pin solder process, which used the $N_2$-10%$H_2$ atmosphere, had degraded the TKN/LTCC interface.  In the case of those sub-modules exposed to the $H_2$-bearing atmosphere, strength levels were in the range that was commensurate with the low pull strength phenomenon.   However, the $H_2$ – pull strength correlation *was not conclusive* because it was not observed with the bottom side pull strengths.  First, this trend simply was not duplicated for the sub-modules in the as-fabricated condition.  Then, no consistent trend could be identified after thermal cycling because of the precipitous strength loss caused by this condition to *all* of the sub-modules (low pull strength phenomenon), irrespective of whether or not they were exposed to the $H_2$-bearing atmosphere.

1.5.4 Air annealing ( "healing") treatment

The experiments described in 1.5.3 provided evidence, albeit not wholly conclusive, that $N_2$-10%$H_2$ atmosphere may have contributed towards the low pull strength phenomenon.  Therefore, it was deemed necessary to address the effects of the $H_2$-bearing atmosphere and, specifically, the reduction of Bi- or Pb-oxides in order to salvage the stock sub-floors that could be used for sub-module construction.

A mitigation strategy was developed that was based upon the premise of re-oxidizing the elemental Bi and/or Pb that was suspected to have formed upon exposure to the $N_2$-10%$H_2$ atmosphere.  The task was to subject the sub-floors to an **air annealing**

treatment prior to their assembly into sub-modules.  This annealing treatment, or "healing" treatment as it was termed, was established as **250°C**, **260 hours, in air**.

The success of the re-oxidation process would have to be inferred from the die pull strength metric of sub-modules.   That is, sub-floors *suspected* of having been exposed to the $N_2$-10%$H_2$ atmosphere would then be exposed to the healing treatments.  Then, the pull strengths would be measured to provide an indication of the effectiveness of the procedure. It was not possible to determine, expressly, that elemental Bi or Pb had been, in fact, re-oxidized into their respective glassy compounds by this healing treatment.

The LTCC base material and the Au-Pt-Pd TKN are complex materials systems as is the TKN/LTCC interface between them. The interface microstructure is further complicated by the addition of the soldered interconnection above it. Therefore, it was possible that the healing process could cause ancillary effects on the solder joint pull strength, either to its improvement or to its degradation. Of course, there remained the likelihood that an entirely different phenomenon was controlling the low pull strength phenomenon, all together, and that the Bi and/or Pb reduction was inconsequential.

The sub-floors that were selected for analysis were taken from lots #7, #14, #17, #18, and #20, which had low die pull strengths from earlier tests.  Thus, it had to be assumed that (a) the low pull strength trends stood a high probability of being reproduced in at-least one of these cases and (b) the low strengths were caused by the possible exposure to processing to the $N_2$-10%$H_2$ environment.  Also, because earlier tests determined that the pull strengths of one sub-module from a given lot would not necessarily be duplicated on a second sub-module of the same lot, this initial study used a single sub-module of each lot and partitioned the different test conditions amongst the dice on that sub-module in the following manner:

1. As-fabricated, no healing treatment:          Top side:      U02, U03, U04

Bottom side: U10, U11, U12


2. Healed; as-fabricated:                Top side:    U06, U07, U08
                                        Bottom side: U14, U15, U16


3. Healed; thermal cycled:               Top side:    U01, U05
                                        Bottom side: U09, U13


The impetus was given to the two as-fabricated conditions for providing a success/failure determination of the healing process. Previous studies indicated that (1) the as-fabricated data were more consistent and (2) the post-thermal cycled strength trends tended to mirror those of the as-fabricated condition, anyways. An evaluation could not be performed to determine the die pull strength after thermal cycling, but without the healing treatment, because the entire sub-floor would have been exposed to the healing treatment after dice had been tested in the "as-fabricated, no healing treatment" condition.

Shown in Fig. 26 are (a) the top side and (b) the bottom side pull strength data taken from the sub-modules tested in the as-fabricated condition. The sub-module serial number and LTCC lot number appear on the bottom and top x-axes, respectively. The half-error bars are one standard deviation. The blue symbols are the pull strengths of dice not exposed to the healing treatment; the red symbols are from the dice that were pull tested after the healing treatment. In Fig. 26a (top side), the mean pull strength values had slightly higher values following the healing treatment. Also, to a limited degree, the magnitudes of the mean pull strength increases after healing were inversely proportional to the initial pull strength magnitude. Nevertheless, in each of these cases, the strength improvements were within the experimental error.
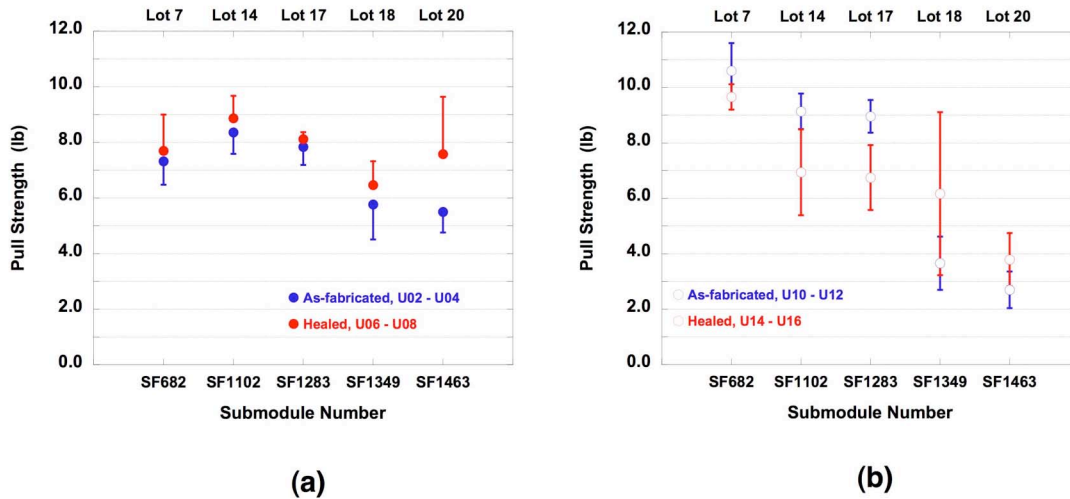
**Fig. 26** Pull strengths as a function of sub-module (lot) units in the as-fabricated and healed conditions: (a) top side dice and (b) bottom side dice. These sub-modules were suspected of being exposed to the $N_2$-10%$H_2$ furnace environment: The half-error bar is one standard deviation.

The plot in Fig. 26b shows the die pull strengths measured on the bottom side of the sub-modules in the as-fabricate or healed condition. There was no one trend that applied to all of the sub-modules. Instead, there were two behaviors. The sub-modules SF682, SF1102, and SF1283, which exhibited relatively high, as-fabricated pull strengths, had the pull strength decrease after the healing treatment. In fact, for the SF1102 and SF1283 units, the strength losses were statistically significant. This trend was opposite to that observed on the top side (Fig. 26a). The healing treatment also caused a greater scatter to the strength data. (The preferred scenario would have been that the healing treatment had a null effect on *these* strength values.) The sub-modules, SF1349 and SF1463, had very low pull strengths in the as-fabricated condition. The healing treatment caused the mean pull strengths to increase, more so for SF1349 than for SF1463. Unfortunately, so did the data scatter increase with the healing treatment. The consequence was that the latter strength improvements were not statistically significant.

The data presented in Fig. 26 can be summarized by the following trends:  (a) For low pull strengths of < 4 lb, the healing treatment improved the top side and bottom side as-fabricated, pull strengths (sub-modules SF1349 and SF1463).  The caveats were that the increases were not statistically significant due to the increased scatter that appeared to accompany the healing treatment and, secondly, the pull strengths could not be consistently raised to, or above, the acceptance criterion.  (b) In the case of nominal pull strengths of 7 – 8 lbs, there was a slight improvement in the mean strength, but generally not of statistical significance.  (c) When die pull strengths were high, having values > 8 lb, the healing treatment caused a loss of pull strength, but to values that remained above acceptance limits.

Next, the analysis turned to the pull strengths of dice sites that were subjected to the healing treatment, and subsequently, exposed to 20 thermal cycles (-55°C/125°C). Unfortunately, there were only two dice remaining on each of the top sides and bottom sides so that a comparison could not be drawn between data scatters of the healed versus healed-plus-thermal cycled conditions. The pull strength data are presented in Fig. 27. The error bars represent one standard deviation. On the top side (Fig. 27a), there was a decrease in the pull strength after thermal cycling.  The magnitude of that decreases were generally similar between the five sub-modules and were commensurate with earlier data. Therefore, the healing treatment did not appear to either improve upon, nor further aggravate, the pull strength drop that is usually observed after thermal cycle.  The same result was observed for the bottom side pull strength data (Fig. 27b).

In summary, the healing treatment did not provide a statistically significant improvement to the die pull strength, especially those sub-modules for which the initial pull strengths were too low to meet the acceptance criteria.  The post-thermal cycle data indicated that the "inherent" pull strength loss that follows thermal cycling overwhelmed any effect caused by the healing treatment.  Therefore, as was determined primarily by the as-fabricated data, the healing treatment provided a slight improvement to the low pull
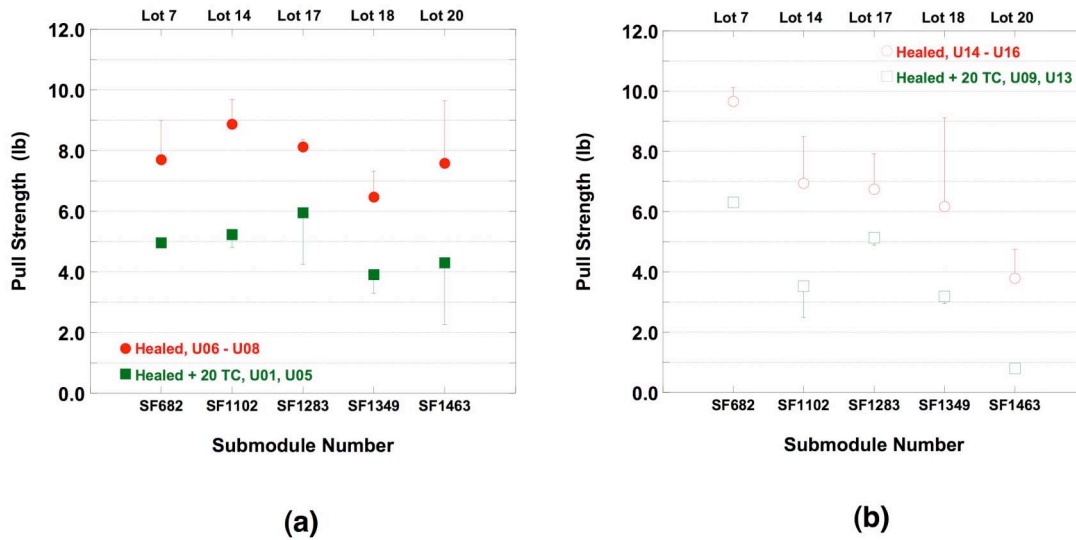
**Fig. 27** Pull strengths as a function of sub-module (lot) units in the healed (as-fabricated) and healed-plus-thermal cycled (20 cycles, -55°C/125°C) conditions: (a) top side dice and (b) bottom side dice. These sub-modules were suspected of being exposed to the $N_2$-10%$H_2$ furnace environment: The half-error bar is one standard deviation.

strength, but did not do so to a sufficient degree that allowed the sub-modules to meet the acceptance criteria. This result implies that the healing treatment was not very effective against the degradation that was suspected of having been caused by exposure to the $N_2$-10%$H_2$ environment. From a positive viewpoint, this exercise confirmed a level of robustness of the thick film, the LTCC substrate, and the TKN/LTCC interface. The exposure of the post-process sub-floors to conditions of 250°C for 260 hours in air did not significantly affect the pull strength of subsequently-formed, solder interconnections.

The failure modes were also analyzed, which accompanied the strength data. The failure modes were separated into two groups: (a) TKN/LTCC interface failures, including those accompanied by an LTCC divot (Figs. 1d and 1e) and (b) the combination of Si/solder and Si/solder + Si UBM modes (Figs. 1b and 1c). Since these

two failure mode groups were mutually exclusive, only the TKN/LTCC interface failures are discussed.  It is important to have a historical perspective on the frequency of the TKN/LTCC and TKN/LTCC + LTCC divot failure modes.  The TKN/LTCC failure mode accounted for 50 – 75% of the fractures on sub-modules in the as-fabricated condition.  Divots were largely not observed in the as-fabricated condition.  After 20 thermal cycles, the percentage of TKN/LTCC failures was 80 – 100%.  The percentage of TKN/LTCC + divot failure sites was historically 5 – 10% after thermal cycling.

Plotted in Fig. 28a are the percentages of top side solder joints having the TKN/LTCC failure mode as a function of the sub-module.  The data sets are for the as-fabricated and healed (250°C, 260 hour) conditions.  In nearly all cases, the percentage of TKN/LTCC failures tended to be higher than the historical values.  There was no statistical difference in the percentages of the TKN/LTCC failure mode between the as-fabricated and healed conditions for the SF682, SF1102, and SF1283 sub-modules.  This trend appeared to corroborate the observed, minimal pull strength differences between the as-fabricated and healed conditions.  On the other, the two sub-modules that experienced the increase of mean strengths after the healing treatment, also experienced a decrease in the TKN/LTCC failure mode, although the decrease was statistically significant only for SF1349.  Mechanistically, the latter trend implied that the TKN/LTCC interface had developed a higher strength, which caused the failure site to move to the die side of the interconnection.  However, it was not possible to draw a correlation, quantitatively, between pull strength and TKN/LTCC failure mode for either the as-fabricated or post-healed data.  This point is illustrated in Fig. 28b, which is a plot of the percentage of the TKN/LTCC failure mode as a function of pull strength.
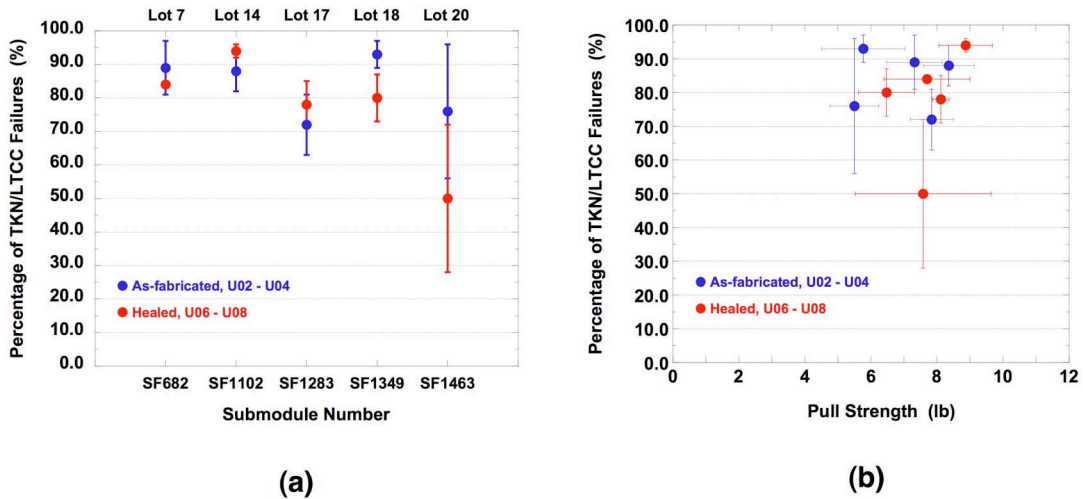
**Fig. 28** (a) Plot of TKN/LTCC failure mode percentage as a function of sub-module pedigree for the pull strengths representing the as-fabricated dice and those dice subjected to the healing treatment (250°C, 260 hours) located on the *top side* of each sub-module. (b) Graph of TKN/LTCC failure mode percentage as a function of pull strength showing the lack of correlation between the two metrics. The symbol colors designate the source of the respective data groups. The error bars are ±one standard deviation.

The failure mode data were similarly analyzed for the sub-module bottom-side die. The data are presented in Fig. 29a. First of all, the TKN/LTCC failure mode percentage remained relatively high compared to historical data. Secondly, the healing treatment did not cause a statistically significant change to the TKN/LTCC failure mode percentage for the SF682 SF1102, and SF1283 sub-modules as also observed on the top side. Similarly, the other two sub-modules SF1349 and SF1463 showed no significant change to the failure mode behavior. The failure mode data in Fig. 29a, like that in Fig. 29a, a lack of impact had by the healing treatment on the failure mode.

The plot in Fig. 29b shows the TKN/LTCC failure mode percentage as a function of pull strength for the sub-module bottom sides. A weak correlation was developed between the two metrics for both the as-fabricated and healed conditions. However, there was no difference between the respective correlations.
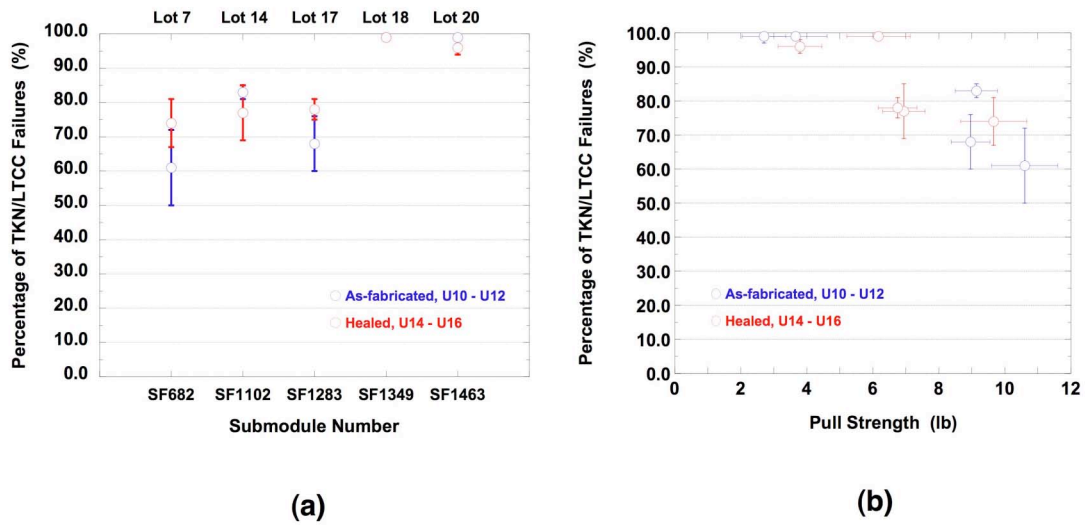
**Fig. 29** (a) Plot of TKN/LTCC failure mode percentage as a function of sub-module pedigree for the pull strengths representing the as-fabricated and post-healing treatment (250°C, 260 hours) conditions for the *bottom side* of the sub-modules. (b) Graph of TKN/LTCC failure mode percentage as a function of pull strength. The symbol colors designate the source of the respective data groups. The error bars are ±one standard deviation.

The die pull failure mode analysis was also performed on the sub-modules after they had been exposed to the healing treatment followed by the thermal cycling step. The low strengths observed in Fig. 27 (top and bottom) were accompanied by the 100% TKN/LTCC failure mode frequencies, or very nearly so, in all cases.

A summary is made of the failure mode data obtained from the experiments described above. The important points are listed below:

1.  The percentages of TKN/LTCC failures tended to be higher than the historical values for the top side data. There was no statistical difference in the percentages of the TKN/LTCC failure modes between the as-fabricated and healed conditions for the SF682, SF1102, and SF1283, sub-modules. The two sub-modules that experienced

an increase of top side, mean strengths after the healing treatment, also experienced a decrease in the TKN/LTCC failure mode, although the small decrease was statistically significant for only one of the two sub-modules, SF1349.  It was not possible to draw a correlation, quantitatively, between pull strength and TKN/LTCC failure mode for either the as-fabricated or post-healed data.

2. Very similar trends were observed for the bottom side data.

3. After thermal cycling, the TKN/LTCC failure mode occurred nearly 100% of the time for all sub-modules; thus, it was not possible to identify any specific trends from these results

The above results *suggested* that the healing treatment could potentially improve upon the low pull strengths, again, under the suspicion that they were caused by exposure to the $N_2$-10%$H_2$ atmosphere.  It was decided that more tests data were required in order to improve the statistical basis needed to confirm this premise.  Therefore, a second set of experiments were performed, the overall goal of which was to "improve upon the statistics" of the analysis so as to better ascertain the effects of the healing treatment.

Sub-modules were selected from LTCC lots 4 – 20 with particular emphasis placed on those lots that demonstrated low pull strengths (Fig. 3) and, which were not part of lots 9 – 11 that the supplier could confirm had were *not* exposed to the $N_2$-10%$H_2$ furnace atmosphere. It had to be inferred that any of sub-module assembled from the LTCC lot that exhibited low pull strengths, previously, stood an higher likelihood – not a certainty given the intra-lot variability of die pull strengths – of having poor pull strength in subsequent units used in the present experiment.

In these experiments, the process monitor methodology was used; that is, for each of the *healed* units.  That is, four dice were tested from both the top and bottom sides in the as-fabricated conditions.  Then, the sub-module was exposed to 20 thermal cycles (-55°C/125°C) after which, the remaining dice on both top and bottom sides were pull tested.

This set of experiments was designated "Revision 1" or "Rev 1." Sub-modules were assembled from sub-floors of lots #13, #17, #18, and #20. The specific sub-module designations were as follows: lot #13 (two units), SF1069 and SF1080; lot #17, SF1329; lot #18, SF1394; and lot #20, SF1504. As can be seen in Fig. 3, lot #13 represented marginal-to-poor pull strengths per SF1090 while the lots #17, #18, and #20 showed very poor pull strengths according to the tested sub-modules, SF1320, SF1392, and SF1494, respectively. In fact, the pull strengths of these four sub-modules formed individual lot "baselines" (i.e., no healing treatment) against which to compare the respective Rev 1 sub-module pull strengths (all of which had received the healing treatment prior to flip chip soldering of the dice). These sub-module test data were referred to as Revision 0 or "Rev 0."

Shown in Figs. 30a is a plot of the as-fabricated, top side pull strength as a function of sub-floor LTCC lot number. The red symbols are the Rev 1 experimental results for which, the sub-floors were exposed to the healing treatment prior to dice assembly; the Rev 0 results from sub-modules that were not healed and are represented by the blue symbols. The specific sub-floor numbers are above and below the respective data points. It was clear that the healing treatment improved significantly the pull strengths of the solder joints. Irrespective of the magnitude of the non-healed pull strengths, the healing treatment caused the pull strengths to meet or exceed the acceptance criteria. In three of the four cases, the healing treatment caused an increase in the data scatter, an effect that was previously observed.

The healing treatment similarly improved significantly the bottom side, as-fabricated pull strengths as shown in Fig. 30b. In all but one case, the healing treatment increased the data scatter.

(a)                                    (b)
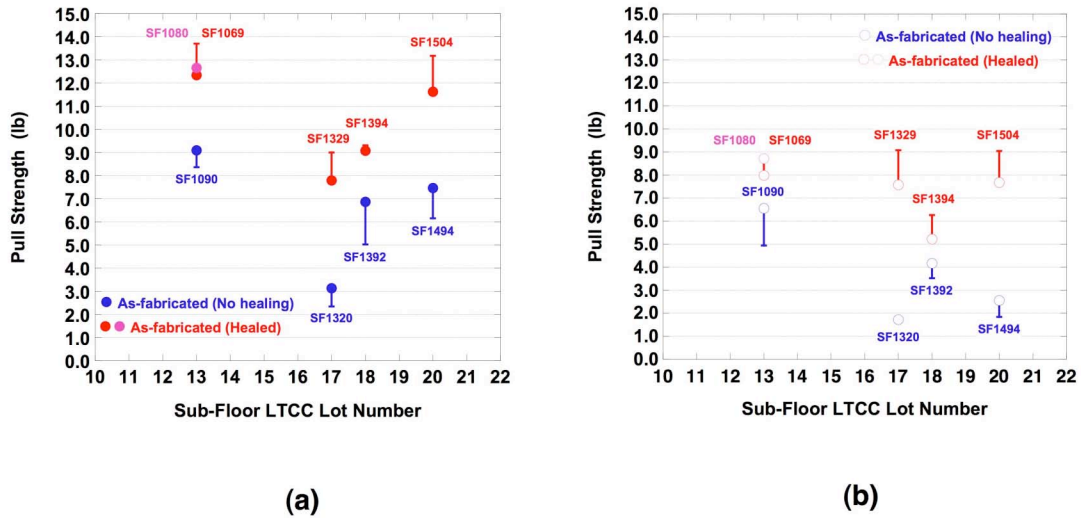
**Fig. 30** Pull strength as a function of sub-floor LTCC lot numbers for (a) top side and (b) bottom side dice. The sub-modules were in the as fabricated condition. The red symbols ("Rev 1") were data from sub-modules that were exposed to the healing treatment (250°C, 260 hours, air). The blue symbols ("Rev 0") were the strength values of sub-modules from the same respective lots, which were not subjected to the healing treatment. All sub-modules were suspected of having been exposed to the $N_2$-10%$H_2$ atmosphere. The one-half error bars were equal to one standard deviation.

The data presented in Fig. 30 were encouraging, more so from the statistical sense that the strength improvements were realized in all four cases and, moreover, on both sides of the sub-modules. Lastly, a comparison of the data between the top side (Fig. 30a) and bottom side (Fig. 30b) indicated that, in the three of four lots for both Rev 0 and Rev 1 experiments, the top side pull strengths exceed the bottom side strengths. The one exception was SF1329 of lot #17 and likely represents a one-time "outlier".

Next, the Rev 1 sub-modules were exposed to the process monitor thermal cycling treatment. The pull strength data appear in Figs. 31a and 31b for the top side and bottom side test results, respectively. Once again, the results were very encouraging as Rev 1 sub-modules (healing treatment) experienced a dramatic increase in the pull

strengths compared to sub-modules in the Rev 0 (no healing treatment). In nearly all Rev 1 cases, the healing treatment caused a small increase in the data scatter. And, in all but one case, the bottom side strengths of the Rev 1 sub-modules remained lower than the top side strengths, but by significantly lesser margins that were observed in the Rev 0 cases. The one exception was the sub-module, SF1329, which exhibited the same trend that was recorded for the as-fabricated condition.
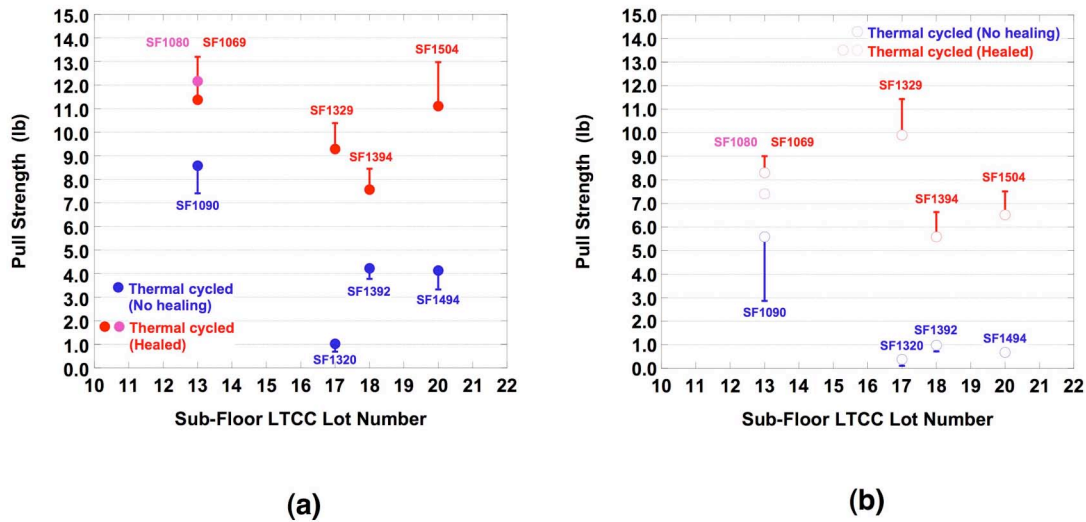


**Fig. 31** Pull strength as a function of sub-floor LTCC lot numbers for (a) top side and (b) bottom side dice. The sub-modules were exposed to 20 thermal cycles (-55°C/125°C) prior to testing. The red symbols ("Rev 1") were data from sub-modules that were exposed to the healing treatment (250°C, 260 hours, air). The blue symbols ("Rev 0") were the strength values of sub-modules that were not subjected to the healing treatment. The one-half error bars were one standard deviation.

The failure modes were examined for pull test sites of the healed (Rev 1) sub-modules. The predominant failure modes were grouped as TKN/LTCC (with or without LTCC divot) and Si/solder (with or without UBM pull out), which were mutually exclusive. Therefore, only the TKN/LTCC mode was plotted for the analysis. The following observations were made from the failure mode data, which were not apparent in the plots discussed below: (a) The LTCC divots did not accompany the TKN/LTCC interface

failures for the as-fabricated condition.  (b) The divots were observed with some TKN/LTCC failures after the thermal cycling exposure, but at a frequency that was considerably lower than by historical accounts.  Therefore, the LTCC divot observations indicated that the healing treatment did not introduce added damage into the bulk LTCC material that was under the thick film pads.

The failure modes were evaluated in a manner that did *not* distinguish between top side and bottom side.  Instead, the TKN/LTCC failure mode percentages were the averages of both sides together.  In order to be consistent, the pull strength data were similarly averaged between the top side and bottom side for both Rev 0 as well as the Rev 1. The failure mode and pull strength data are plotted separately in Figs. 32a and 32b, respectively, which represented the as-fabricated condition.



(a)                                           (b)
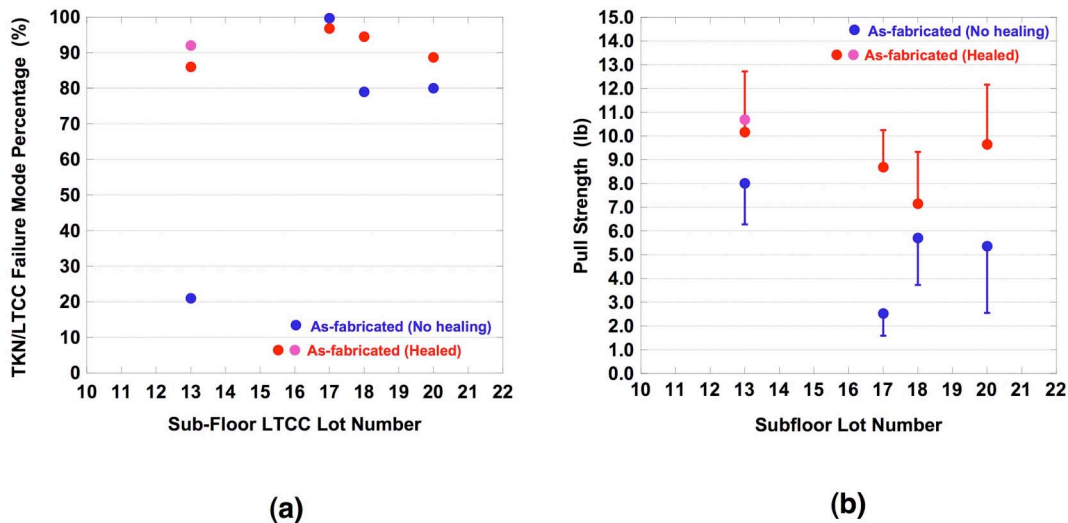
**Fig. 32** (a) TKN/LTCC failure mode percentage and (b) pull strength as a function of sub-floor LTCC lot numbers.  The respective data were averaged between the top side and bottom side dices of the sub-modules.  The sub-modules were in the *as-fabricated condition*.  The red symbols ("Rev 1") were data from sub-modules that were exposed to the healing treatment (250°C, 260 hours, air).  The blue symbols ("Rev 0") were the strength values of sub-modules that were not subjected to the healing treatment. The one-half error bars were one standard deviation.

(Individual sub-module numbers can be obtained from Figs. 30 and 31.)  The improvement in pull strength created by the healing treatment was replicated in Fig. 32b

The improvement to pull strength brought about by the healing treatment did not give rise to an expected decrease of the percentage of TKN/LTCC failure mode percentage. In fact, the percentages of the TKN/LTCC failure mode *increased* in three of four instances.  The one exception, lot #17, had already shown a 100% TKN/LTCC failure mode percentage for the non-healed case; thus, the slightly lower value for the heeled case was a result of experimental variability.  The only scenario in which the strength increase could be accompanied by an increase in the TKN/LTCC failure mode, given the finite percentage of solder/die UBM failures and presuming that the healing treatment improved the TKN/LTCC interface strength, is that there was also a dramatic improvement to the solder/die UBM interface strength.  Now, the solder/ die UBM interface was not present during the healing treatment so the latter could not have *directly* improved the latter.  Therefore, it was concluded that the healing treatment had an *indirect* effect on the solder/die UBM interface.  The likely mechanism was a change to the dissolution behavior of Au-Pt-Pd alloy component of the thick film pad. Those elements appeared at the solder/UBM interface as intermetallic compounds (IMC) formed with the Ni UBM layer.

The failure mode data were similarly analyzed for the units after thermal cycling.  The averaged TKN/LTCC failure mode percentage and averaged pull strength data are shown in Figs. 33a and 33b, respectively.  The averaged pull strengths also reflected the improvement resulting from the healing treatment performed on the Rev 1 sub-floors.  Also added to the graph in Fig. 33b were the as-fabricated, mean pull strengths of the Rev 1 sub-modules (triangles) in order to illustrate that the healing treatment resulted in an uncharacteristically small differences between the two data sets.  (The non-healed Rev 0 data showed the expected trend.)  In fact, the trend was reversed in

three of four cases whereby the mean post-thermal cycled pull strength were higher than those of the as-fabricated condition.



(a)

(b)
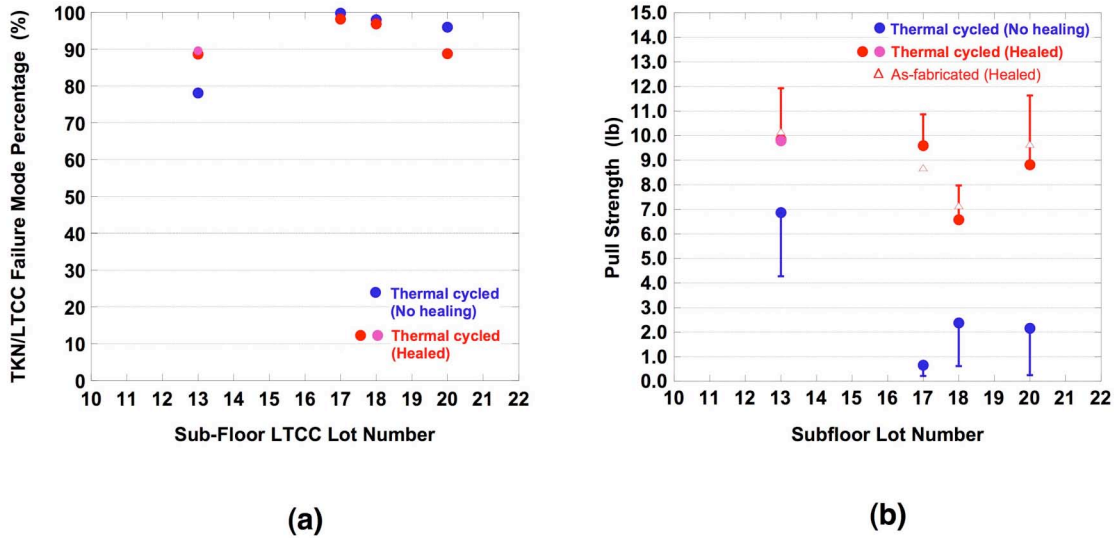
**Fig. 33** (a) TKN/LTCC failure mode percentage and (b) pull strength as a function of sub-floor LTCC lot numbers. The respective data were averaged between the top side and bottom side dices. The sub-modules were in the *thermal cycled condition*. The red symbols ("Rev 1") were data from sub-modules that were exposed to the healing treatment (250°C, 260 hours, air). The open triangles were the as-fabricated pull strength values. The blue symbols ("Rev 0") were the strength values of sub-modules that were not subjected to the healing treatment. The one-half error bars were one standard deviation.

Referring Fig. 33a, it was observed that, in the case of the non-healed Rev 0 case, the TKN/LTCC failure mode percentages were generally higher than for the as-fabricated case (Fig. 32a), which coincided with generally lower pull strengths after thermal cycling. However, in the case of the healed sub-modules for which there was little difference in the as-fabricated versus thermal cycled pull strengths, there was concurrently little change to the TKN/LTCC failure mode percentages.

A direct comparison was made between the non-healed data (Rev 0) and healed data (Rev 1) in Fig. 33. It would have been anticipated that the significantly higher pull strengths of the Rev 1 sub-modules (Fig. 33b) would have been accompanied by a decrease in the TKN/LTCC failure mode percentages.   This scenario did not materialize in Fig. 33a (except to a small degree, lot #13).  Thus, as was similarly concluded from a similar trend from the as-fabricated condition data in Fig. 32, the healing treatment appears to have had an *indirect* strengthening of the solder/die UBM interface that maintained the preferred failure site at the TKN/LTCC interface, in spite of the latter's hypothesized strength improvement resulting from the healing treatment.

In summary, sub-modules were assembled from sub-floors built of LTCC material lots *suspected* of having been exposed to the $N_2$-10%$H_2$ furnace during attachment of the edge pins because previously-tested sub-modules from these lots exhibited low pull strengths.  The current sub-floors were exposed to the healing treatment of 250°C, 260 hours, in air, then assembled with die into sub-modules, and lastly pull tested using the "process monitor" methodology. The healed sub-modules (Rev 1) exhibited significantly improved pull strengths for both the top side and bottom side dice as well as for both as-fabricated and post-thermal cycled conditions when compared to sub-modules of the same respective lots, which were not exposed to the healing treatment (Rev 0). The strength drop, which was typically observed after thermal cycling, was reduced or eliminated for the healed sub-modules.  The healing treatment appeared to result in slightly higher scatter associated with the strength values. The TKN/LTCC failure mode percentage increased or, remained relatively high, for the as-fabricated as post-thermal cycled dice, respectively.  This trend was contrary to that expected from the improved pull strengths.

The results of the previous experiments were very encouraging, in particular, because the healing treatment had a sufficiently large effect so as to potentially raising the pull strength above acceptance limits.  However, those results are based on an inference that the Rev 1 units would have demonstrated the same strength behaviors as the Rev

0 units of the same lot that were not exposed to the healing treatment. Also, it is to be recalled that the same effect was not reproduced in the previous experimental set that examined the role of the healing treatment on an individual sub-module basis. Therefore, before considering the implementation of the healing treatment for flight product, a second set of experiments was performed to confirm the later benefits and that the procedure did not degrade the sub-modules.

In the next series of tests, sub-modules were assembled, using sub-floors from LTCC lots that exhibited roughly three degrees of degradation: lot #14, poor strength; lot #16, excellent strength; and lot #17, very poor strength. Thus, it was assumed – it could not be confirmed by the supplier – that lots #14 and #17 were exposed to the $N_2$-10%$H_2$ atmosphere. It was surmised that the lot #16 sub-floor was either, not exposed to the $N_2$-10%$H_2$ atmosphere or, if exposed to the latter condition, did not show degradation. Irrespective of the presiding scenario, the sub-module from lot #16 would be used to determine if the healing treatment had a detrimental effect on "good" units.

All of the sub-floors were exposed to the healing treatment of an air anneal at 250°C for 260 hours followed by their assembly into sub-modules. The sub-modules were tested per the "process monitor" methodology, one half of the dice (both sides) pull tested in the as-fabricated condition and the other half pull tested after exposure to 20 thermal cycles (-55°C/125°C). The specific sub-floor units were as follows: lot #14, SF1104, SF1105, SF1158; lot #16, SF1252; and lot #17, SF1298. Only the lot #17 sub-module overlapped with the Rev 1 (Rev 0) test specimens. Multiple units were evaluated for lot #14 due to availability.

Shown in Fig. 34a is pull strength as a function of sub-module number, including the lot number designation. The pull strengths were separated into top side (closed symbols) and bottom side (open symbols) results; as-fabricated strengths were in blue while the post-thermal cycle data were in red. These data were compared to those in Fig. 3 per each of the respective lot numbers. The healing treatment did improve the pull

strengths of the sub-modules from lots #14 and #17; however, the strength gains owed

certainly did not match the magnitude of those observed in the Rev 1 experiments.  For

example, the SF1298 sub-module (lot #17) pull strengths can be compared to those of

sub-module SF1329 from the Rev 1 experiments. As a result of the lack of substantial

improvement, the pull strength data mirrored the same general trends of relative

strengths that were observed in non-healed units (Fig. 3).



**(a)**　　　　　　**(b)**
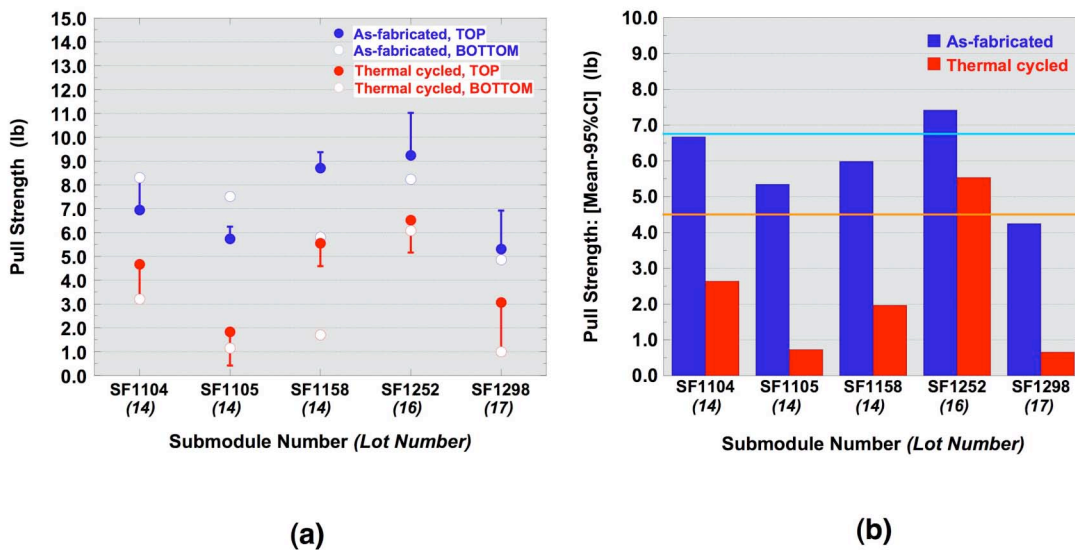
**Fig. 34** (a) Pull strength as a function of sub-module number (lot number in italics).  All of the sub-floors were exposed to the healing treatment (250°C, 260 hours, in air) prior to assembly into the sub-modules. The error bars were one standard deviation.  (b) Pull strength lower acceptance limit (mean – 95% confidence interval) as a function of sub-module number.  The strength data are the average of top side and bottom side.  The turquoise and orange lines note the acceptance limit for the as-fabricated and post-thermal cycled cases.

Several other points were observed in Fig. 34a. The healing treatment did not eliminate

the variability of pull strengths between sub-modules made the same lot, as is illustrated

by the variability of pull strengths between the three lot #14 sub-modules. The healing

treatment decreased only slightly the already-high pull strengths of lot #16; thus, it did

not have a significant, detrimental effect on satisfactory pull strengths.  Also, the healing

treatment did cause the top side and bottom side strengths to be closer together in all cases except SF1158 (lot #14); however, it did not reduce the gap between as-fabricated and post-thermal cycled pull strengths as was observed in the Rev 1 experiments. Therefore, the data presented in Fig. 34a reflected, more so, the results of the experiments that preceded Rev 1, in which were that the healing treatment provided only a slight improvement to the low pull strength of the selected modules.

The minimal effect had by the healing treatment in these experiments was further substantiated by the failure of the post-healed pull strengths in Fig. 34a to meet acceptance criteria; this point is illustrated in Fig. 34b. The pull strengths are averaged between the top side and bottom side. The 95% confidence interval is subtracted from the average; the resulting difference must exceed 6.75 lb for the as-fabricated condition (turquoise line) and 4.5 lb for the post-thermal cycle case. Only SF1262 from lot #16 met both acceptance criteria.

In summary, a third set of experiments were conducted, the objective of which, was to confirm the reproducibility of the healing process with respect to the significant improvement of the pull strengths of sub-modules in the Rev 1 experiments. The data in Fig. 34 indicated that that reproducibility was not realized. Low pull strengths were improved upon, but only slightly, so that the sub-modules would still not have met the acceptance limits. A fallout of the minimal effect of the healing treatment was that there was little improvement on sub-module-to-sub-module variability or on the differences of pull strengths between top side and bottom side as well as those of as-fabricated versus thermal cycled units.

An analysis is made that compiles the results obtained from the three healing experiments. A brief synopsis is provide below of each of those experiments:

**Experiment #1**:

*Approach:* Individual sub-floors, which were suspected of having been exposed to the $N_2$-10%$H_2$ atmosphere, were tested in the as-fabricated, healed, and healed-plus-thermal cycled conditions to remove sub-module-to-sub-module variations.

*Results:* The healing treatment improved the pull strength for units starting with an as-fabricated strength of > 4 lb; had no effect if the as-fabricated strength was 7 – 9 lb; and decreased, slightly, the pull strength of units starting with a strength > 8 lb.  The strength improvement in the first case was minimal and did not always allow the sub-module to reach acceptance limits.

**Experiment #2 ("Rev 1"):**

*Approach:* Sub-modules were selected from LTCC lots within the group, #4 – 20, that previously exhibited low pull strengths, which were assumed to have been caused by exposure to the $N_2$-10%$H_2$ atmosphere. The units were exposed to the healing treatment. The process monitor, pull test methodology was used (after the healing treatment); that is, pull tests were performed in the as-fabricated and post-thermal cycled conditions.  These results were compared to corresponding pull strength data from non-healed, sub-modules from the same lot (Rev 0).

*Results:* Both the as-fabricated and post-thermal cycled pull strengths of the healed sub-modules (Rev 1) were significantly improved vis-à-vis the pull strengths of the Rev 0. The healing treatment also caused a reduced difference between top side and bottom side strengths as well as reduced the gap between as-fabricated versus post-thermal cycled pull strengths.

**Experiment #3:**

*Approach:* Reproduce experiment #2 (Rev 1) results. Sub-modules were selected from LTCC lots #4 – 20 with particular emphasis on lots with low pull strengths. The units were exposed to the healing treatment. The process monitor, pull test methodology was used (after the healing treatment) to assess the effect of the healing treatment.

*Results:* The sub-modules did not reproduce the pull strength gains observed in the Rev 1 experiments; the results were comparable to those of experiment #1.  That is, the healing treatment caused a slight pull strength improvement, but not to the magnitude that allowed the sub-modules to meet acceptance limits.  On the other hand, the healing treatment caused only a very slight pull strength loss of sub-modules already having a high pull strength; thus, it did not degrade the "good" sub-modules.

Because the above experiments could not establish that the annealing (healing) treatment (250°C, 260 hours, air) could reproducibly improve low pull strengths to the degree that it allowed sub-modules (of suspect lots) to meet the acceptance criterion, this process was not recommended for implementation into the sub-module process flow.

The following general observations were also made from the healing experiments:

(a) Their was concern that the 250°C, 260 hour, air annealing treatment would oxidize the Pd component of the Au-Pt-Pd thick film layer, thereby potentially degrading solderability.  However, there was no such evidence of poor solderability, which would have been indicated by an increase in the frequency of mechanical opens recorded during the failure mode analysis.  Thus, the burnishing process remained effective in this regard[5].

(b) The healing treatment increased the scatter in the pull strength measurements.

(c) The TKN/LTCC separation failure mode remained higher than historical trends and did not decrease with improved pull strengths after healing.  The occurrence of LTCC divots accompanying the TKN/LTCC failure mode was also diminished as compared to historical data.

---

[5] However, the surfaces of pores within the thick film layer would have also been susceptible to addition Pd-O formation as the burnishing would not have been able to reach those surfaces.  A loss of wettability on the pore surfaces would not have been apparent on the surface, but would have potentially limited penetration by the molten solder towards the TKN/LTCC interface.

1.5.5 Summary: Hydrogen-Nitrogen Firing Environment and Annealing ("Healing")
Experiments

1.  The suspect role of the $N_2 - 10\%H_2$ braze pin furnace atmosphere was examined as
    a potential source the low pull strength phenomenon.  Existing sub-module pull
    strength data could not provide a clear correlation between the potential of exposure
    and pull strength performance.  An active approach was taken in which sub-floors
    were exposed to either $N_2 - 10\%H_2$ atmosphere or the standard $N_2$ conditions.  The
    $N_2 - 10\%H_2$ exposure did reduce slightly the top side pull strength for both the as-
    fabricated or post-thermal cycled conditions.  However, the correlation was not
    reproduced on the bottom side.

2.  Sub-floors were exposed to a post-process annealing or "healing" treatment (250°C,
    260 hours, air) in order to mitigate the effects of the $N_2 - 10\%H_2$ exposure.  The
    healing treatment did not degrade sub-modules that had high pull strengths to start.
    The healing treatment did improve upon low pull strengths, but to such widely
    varying degrees that the procedure was not recommended for implementation into
    the sub-floor process flow.

3.  The low pull strength phenomenon continued to appear in later process monitors
    despite the increased scrutiny given by the supplier to post-processes. This point,
    together with a persistent sub-module-to-sub-module variability within lots and the
    high frequency of TKN/LTCC failure modes (without a low occurrence of LTCC
    divots) demonstrated that the $N_2$-10%$H_2$ exposure was *not* the root cause of the low
    pull strength phenomenon.  Rather, the root-cause of the low pull strength appears
    to be intrinsic to the overall materials set that includes the LTCC, the thick film, the
    TKN/LTCC interface, and the Sn-Pb solder.

4.  The 250°C, 260 hours, air treatment, in-and-of-itself, has the potential to improve
    upon low pull strengths, but not as a healing treatment for the $N_2$-10%$H_2$ exposure.

# 2.0 Materials and Process Control Improvements Addressing the Low Strength Phenomenon

*2.1 Review*

Recall that the overall objective of this study was to determine the root-cause of the low pull strength phenomenon. It has been shown that a correlation cannot be drawn between pad height and pull strength.  Similarly, the low pull strength phenomenon did not appear to be sensitive to the post-processing sequence, the dice assembly sequence, or the pull test sequence.  The exposure of the sub-floors to the $N_2$-10%$H_2$ atmosphere prior to post-processing may have caused a small loss of pull strength; but, it did so only on the top side.  The air annealing ("healing") treatment increased pull strength; but, it did not so reproducibly, which suggests that a mechanism other than the $N_2$-10%$H_2$ atmosphere effect, was being mitigated.  Moreover, it was concluded that the root-cause of the low pull strength rested, instead, with a behavior that was intrinsic to the overall materials set, which includes the LTCC, the thick film, the TKN/LTCC interface, and the Sn-Pb solder.

*2.2 New sub-floor lot fabrication*

The supplier exercised improved measures to control the materials and manufacturing processes used to make the sub-floors.  Subsequently, a new group of sub-floors were fabricated, which were identified as lot #29.  Two sub-floors, designated S-Lot29-1 and S-Lot29-2, were post-processed with print-dry-fire steps that placed the flip chip Au-Pt-Pd thick film bond pads and dielectric layers onto the LTCC surface.  However, after the bottom side, post-process step was completed (which is the designated order), it was observed that the dielectric layer did not completely cover one end of the thick film pad. This observation is illustrated schematically in Fig. 35.  It was determined that the viscosity of the thick film paste used to make S-Lot29-1 and -2 was too high, which did not allow it to flow effectively through the screen.  The result was an incomplete printing of the full, thick film pad area.
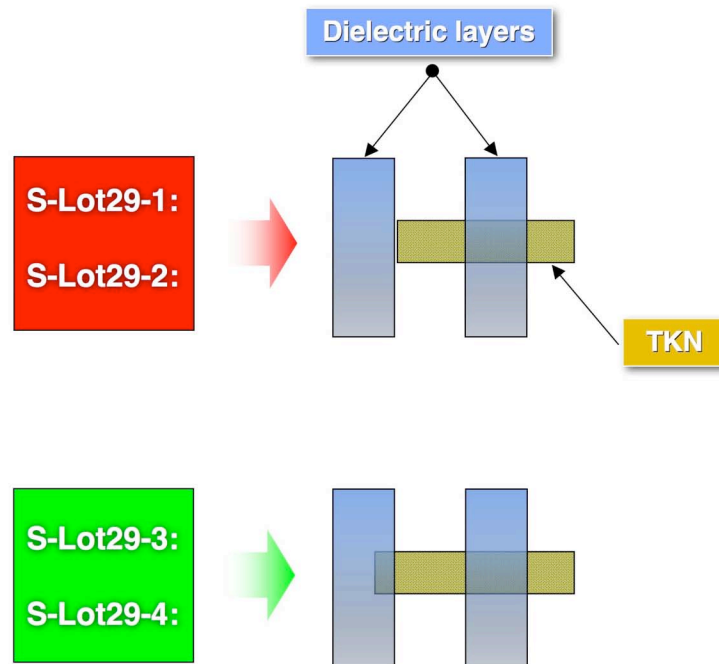
**Fig. 35** Illustration of the location of the Au-Pt-Pd thick film flip chip pad relative to the dielectric layers in the initial sub-floor manufacturing step with lot #29 material. The illustration shows the configuration of the two sub-floors, S-Lot29-1 and -2, which were made with the higher viscosity, thick film paste while the sub-floors, S-Lot29-3 and -4, were made with for the TKN paste having the correct viscosity.

There were two potential degradation scenarios contributing to a low pull strength. First of all, failure of the thick film pad to extend completely over its required length exposed that edge to the molten solder. As a result, there became an additional pathway for Sn to reach the TKN/LTCC interface, resulting is potential degradation to the TKN/LTCC interface bond strength. Of course, per Fig. 35, even with correct registration between the dielectric layer and TKN pad, there remained two edges of the pad that remained exposed to the Sn-Pb solder. Thus, the effect may have been only minimal. The second scenario was simply a loss of a purely mechanical anchor. The dielectric layer serves as "Scotch™ tape" to hold the thick film pad under it, to the LTCC surface.

Upon discovery of the use of the high viscosity, thick film paste, the processing of the S-Lot29-1 and -2 units was halted with only the bottom side having received the post-process features.  New paste was placed into the process.  The two sub-floors S-Lot29-3 and S-Lot29-4 were fully, post-processed with the correct registration that is illustrated at the bottom of Fig. 35.  The four S-Lot29-X sub-floors were assembled into sub-modules (or partial sub-modules in the case of -1 and -2) and then had the dice pull tested according to the standard process monitor methodology.  The strength data are shown in Fig. 36.
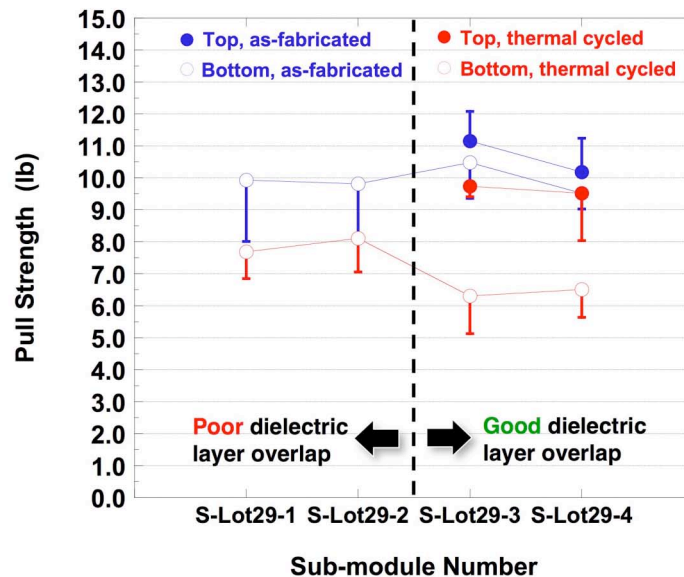


**Fig. 36** Pull strength as a function of sub-floor number of the four sub-module units assembled with lot #29 LTCC material designated S-Lot29-X (X = 1, 2, 3, and 4).  The half-error bars are one standard deviation.

Several observations were drawn from Fig. 36.  First of all, attention is turned to the S-Lot29-3 and -4 units.  The as-fabricated pull strengths were very high for both the top side and bottom side dice; the top side strength was only slightly higher.  After exposure to the thermal cycling environment, there was a modest drop of top side strength.  However, a more significant strength drop was measured for the bottom side dice.

Nevertheless, all strength values of the S-Lot29-3 and -4 units would have passed acceptance criteria.

Next, the pull strengths of the S-Lot29-1 and -2 sub-modules were considered in the analysis.  Again, only bottom side strength data were available. In the case of the as-fabricated condition, the bottom side pull strengths were comparable with those of the S-Lot29-3 and -4 units.  This comparison suggested that the mis-registration between the thick film pad and the dielectric layer did not significantly affect the mechanical properties.

However, the analysis became more interesting for the thermal cycled case.  After thermal cycling, the S-Lot29-1 and -2 pull (bottom side) strengths decreased when compared to the as-fabricated condition – this trend and magnitudes were not unexpected.  Yet, the mean pull strength values *were higher than* those of the units S-Lot29-3 and -4.  Statistically, they were the same to within the experimental error.  Some of the scatter is likely due to the persistent variability between sub-floor units that has been noted, previously.  (It was interesting that mean strengths of S-Lot29-1 and -2 grouped together as did S-Lot29-3 and -4 pull strengths.)  So, again, the misregistration between the dielectric pad and thick film conductor pad did not affect the pull strength after thermal cycling.

A minor point was made from the observations made in Fig. 36. There was the absence of a second post-processing step for the S-Lot29-1 and -2 units that would have been used for the top side structures. Thus, the slightly higher pull strengths of the S-Lot29-1 and -2 sub-modules after thermal cycling would be attributed to the omission of the post-processing steps for the top side of the sub-floors.  A similar trend was also observed in Fig. 16 and, like the present case, it was relatively weak and not statistically significant.

In order to confirm the pull strength improvements indicated by S-Lot29-3 and -4 units, two sub-modules were subsequently assembled from sub-floors made with the LTCC lot #29 material. The sub-modules, which were identified as SF1594 and SF1599, were evaluated using the process monitor methodology. Shown in Fig. 37 are the pull strength data for SF1594 and SF1599, together with the S-Lot29-3 and -4 results. The half-error bars are one standard deviation. Overall, SF1594 and SF1599 exhibited excellent pull strengths. The as-fabricated values were slightly lower than those of S-Lot29-3 and -4. The bottom side strengths were no longer consistently less than the top side values; in fact, the sub-module SF1599 exhibited *mean* bottom side strengths that exceeded the top side strengths with statistical significance. The thermal cycling caused the expected decrease of pull strength for both sides. However, the values remained relatively high. The data scatter was commensurate with that observed in prior studies.
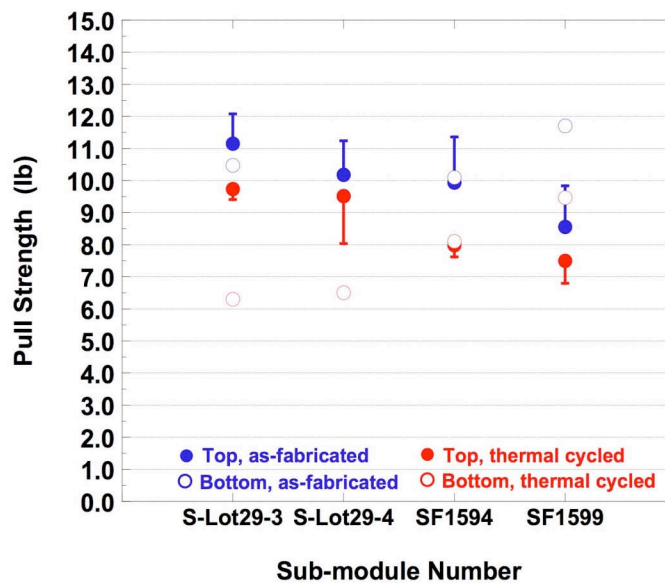


**Fig. 37** Pull strength as a function of sub-module number of the four sub-module units assembled with lot #29 LTCC material: SF-Lot29-3, S-Lot29-4, SF1594, and SF1599. The data were separated into top side and bottom side strengths for the as-fabricated or thermal cycled conditions. The half-error bars are one standard deviation.

The [Mean-95%CI] values were plotted as a function of sub-module number in Fig. 38 in order to compare the strength performances of with the process monitor acceptance limits of 6.75 lb and 4.5 lb for the as-fabricated and post-thermal cycled conditions, respectively. (Recall that the acceptance criteria combined top side and bottom side strengths per the two conditions.) Both strength criteria were exceeded by the pull strengths of the four sub-modules. Clearly, these data indicated a significant improvement had been made to the quality of the process monitors.
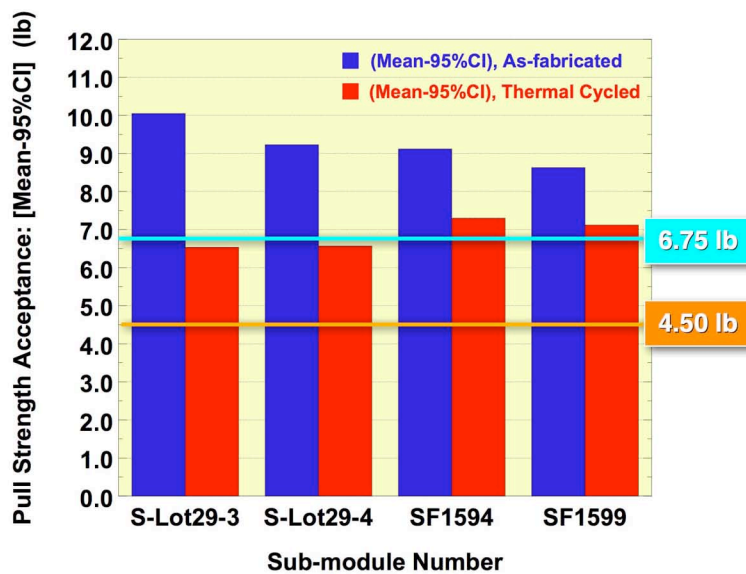


**Fig. 38** Pull strength acceptance metrics, [Mean-95%CI] as a function of sub-floor number SF-Lot29-3, S-Lot29-4, SF1594, and SF1599 assembled from lot #29 LTCC material. The metric acceptance criteria are a minimum of 6.75 lb, as-fabricated (turquoise line) and 4.5 lb, post-thermal cycled (orange line).

The failure modes were also surveyed for the lot #29 units. Shown in Fig. 39 are bar graphs showing each of the three following failure modes (color coded) as a function of the four sub-modules:

- **Si/solder: combination of both with and without UBM pull out**;
- **TKN/LTCC interface; and**

- **TKN/LTCC interface with LTCC divots.**

The data were separated into the top side (a) and the bottom side (b). The TKN/LTCC failure mode predominated at values that were still higher than those observed historically, prior to the appearance of the pull strength losses. An increase of the Si/solder failure mode accompanied the higher pull strengths of the bottom side dice of SF1599 versus the top side pull strengths. There was no occurrence of LTCC divots (green) as had been the case with previous, as-fabricated test results.



(a)                                        (b)
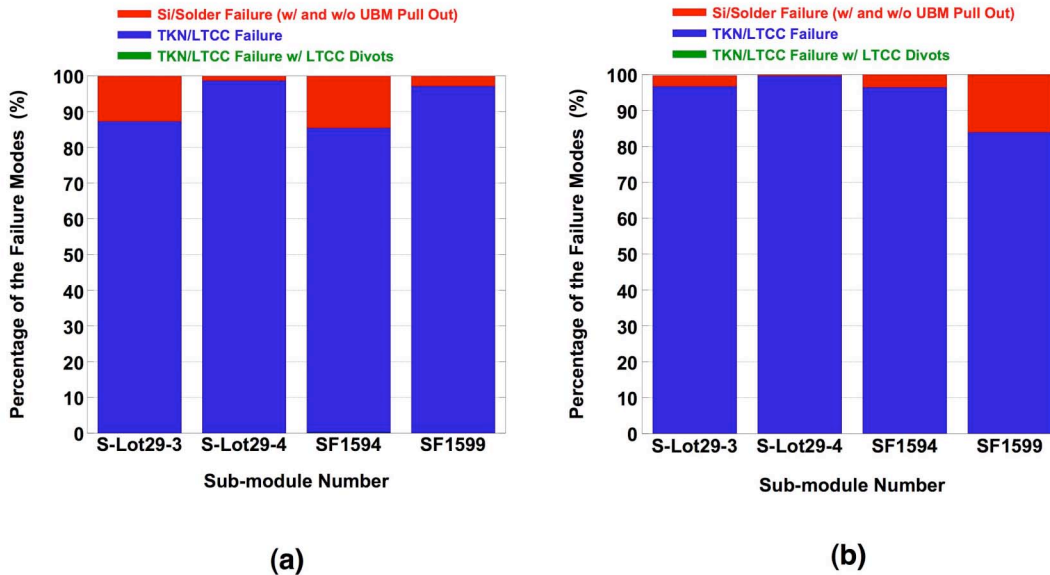
**Fig. 39** Failure mode analysis of sub-modules SF-Lot29-3, S-Lot29-4, SF1594, and SF1594 assembled from lot #29 LTCC material. The pull tests were made on units in the as-fabricated condition. The plots represent (a) the top side and (b) the bottom side.

The same failure mode analysis was performed on dice that were pull tested after exposure of the process monitor, thermal cycling environment. The failure mode data appear in Fig. 40. In this graph, the strength data were tracked in yellow over the bar graphs. Again, there was a predominance of the TKN/LTCC failure mode. However, the Si/solder failure mode was observed for SF1594 and SF1599, bottom side (Fig. 40b) dice that exhibited higher strengths. The failure mode data in Figs. 39 and 40 and, in

particular, the increased frequency of the Si/solder failure mode, coincided with the improved pull strength values.  Only a few instances were recorded in which an LTCC divot accompanied the TKN/LTCC failures after thermal cycling, so few, that it is difficult to discern the green bar in Fig. 40. Lastly, the number of mechanical opens remained commensurate with historical data, indicating that the solderability of the thick film pads was unchanged vis-à-vis prior sub-modules.



(a)                                     (b)
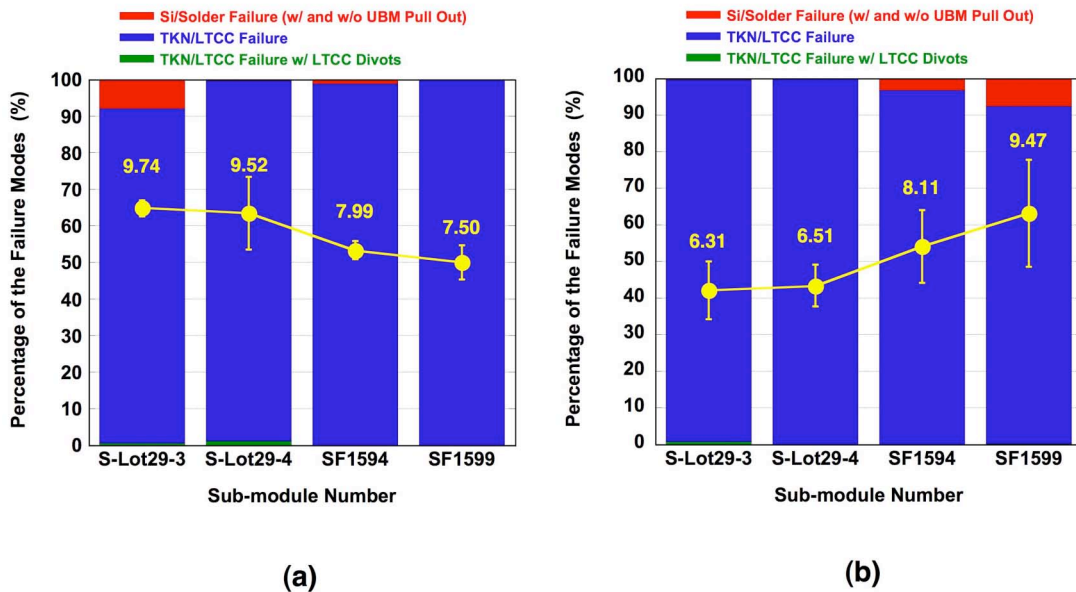
**Fig. 40** Failure mode analysis of sub-modules SF-Lot29-3, S-Lot29-4, SF1594, and SF1599 assembled from lot #29 LTCC material.  The pull tests were made on units after exposure to the thermal cycling environment.  The plots represent (a) the top side and (b) the bottom side.  In addition, the pull strength data were overlaid on the bar graphs; the error bars are ±one standard deviation.

As a result of the data described above, the assembly of flight process monitors was resumed using sub-floors from the lot #29 LTCC material.  Two process monitors, rather than one, were built for the Flight 11 sensor in order to be assured of assembly quality.  Those process monitor units were designated SF1591 and SF1608.  Shown in Fig. 41 are the pull strengths of SF1591 and SF1608, together with those of the four predecessor sub-modules of lot #29 sub-floor material.  The data were separated into

top side (closed symbols) and bottom side (open symbols) results.  The as-fabricated (blue symbols) and thermally cycled (red symbols) data were combined on the plot.
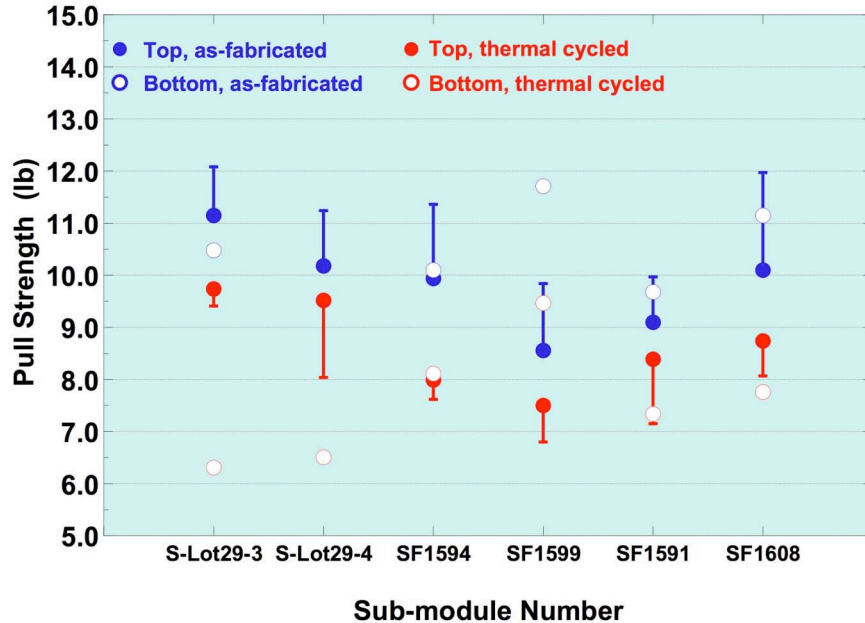


**Fig. 41** Pull strengths of SF-Lot29-3, S-Lot29-4, SF1594, SF1599, and Flight 11 process monitors SF1591 and SF1608 assembled from lot #29 LTCC material.  Top side and bottom side data were indicated by closed and open symbols, respectively.  The as-fabricated condition symbols are in blue; the thermal cycled data are in red.  The half-error bars are one standard deviation.

Overall, the pull strength levels remained very good.   The process monitors SF1591 and SF1608 performed very similarly to SF1594 and SF1599, indicating a greater level of consistency to the lot #29 sub-modules.  In the as-fabricated condition, the bottom side strengths were *greater* than the top side strengths for SF1591 and SF1608 units.  Recall that the same trend was observed for SF1599 and, to a lesser magnitude, SF1594.  Thermal cycling caused the expected drop in pull strength for SF1591 and SF1608, more so for the bottom side than for the top side dice, so that the top side strength was higher.  Yet, all of the strength values remained satisfactory.  The degree of data scatter remained consistent for all cases.

It was confirmed that the SF1591 and SF1608 pull strengths met the acceptance limits. The parameter, [Mean-95%CI], was plotted in Fig. 42 for each of the sub-modules. The Flight 11 process monitors met the as-fabricated and post-thermal cycle acceptance criteria.
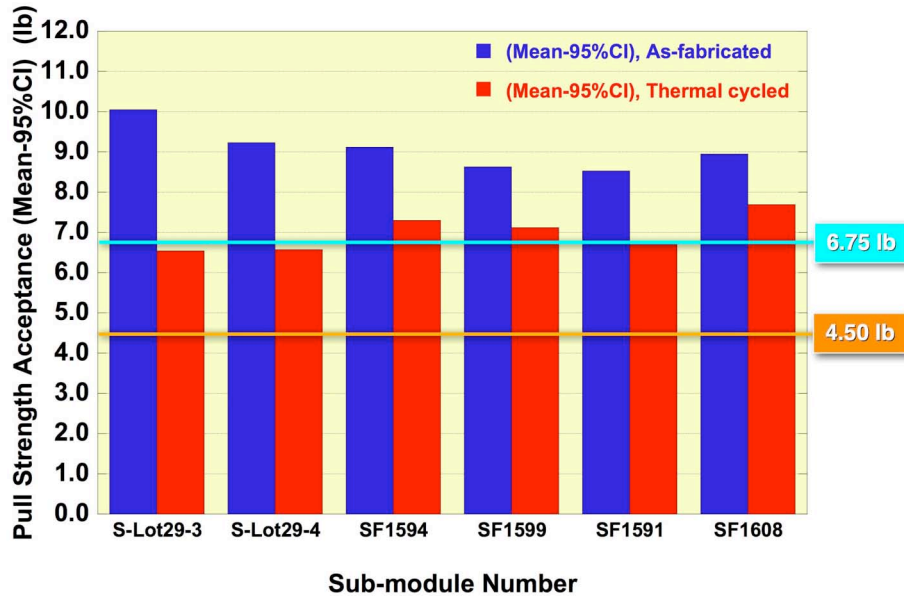


**Fig. 42** Acceptance parameter, [Mean-95%CI] as a function of the sub-modules: SF-Lot29-3, S-Lot29-4, SF1594, SF1594, and Flight 11 process monitors SF1591 and SF1608 assembled from lot #29 LTCC material. The flags, 6.75 lb and 4.5lb, are the acceptance limits for the as-fabricated and post-thermal cycled pull strengths, respectively.

The failure mode analysis was also performed on the sub-modules. Shown in Fig. 43 are bar graphs depicting the TKN/LTCC and TKN/LTCC+divot failure modes for the sub-modules SF1594, SF599, SF1591, and SF1608. The as-fabricated data appear in Fig. 43a and the post-thermal cycle results are shown in Fig. 43b. Referring to the as-fabricated data in Fig. 43a, the TKN/LTCC+divot failure mode had a single occurrence for SF1594; otherwise, this failure mode was absent from the other units as indicated by the gaps in the bar chart (because the dark colors representing this failure mode, had

values equal to zero).  The process monitors SF1591 and SF1608 exhibited TKN/LTCC failure mode percentages that occurred to a lesser degree on the bottom side as compared to the top side, which also corresponded to the higher pull strength values in the former case.
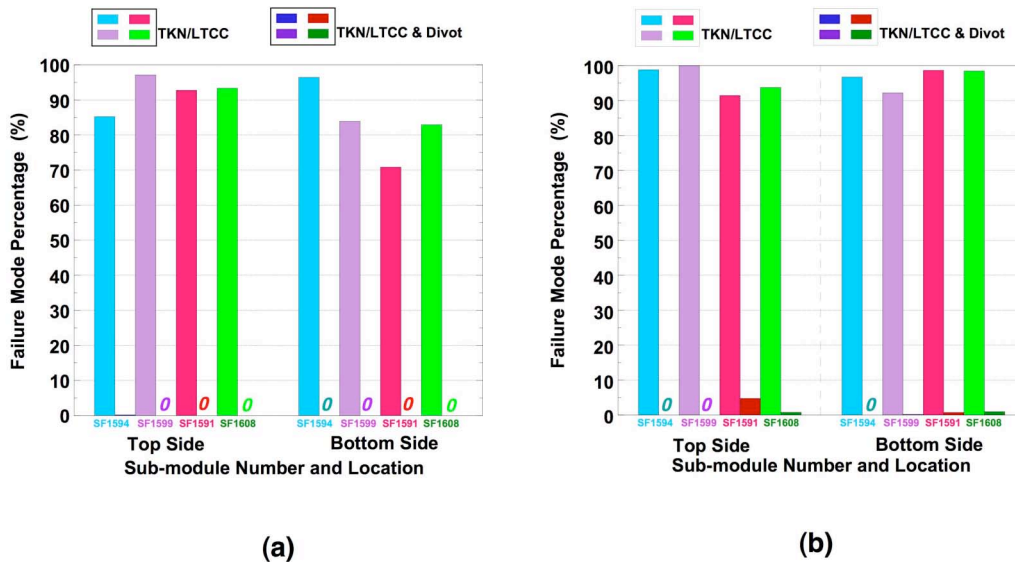


**Fig. 43** Failure mode analysis of sub-modules SF1594, SF1594, and Flight 11 process monitors SF1591 and SF1608 assembled from lot #29 LTCC material: (a) as-fabricated and (b) post-thermal cycle.  Per the legends, the lighter shades of colors are the TKN/LTCC failure mode and darker shades are the TKN/LTCC+divots mode.  Top side (left) and bottom side (right) data were separated within each plot.

After thermal cycling, the TKN/LTCC failure mode increased slightly for SF1594 and SF1599, but did not change significantly for SF1591 or SF1608 on the top side.  On the bottom side, the LTCC divots were observed at levels that were commensurate with prior data.  Therefore, when the latter mode was added to the purely TKN/LTCC failures, the combination resulted in the expected increase of TKN/LTCC separate after thermal cycling.  An increase in the occurrence of the TKN/LTCC separations (with or without divots) was more pronounced for the bottom side.  These observations, when combined with the pull strength data, continued to indicate a reversed relationship

between pull strength and the percentage of failure modes having TKN/LTCC interface separation.

At this point, the sub-floor manufacturing process appeared to be in control.  Assembly continued with the sub-module SF1660, which was constructed from LTCC lot #30, and was the process monitor for the Flight 12 sensor. Unfortunately, the pull strength data were *disappointing*.  Shown in Fig. 44a are the SF1660 pull strength data for the top and bottom sides, including the as-fabricated and thermally cycled conditions, together with the data corresponding to the two Flight 11 process monitors, SF1591 and SF1608. The process monitor SF1660 exhibited a significant loss of strength for all conditions – that is, top side, bottom side, as-fabricated and post-thermal cycled.  Interestingly, the



(a)                                                                  (b)

**Fig. 44** (a) Pull strength as a function of sub-module designation for the Flight 12 process monitor, SF1660 (sub-floor lot #30).  The pull strength data from the Flight 11 process monitors, SF1591 and SF1608 were also included. The as-fabricated and thermal cycle conditions were represented by the blue and red symbols, respectively; top side data were designated by the solid symbols while open symbols indicated the bottom side data.  The error bars are one standard deviation.  (b) Pull strength acceptance data as a function of the process monitor sub-module.  The minimum strength criteria (which are averages of the top side and bottom side results) are 6.75 lb and 4.5 lb for the as-fabricated and post-thermal cycled conditions, respectively.

108

bottom side strength remained higher than the corresponding top side value.  As shown in Fig. 44b, neither the as-fabricated nor thermal cycled pull strengths (average of top side and bottom side data) met the respective acceptance criteria.

The failure mode analysis was also performed on SF1660. The TKN/LTCC and TKN/LTCC+divot failure modes were illustrated by the bar graphs in Fig. 45: (a) for the as-fabricated condition and (b) for the post-thermal cycled condition.  The top side and bottom side data were distinguished from one-another. Again, the Flight 11 process monitor results (LTCC lot #29) were also included for comparison purposes.  The reduced strengths of the SF1660 were accompanied by consistently elevated percentages of the TKN/LTCC failure mode.  Although the TKN/LTCC+divot failure



(a)                                                         (b)
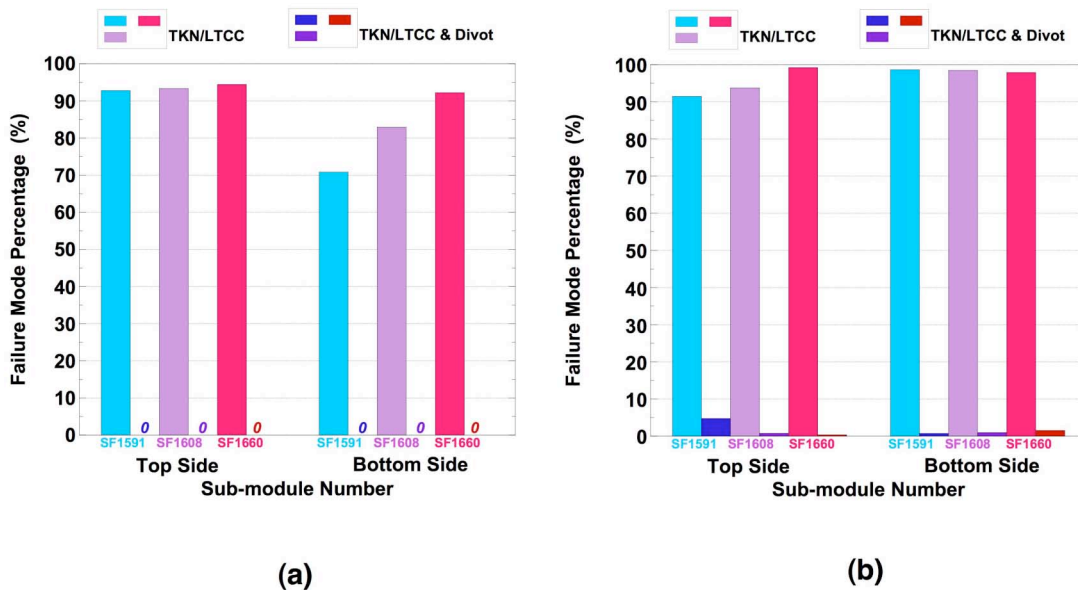
**Fig. 45** Failure mode analysis of sub-modules SF1591 and SF1608 (both Flight 11) as well as SF1660 (Flight 12) assembled from lot #30 LTCC material: (a) as-fabricated and (b) post-thermal cycle conditions.  Per the legends, the lighter shade of colors are the TKN/LTCC failure mode and darker shades are the TKN/LTCC+divots mode.  Top side and bottom side data were distinguished in each plot.

mode was absent from as-fabricated pull strength measurements, it was observed after thermal cycling, but to a limited degree.  In summary, the process monitor SF1660 indicated the recurrence of the "low pull strength" phenomenon.

The Flight 12 build was allowed to proceed, in spite of the as-fabricated pull strengths not reaching the acceptance criteria.  Recall that it is the as-fabricated strength metric that provides the "go/no-go" decision on whether to assemble the sub-modules.  (The thermal cycle data provide input as to whether the sub-module assemblies will continue with testing and being joined to a detector assembly in the cage.)  The technical basis for allowing the flight sub-modules to proceed were: (1) the strength values were sufficiently close to the acceptance limits and (2) it was becoming evident, based upon the data accumulated to date, that the low pull strength phenomenon may occur randomly as an intrinsic property of this material set.

Nevertheless, an increased degree of scrutiny was given to sub-module performance by having two process monitors assembled for the Flight 13 build.  The two sub-modules were designated SF1659 and SF1662.  These units originated from sub-floors built of lot #30 LTCC material.  Shown in Fig. 46a are the pull strength data.  Again, the top side and bottom side pull strengths were separated.  The LTCC lot numbers were included on the x-axis.  Low pull strengths were observed for these latest sub-modules.  As observed with the previous three sub-modules, the as-fabricated, bottom side pull strengths of SF1659 and SF1662 were greater than those of the top side, particularly for SF1662 where the difference was very significant.  This trend was diminished after thermal cycling because of the substantial strength loss that occurred for both the top sides and bottom sides.

(a)



(b)

**Fig. 46** (a) Pull strength as a function of sub-module designation for the Flight 13 process monitors, SF1659 and SF1662 (both lot #30). The pull strength data from the process monitors of Flight 11 (SF1591 and SF1608, lot #29)) and Flight 12 (SF1660, lot #30) were also included. The as-fabricated condition was represented by the blue symbol

color; top side data used the solid symbols while open symbols designated the bottom side data. The error bars are one standard deviation. (b) Pull strength acceptance data as a function of the process monitor sub-module. The minimum strength criteria (which are averages of the top side and bottom side results) are 6.75 lb and 4.5 lb for the as-fabricated and post-thermal cycled conditions.

The pull strength performances were converted to the acceptance criteria parameter, [Mean-95%CI], and plotted in Fig. 46b. In the cases of SF1659 and SF1662, the as-fabricated pull strengths were slightly above and slightly below, respectively, the minimum value. Under these circumstances, the assembly of the Flight 13 sub-modules was allowed to proceed. Following thermal cycling, the pull strengths of the two Flight 13 process monitors were, in both cases, below the 4.50 lb criterion. It was clear in Fig. 46 that all three lot #30 sub-modules exhibit similar strength performances.

The failure modes of SF1659 and SF1662 were also evaluated, although the results were not shown graphically. The TKN/LTCC failure mode exceeded 90% for all test cases. In the as-fabricated condition, the TKN/LTCC failure mode was slightly less than 94% on the bottom side of both sub-modules while the top side percentages were 97 – 98%; the difference coincided with the different strength behaviors. Divots were not observed in the TKN/LTCC failures of the as-fabricated case. The TKN/LTCC failure mode accounted for 99 – 100% of the solder joints after thermal cycling for both sub-modules. Divots accompanied the TKN/LTCC failures to levels that were commensurate with historic data.

In summary, the good pull strength behavior that was observed for process monitors made from lot #29 LTCC material was not reproduced by the process monitors from lot #30 material that were used for Flights 12 and 13 process monitors. The latter units were characterized consistently by low pull strengths that did not meet the acceptance criteria in two of three units. A consistent property of the process monitors made from the lot #30 as well as lot #29 sub-floors was that, in the as-fabricated condition, the

bottom side die pull strengths were consistently higher than the top side strengths, albeit, not always so by statistical significant level. After thermal cycling, this trend repeated in only two of the five cases due to the dramatic loss of pull strengths.

Prior to the beginning of the Flight 14 assembly sequence, a sub-module SF1680 (lot #30) that was being electrically evaluated for the previous flight build, was observed to fail electrical functionality tests. Therefore, the unit provided an additional opportunity to investigate lot #30 pull strength performance. It was decided to pull test *all* of the top side and bottom side dice.

The "official" pull strength for the top side was calculated, but using only the U01, U03, U06 and U08 pull strength values so as to be consistent with process monitor practice; that value was 8.1±0.9 lb. The bottom side strength, which was calculated using U09, U11, U14, and U16 pull strengths, only, was 10.0±1.3 lb. (The pull test values from the remaining top side and bottom side dice were commensurate with the respective measurements.)  The two strength values were considerably higher than those of the other lot #30 process monitors, indicating the absence of the low pull strength phenomenon.  The trend was maintained, which was higher pull strengths for the bottom side dice versus the top side dice.  The TKN/LTCC failure mode percentages were: top side, 91.7% and bottom side, 80.0%, again showing an inverse relationship with respect to pull strength.  (There were no divots for the as-fabricated pull strength fracture surfaces.)  In conclusion, the seemingly consistent trend of low pull strengths for sub-modules assembled from lot #30 sub-floors, was contradicted by the performance of the SF1680 sub-module, which further substantiated the unpredictability of the low pull strength phenomenon.

The assembly of process monitors continued for Flights 14, 15, 16 and 17 sensors.  The LTCC material came from lot #31 for the Flights 14 and 15 and lot #32 for the Flights 16 and 17 sub-modules.  The pull strength results were evaluated together for the following analyses.

The process monitor sub-modules for Flight 14 were SF1731 and SF1751(LTCC sub-floor lot #31).  The pull strength performances of these units are shown in Fig. 47a.



(a)
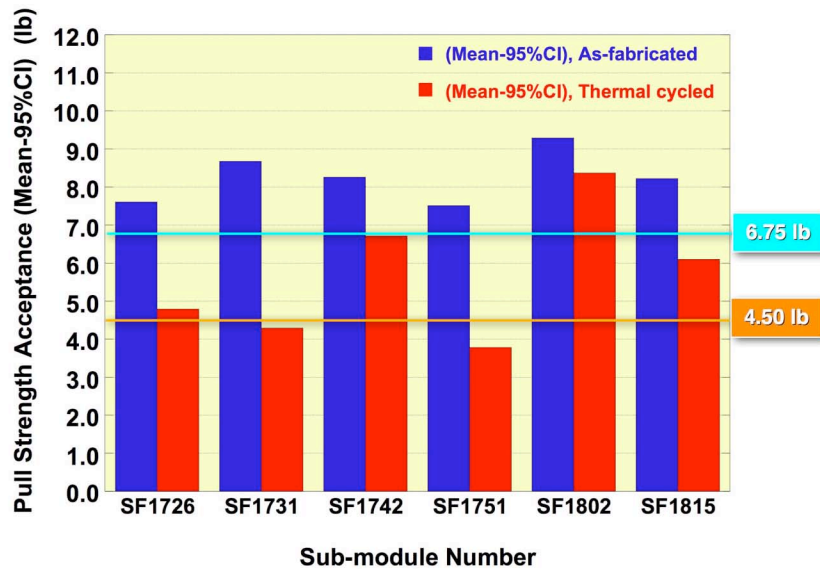


(b)

**Fig. 47** (a) Pull strength as a function of process monitor sub-module designations as follows: Flight 14, SF1731 and

SF1751; Flight 15, SF1726 and SF1742; Flight 16, SF1802; and Flight 17, SF1815. The data were distinguished according to top side and bottom side as well as as-fabricated and post-thermal cycled. The error bars are one standard deviation. (b) Pull strength acceptance data as a function of the process monitor sub-module. The minimum strength criteria (which are averages of the top side and bottom side results) are 6.75 lb and 4.5 lb for the as-fabricated and post-thermal cycled conditions. The strengths are an average between the top side and bottom side.

(The data in Fig. 47 were plotted in the order of increasing SFXXXX number, not by increasing flight number, to maintain the prior presentation methodology.) The as-fabricated pull strengths were very high with the strength metric exceeding minimum acceptance criteria as shown in Fig. 47b. The trend was that the bottom side joints had higher strengths than did the top side solder joints for the as-fabricated condition. However, in both cases, the post-thermal cycling strength exhibited a large decline, falling short of the acceptance criterion. The bottom side pull strengths remained greater than the top side values, and moreover, by statistically significant margins.

The TKN/LTCC failure mode percentage remained in excess of 85% for all as-fabricated cases. The percentages exhibited a reverse trend with respect to pull strength within that 85 – 100% range. After thermal cycling, the TKN/LTCC failure mode percentage remained greater than 99% and any trend versus pull strength was indistinguishable.

The observation was made that the TKN/LTCC fracture surface footprint was noticeably bigger on the bottom surface than on the top surface. This characteristic was not observed in previous units. Assuming that the TKN/LTCC fracture surface area is indicative of the bond surface area, then the larger solder joint footprint could have contributed to the significantly higher pull strength of the bottom side interconnections. The occurrence of LTCC divots accompanying the TKN/LTCC failures was commensurate with past performance.

The sub-modules SF1726 and SF1742 were the process monitors for Flight 15 and were also assembled from lot #31 sub-floors.  The bottom side strengths exceeded the top side strengths.   Similarly, there was a substantial strength loss after thermal cycling, more so for SF1726 than SF1742; still, the bottom side solder joints remained stronger than the top side interconnections.  The excellent pull strength performance allowed these two process monitors to exceed the acceptance criteria for both the as-fabricated and thermal cycled conditions.

The TKN/LTCC failure mode percentages were greater than 95% for both the top side and bottom side pull tests for the as-fabricated condition.  The percentages increased to a range of 98 – 100% after thermal cycling.  However, as was noted above for units SF1731 and SF1751, the footprint of the TKN/LTCC fracture surfaces were larger on the bottom side than on the top side, which likely contributed to the higher strengths of those latter joints.

At this point, a short compilation is constructed of the observations made of sub-modules fabricated with lot #29 sub-floors, which the supplier stated that improvements had been made with respect to control of materials and processes, through lot #31.  The following trends were noted: The *lot #29* showed excellent strength performance for both as-fabricated and post thermal cycled units.  The *lot #30* sub-modules exhibited only marginally acceptable, as-fabricated strengths and poor pull strengths after thermal cycling.  The *lot #31* units exhibited excellent, as-fabricated pull strengths and pull strengths after thermal cycling that were either marginally good or marginally poor with respect to the acceptance limit.  In most cases, the bottom side strength exceeded the top side strength, albeit, not always with a statistically significant difference.  Thus, there remained a high degree of lot-to-lot and sub-module-to-sub-module variability for pull strength performance that was particularly evident in the post-thermal cycle data. In general, the TKN/LTCC failure modes remained high (<90%) when compared to historical records.  The accompaniment of LTCC divots with the TKN/LTCC failure mode was not excessive and mechanical opens were comparable to earlier results.  Lastly, it

was observed for lot #31 sub-modules that the bottom side, TKN/LTCC fracture surface foot-prints were *larger* than those of the top side, which suggested that the bottom side thick film pads had a larger (bond) area than the top side solder joints.  Certainly, this geometric difference could contribute to the higher bond strengths for the bottom side. It also implies that, despite the added measures taken by the supplier to control materials and/or processes, there remained a significant – perhaps unavoidable – variability in the sub-floor structures that affects the reproducibility of sub-module pull strengths.

There was a period of inactivity after the Flight 15 build.  Sub-module manufacturing was resumed for the Flight 16 and 17 detectors.  In order to be assured that the SNL assembly process was ready, a sub-module SF1795 was run through those steps.  This sub-module was built from lot #31 material.  Only the top side of the sub-floor was assembled with dice due to a shortage of the latter. The pull strength of the U01, U03, U06 and U08 joints was 9.1±1.6 lb, which corroborated the values observed in Fig. 47a. Therefore, the directive was given to continue the assembly of sub-modules.

However, during the course of sub-floor manufacturing and sub-module assembly exercises, it was learned that grit blasting was used by the supplier on *some* LTCC sub-floors after the (lamination) process.  (The grit blasting was limited to those areas of the LTCC surface that would receive the post-process, thick film bond pads for the dice.) The decision to blast the sub-floor surfaces was made at the discretion of the operator. The criterion was qualitative:  *If the surface appeared to be "too shiny", the surface was grit blasted in order to remove the excess glassy phase.*  The basis for this step was as follows: An excessively shiny surface indicated the presence of too much glass phase. The supplier had experienced poor adhesion of post-process thick film layer under this situation and, thusly, introduced the grit-blasting step in their LTCC processes.

The objectivity associated with the decision to perform the surface treatment, coupled with personnel changes, prevented there from being made a determination whether or

not each of the sub-floors from lots prior to #29 were exposed to the surface blasting process. Fortunately, there were adequate records to determine that, in fact, the sub-floors fabricated from the LTCC lots #29, #30, and #31 were *not* grit blasted. Certainly, the variability of the pull strength performances in Figs. 46 and 47 would support a hypothesis that, although high strengths can be achieved in the absence of the grit blasting step, the absence of grit blasting may account for the variability of pull strength performance.

The sub-module process monitors, SF1802 (Flight 16) and SF1815 (Flight 17) were made from a new lot of LTCC material, lot #32, for which, the sub-floors were grit blasted prior to the post-processing steps. In fact, all sub-floors lots subsequent to #31 were blasted prior to any post-processing steps. The sub-modules SF1802 and SF1815 exhibited excellent pull strengths as shown in Fig. 47a. Also, the bottom side strengths were higher than those measured on the top side so that this characteristic was not a function of grit blasting. Although exposure to thermal cycling caused a drop in pull strength, the magnitude of that strength loss was less severe than was observed in other units. Lastly, the pull strengths of these two units readily met acceptance requirements for both the as-fabricated and post-thermal cycled conditions (Fig. 47b).

The failure mode analysis was also performed on these two units. The TKN/LTCC interface fracture still predominated, in spite of the relatively high strengths. The higher as-fabricated pull strengths of SF1802 were accompanied by a 85 – 97 % occurrence of TKN/LTCC failure modes. This same failure mode was slightly more prevalent for SF1815 (90 – 100%), which coincided with the slightly lower pull strengths. In both cases, although the post-thermal cycling pull strengths remained high, the failure mode was ≥98% TKN/LTCC interface separation. The occurrence of divots remained relative infrequent; they occurred to a lesser degree with SF1802 (85 – 98%). A more in-depth analysis of the failure mode trends of these and other units is presented in a follow-up section.

In summary, at first glance, the pull strength data for sub-modules SF1802 and SF1815 (lot #32, grit blasted) in Fig. 47a would imply that the grit blasting procedure improved the pull strength.  However, several observations limit the significance of this statement. First of all, the as-fabricated pull strengths were not all that different from those of sub-modules from lots #29 or #31.  Second, the largest improvement of pull strength was observed *after* thermal cycling for the SF1802 and SF1815 sub-modules.  It would have been expected that the most pronounced effect would have been in the as-fabricated condition. Third, the grit blasting did not reduce or eliminate the difference of pull strengths between top side and bottom side.  Fourth, the failure mode did not appear to be very sensitive to the differences in pull strengths or any changes to the LTCC surface and TKN/LTCC bond that were brought about by the grit blasting step.  Therefore, it cannot be ruled out that the improved strengths exhibited by the lot #32 sub-modules were simply a coincidence brought about by the sub-module-to-sub-module variability of the pull strength property.

# 3.0 SCRANTOM VERSUS DUPONT™ STUDY

Several potential causes have been investigated above that could be responsible for the low pull strength phenomenon. Those factors included thick film pad height, the edge pin attachment process being conducted in a $N_2$-$H_2$ gas atmosphere, materials and process controls at the supplier (e.g., thick film paste viscosity), and lastly the media blasting the LTCC sub-floor surfaces prior to post-processing steps. None of these factors was, explicitly, a root-cause. Instead, only minor correlations could be drawn between pull strength and the material and/or process variable. Nevertheless, these results further substantiated the premise the potential root cause was associated with the microstructure (physical, chemical, or both) of the TKN/LTCC interface. The actual "defect" has not been identified to this point.

The next evaluation addressed, once again, the post-processing print-dry-fire sequence that was used to place the thick film pads for the flip chip solder joints. A comparison was made between the firing processes of the supplier, Scrantom, to those of DuPont™, the manufacturer of the LTCC 951™ tape and the 4596™ Au-Pt-Pd TKN ink. The metric used to compare the two processes was the die pull test and follow-up failure mode analysis. Only the bottom side of the sub-floors was assembled with dice and tested due to a shortage of material.

The test vehicle build was performed as follows: Two (2) sub-floors were fabricated at Scrantom, having no specific lot number designation. One sub-floor was identified as "S" for Scrantom and the other "D" for DuPont. The (Au-Pt-Pd) thick film flip chip pads and traces were printed and dried on both sides of the sub-floors at Scrantom, *but not fired.* The thick film paste thickness was 8 $\mu$m. One of the sub-floors was shipped to DuPont™ for post-process firing per their equipment and parameters (nominally, 850°C for 10 min). The other unit remained at Scrantom where it was similarly fired per their respective processes.

The parts were returned to Sandia where the thick film pad heights were measured. Then, both parts were shipped to Scrantom where the 5704 dielectric layer was print and dried on the bottom side to define the solderable area of the flip chip pads.  The "D" part was returned to DuPont™ for exposure to six (6) additional firing steps, which included the firing step for the 5704 dielectric layer.  The same sequence was performed on the "S" part at Scrantom.

The two sub-floors were returned, once again, to Sandia for assembly of dice on the bottom side.  Four of the dice were pull tested in the as-fabricated condition.  Then, the two partially-assembled sub-modules were exposed to 20 thermal cycles (-55°C/125°C) after which, the four remaining dice were tested for pull strength.

Shown in Fig. 48 are the pull strengths as a function of the DuPont™ and Scrantom pedigrees, including data for both the as-fabricated and post-thermal cycled conditions.
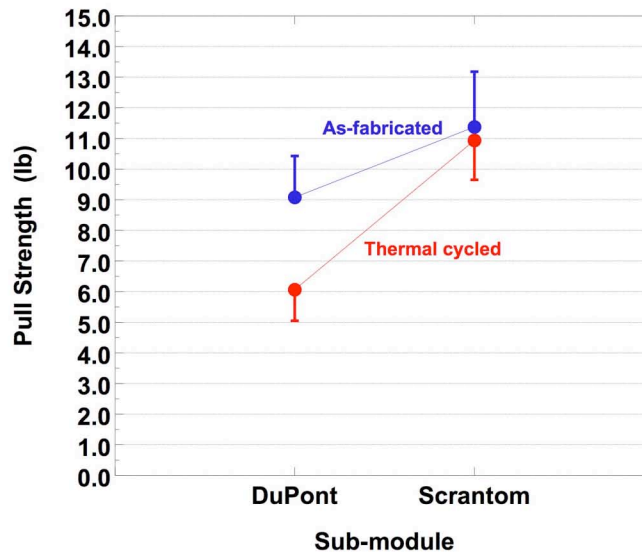


**Fig. 48** Pull strength as a function of sub-module pedigree per the thick film (post-process) firing location: DuPont™ and Scrantom.  Both the as-fabricated and post-thermal cycle (20 cycles, -55°C/125°C) data are combined on the same plot.  The pull tests were performed only on dice on the bottom side.   The error bars are one standard deviation.

Both sub-modules exhibited very high strengths in the as-fabricated condition.  Although the Scrantom unit had a higher mean strength, it was not statistically different from that of the DuPont™ sub-module. The relative difference of pull strengths between the two sub-module pedigrees that was established by the as-fabricated test data, was reproduced after exposure to the 20 thermal cycles (-55°C/125°C).  In both cases, the thermal cycling caused a decrease in the pull strengths.  The Scrantom unit exhibited a considerably lesser degree of pull strength loss so that there was no statistical difference between the as-fabricated and post-thermal cycled pull strengths for this unit.  On the other hand, the DuPont™ unit experienced a substantial drop in pull strength.

The failure modes were also analyzed for the two sub-modules; those results are shown in Figs. 49a and 49b for the as-fabricated and thermal cycle cases, respectively.  In the as-fabricated condition, the predominant failure mode was separation at the TKN/LTCC interface; divots did not accompany this failure mode for either sub-module.  However, there was a significant presence of Si/solder interface failures accompanying the relatively high pull strengths of the Scrantom sub-module.  After thermal cycling, the TKN/LTCC failure mode increased only slight for the Scrantom unit, reflecting the minimal change of pull strength.  Divots appeared with some of the TKN/LTCC fracture surfaces.  In the case of the DuPont™ unit, the TKN/LTCC failure mode increased from 92% to 98% from as-fabricated to the post-thermal cycled condition; recall that there was significant drop in pull strength.  Interestingly, the DuPont™ unit did not exhibited LTCC divots with any of the TKN/LTCC failures. Therefore, it was clear that both sub-modules exhibited the inverse relationship between pull strength and the presence of the TKN/LTCC failure mode.
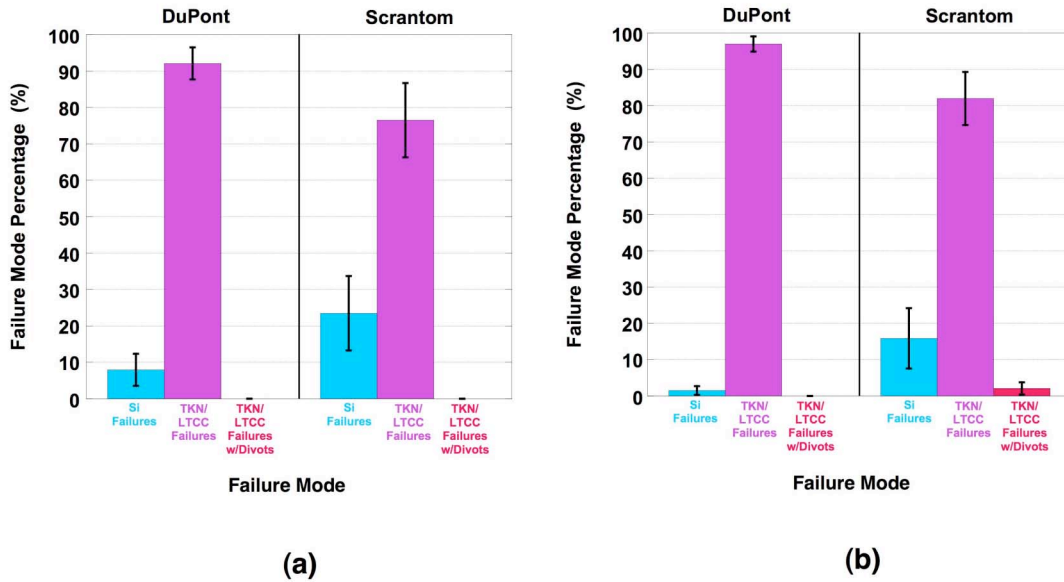
**Fig. 49** Graphs showing the failure mode percentages for the DuPont™ and Scrantom post-processed sub-modules. The error bars are ±one standard deviation.

It was concluded that there did not appear to be a discrepancy in the thick film post-process used by Scrantom, based upon the presumption that DuPont™ expertise in thick film post-processing provides the industry "baseline" for this technology. Furthermore, these data indicate that the pull strength properties of the flip chip solder joints and thusly, also the low pull strength phenomenon, can be sensitive to the post-processing step(s). Of course, it remains to be determined as to the correlation between the strength and the thick film and TKN/LTCC interface microstructures for identifying the cause of the low pull strength phenomenon.

The analysis included a scanning electron microscopy (SEM) evaluation of the fracture surfaces of the solder bumps that remained attached to the die after pull testing[6]. The bump locations were identified by the map in Fig. 50. The legend is: "T", top; "B", bottom; "L", left; and "R", right. There are 33 solder joints per side of the die.

---

[6] It is noted that the following analysis represents the first in-depth microstructural evaluation described in this report. In fact, several microstructural studies occurred prior to, and during, this one, which will be described later on in this report.
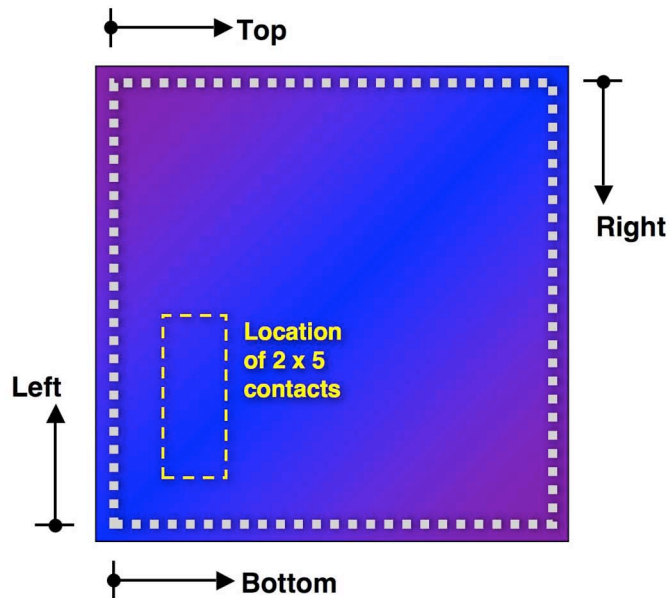
**Fig. 50** Schematic diagram showing the legend used to identify the location of solder bumps examined by SEM or destructively, by metallographic cross sections.

The bumps that were examined are listed below:

**Scrantom**:          U12 (As-fabricated, 12.19 lb)

T28*, T29, R01*, R6, R28, R30*, and L30

U14 (Thermal cycled, 12.21 lb)

T18*, R29, L10*, and B27*

**DuPont™:**          U15 (As-fabricated, 7.33 lb)

T16*, R1*, and R16*

U11 (Thermal cycled, 5.00 lb)

T20*, R16*, L10*, and B13

The solder bumps designated with the asterisk (*) also had energy dispersive x-ray analysis (EDXA) performed on the fracture surfaces.

Shown in Figs. 51a and 51b are SEM, backscattered electron (BSE) images of TKN/LTCC fracture surfaces from the DuPont™ and Scrantom test vehicles, respectively, representing the as-fabricated condition. (The traditional secondary electron (SE) image did not provide necessary detail of the fracture surfaces.)  The Scrantom image was taken from die U12, solder joint L30 (Fig. 50) and the DuPont™ image was from die U15, solder joint R16. These fracture surfaces were created by the TKN/LTCC failure mode.  The images in Fig. 51 are the solder ball side of the fracture (schematic image d in Fig. 1b).

The images in Fig. 51 show the presence of small, dark spots distributed on the fracture surfaces.  Those smaller black spots were not voids but, rather, the glassy phase of the thick film layer. Larger, black areas in Fig. 51a were voids (white arrow).  The relatively bright regions are the Au-Pt-Pd thick film material.  Between the latter regions, are gray areas of Sn or Au-Sn intermetallic compound (IMC), the latter resulting from the reaction between Au component of the thick film and the Sn component of the solder.  The EDXA technique confirmed these elemental compositions, qualitatively.  The extent of glassy phase (small black spots) appeared to be heavier on the DuPont™ fracture surface (Fig. 51a).   It was observed in the case of the Scrantom fracture surface (Fig. 51b) that there was an increased presence of Sn or Au-Sn IMC, implying that the Sn-Pb solder had infiltrated through Scrantom thick film layer to a greater degree than it did in the DuPont thick film layer.  Furthermore, the extensive solder infiltration suggested that there was a greater degree of porosity in the Scrantom thick film layers.  (This inference will be further investigated by metallographic cross sections later on.)
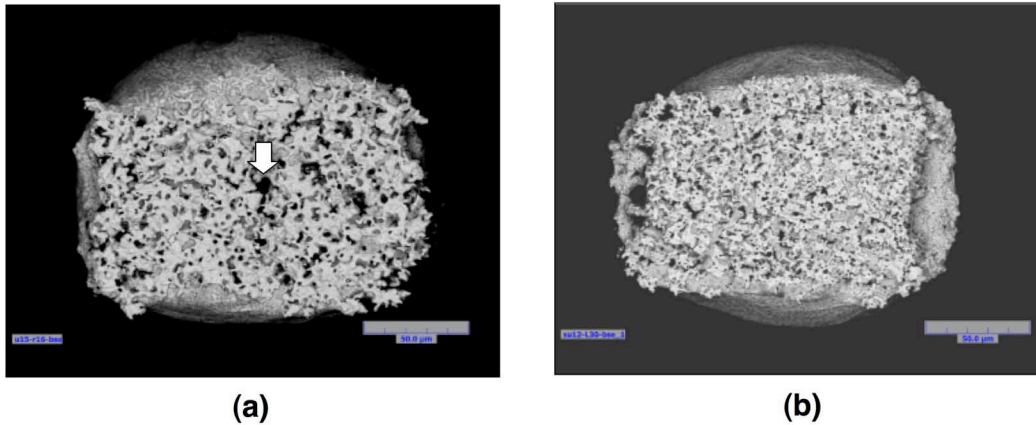
**Fig. 51** Scanning electron microscopy (SEM), backscattered electron (BSE) images of the TKN/LTCC fracture surfaces of solder joints referencing the as-fabricated condition: (a) DuPont™ test vehicle, die U15, joint L16 and (b) Scrantom test vehicle, die U12, joint L30. The white arrow in (a) exemplifies a void.

The same observations were made of solder joint fracture surface taken from the same test vehicles after thermal cycling. Shown at the top of Fig. 52 are SEM/BSE images of the TKN/LTCC failure mode fracture surfaces of solder bumps on dice from (a) the DuPont™ test vehicle (die U11, solder joint L10) and (b) the Scrantom test vehicle (die 14, solder joint L10). The corresponding EDXA data provided on the bottom of Fig. 52 were obtained from scanning over an area footprint the size of which is indicated by the red rectangle. The EDXA technique confirmed that there was higher Sn and lower Au signals on the Scrantom fracture surface (Fig. 52b), which confirmed a decreased presence of glassy phase and, moreover, an increased presence of solder (Sn) at the TKN/LTCC interface.

126
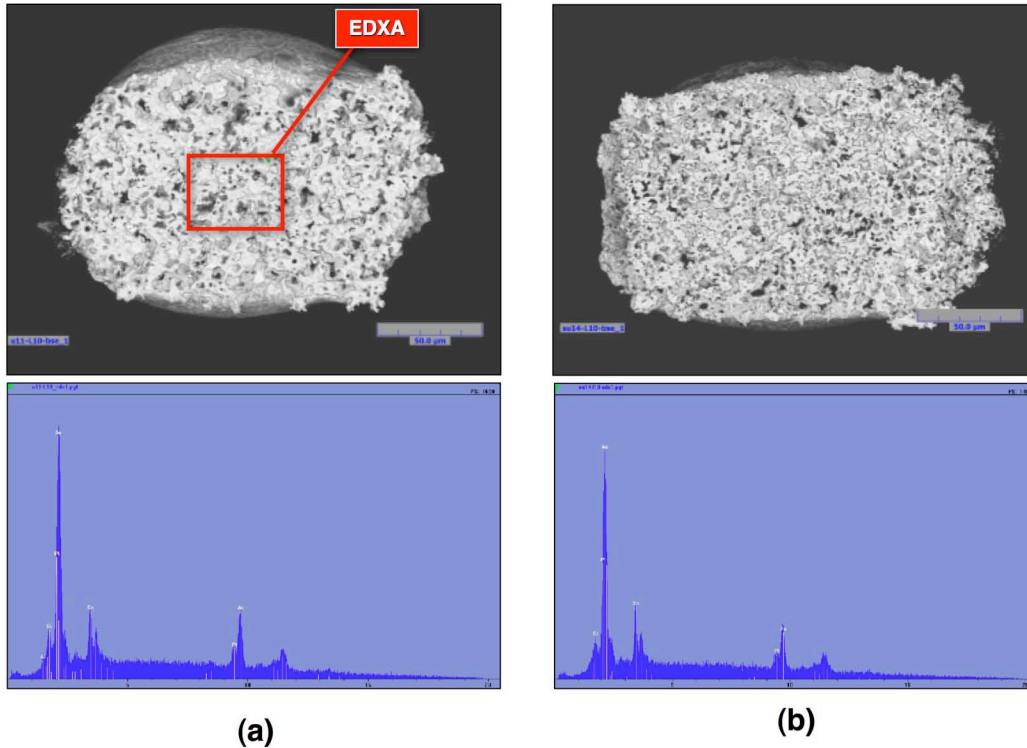
**Fig. 52** Scanning electron microscopy (SEM), backscattered electron (BSE) images of the TKN/LTCC fracture surfaces of solder joints of dice pull tested after thermal cycling: (a) DuPont test vehicle, die U11, joint left 10 and (b) Scrantom test vehicle, die U14, joint left 10. The area that was scanned for the energy dispersive x-ray analysis (EDXA) spectra beneath them is represented by the red rectangle.

Metallographic cross sections were also made of selected rows of the failed solder bumps. The specific die that represented the as-fabricated and post-thermal cycled conditions per the two sub-modules as listed below:

Scrantom:

As-fabricated  ……….        U12

Thermal cycled        …….. U14

DuPont:

As-fabricated  ……….        U15

Thermal cycled ........ U11

Shown in Fig. 53 are SEM (SE) photographs showing the cross sections of two solder joints from the U15 die on the DuPont™ test vehicle that was pulled in the as-fabricated condition. The specific solder joints in (a) and (b) were R4 and L25, respectively. The TKN/LTCC failure mode occurred for both cases. The two solder joints were selected to represent the range of thick film thickness that was observed on the DuPont™ sites. In most cases, however, the thinner layer shown in Fig. 53b occurred more frequently than did the thicker layer shown in Fig. 53a. The presence of thick film and glassy phase particles prevent the solder from reaching the actual fracture surface.



(a)                                              (b)
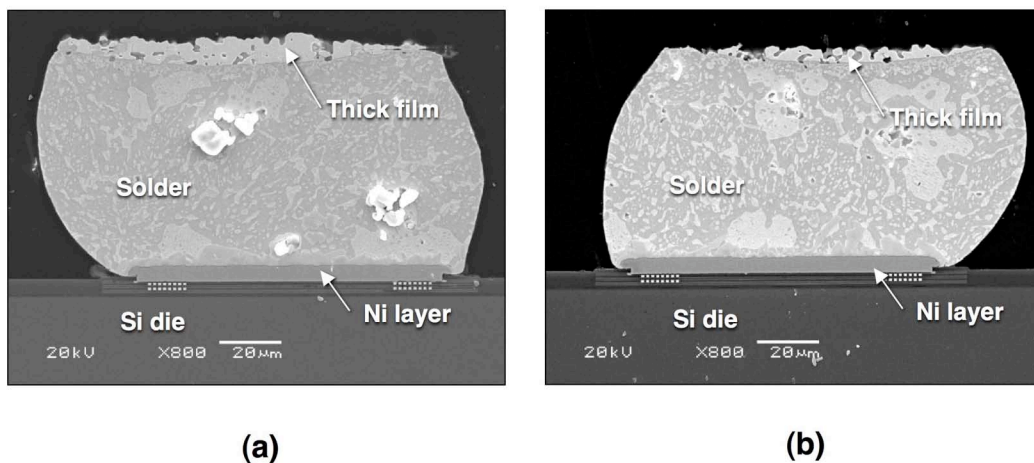
**Fig. 53** SEM (SE) images of the cross sections of two solder joints from the U15 die of the DuPont™ test vehicle. The U15 die was pulled in the as-fabricated condition. The solder joints were: (a) R4 and (b) L25.

Two solder joints from the Scrantom test vehicle were similarly imaged after pull testing in the as-fabricated condition. Both solder joints exhibited the TKN/LTCC failure mode. Shown in Fig. 54 are SEM (SE) micrographs of two solder joints from the U12 die: (a) joint L5 and (b) joint R21. These joints represented the range of thick film structures for the Scrantom test vehicle. It was observed that there was considerably more infiltration

by the Sn-Pb solder into the thicker Scrantom thick film layer, reaching the fracture surface.
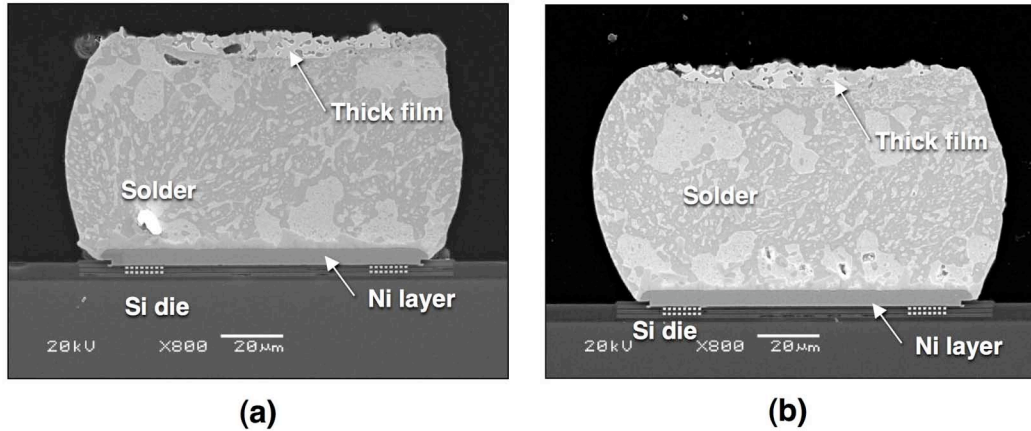


**Fig. 54** SEM (SE) images of the cross sections of two solder joints from the U12 die of the Scrantom test vehicle. The U12 die was pulled in the as-fabricated condition. The solder joints were: (a) L5 and (b) R21.

A direct comparison could be made between the thick film structures of the DuPont™ and Scrantom test vehicles by the low and high magnification SEM images in Figs. 55 and 56, respectively. In spite of the thinner, thick film layer on the DuPont™ solder joint, the solder did not infiltrate the layer as effectively as it did in the Scrantom thick film layer. It was observed in Fig. 56 that the Au-Pt-Pd particles appeared to be better sintered together in the DuPont™ layer, which would explain the reduced layer thickness in this sample given that both samples were printed with the same ink thickness. In addition, the thinner DuPont™ layer was, overall, more "compact" such that the combination of Au-Pt-Pd and glassy phase particles formed an effective barrier against penetration of the (molten) solder to the TKN/LTCC interface. The thicker Scrantom thick film layer (Figs. 55b and 56b) was characterized by more voids that were subsequently filled with solder or IMC. Moreover, those voids often formed more-or-less continuous paths that allowed the molten solder to reach the TKN/LTCC interface.
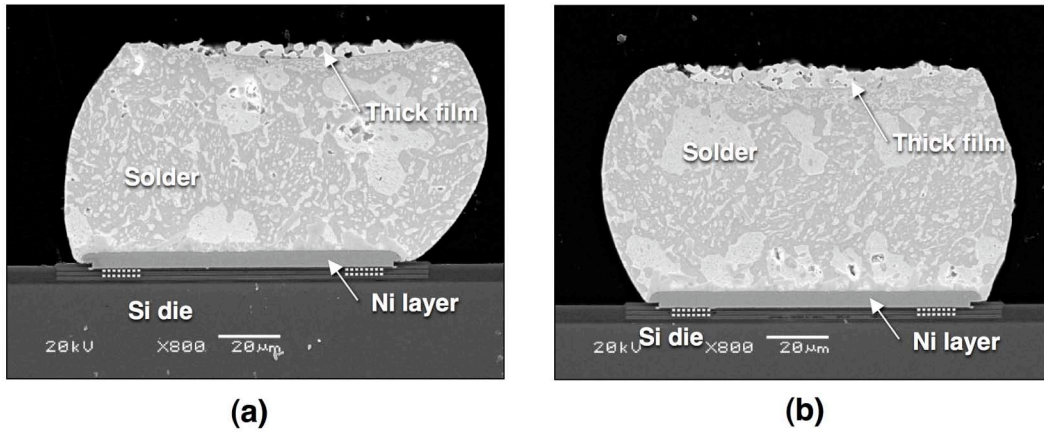
**Fig. 55** Low magnification, SEM (SE) images of the cross sections of two solder joints pull tested in the as-fabricated condition (TKN/LTCC failure mode) comparing the two test vehicles: (a) DuPont™, U15, joint R4 and (b) Scrantom, U12, joint R21.
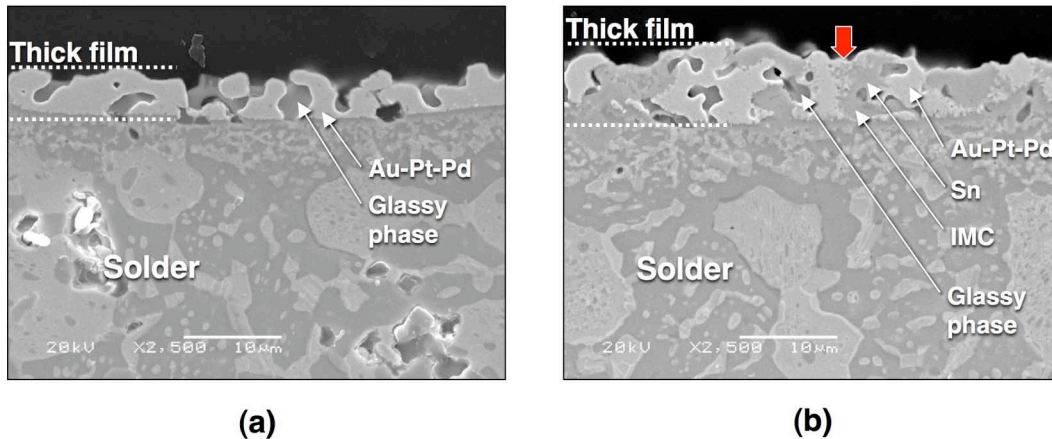


**Fig. 56** High magnification, SEM (SE) images of the cross sections of two solder joints pull tested in the as-fabricated condition (TKN/LTCC failure mode) comparing the two test vehicles: (a) DuPont™, U15, joint R4 and (b) Scrantom, U12, joint R21. The morphology of the partially dissolved Scrantom TKN is identified by the red arrow.

A closer examination was made of the infiltrated regions of the Scrantom thick film layer (Fig. 56b). Based upon the gray tones present in the SEM image, it was observed that only Sn had entered those pores so that upon dissolution of the thick film, predominantly

the Au-Sn IMC, designated $AuSn_4$, was present after solidification[7]. Some Au-Pt-Pd material, which was in the process of being dissolved upon solidification, is identified by the red arrow. There were also small areas of elemental Sn. However, the amount of Pb present in the voids was not commensurate with the solder composition (63Sn-37Pb, wt.%). Therefore, there was preferential entry into, and wetting of, pores within the Scrantom thick film layer by primarily the Sn component of the solder.

It is noted that the solder fields comprising the flip chip ball were also compared between the two test vehicles, using Figs. 53 – 55. There were no repeatable microstructural properties that distinguished the solder joint microstructures or the solder/Si interface between the DuPont™ and Scrantom pedigrees.

The SEM evaluation of solder joint cross sections was also performed on sites that were pull tested after thermal cycling. The IMC layer that developed between the Au-Pt-Pd component and the solder increased only slightly in thickness when compared to the as-fabricated condition.

Shown in Fig. 57 is a view of the cross section of the U11, T33 solder joint from the DuPont™ test vehicle that was pull tested after exposure to the thermal cycling environment. The same relatively thin, yet compact microstructure of Au-Pt-Pd and glassy phase particles was reproduced, again. Consequently, there were no appreciable infiltration by the solder into the thick film layer structure and any further IMC development was limited to the thick film/solder interface.

---

[7] The actual composition of the IMC within the pores as well as at the Sn-Pb/TKN interface is the $(Au, Pt, Pd)Sn_4$ stochiometry [14]. However, given the lesser content of Pt and Pd as well as for brevity sake, the IMC will be written as $AuSn_4$.
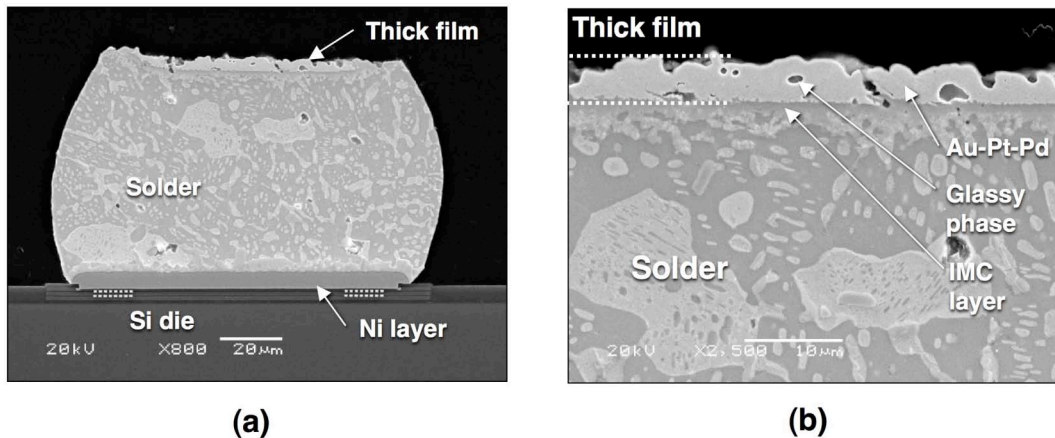
**Fig. 57** SEM (SE) images of the cross sections of the T33 from the U11 die of the DuPont™ test vehicle that was pull tested after thermal cycling: (a) low magnification and (b) high magnification.

The thick film structure of the Scrantom solder joints after thermal cycling was examined by comparing it to that of the of the DuPont™ test vehicle solder joints (exemplified in Fig 57). Shown in Fig. 58 are low magnification SEM images of solder joints from the two respective sub-modules. The TKN/LTCC failure mode was observed for both joints. The solder joint in Fig. 58a, which was from the DuPont™ test vehicle (U11, T6), was chosen because it represented the thickest layer that was as close as possible to the Scrantom thick film layer that in Fig. 58b (U14, T2). The Scrantom thick film (Fig. 58b) still appears as less contiguous than is the DuPont™ layer (Fig. 58a). There was a significant degree of infiltration of the Scrantom thick film by the Sn-Pb solder (specifically, the Sn component of the solder) as indicated of the presence of $AuSn_4$ IMC within the large voids. There was no elemental Sn observed in those infiltrated regions. As was the case for the as-fabricated condition, there did not appear to be any repeatable differences between the solder or solder/Si (UBM) interface microstructures that was distinguishable between the two test vehicles.
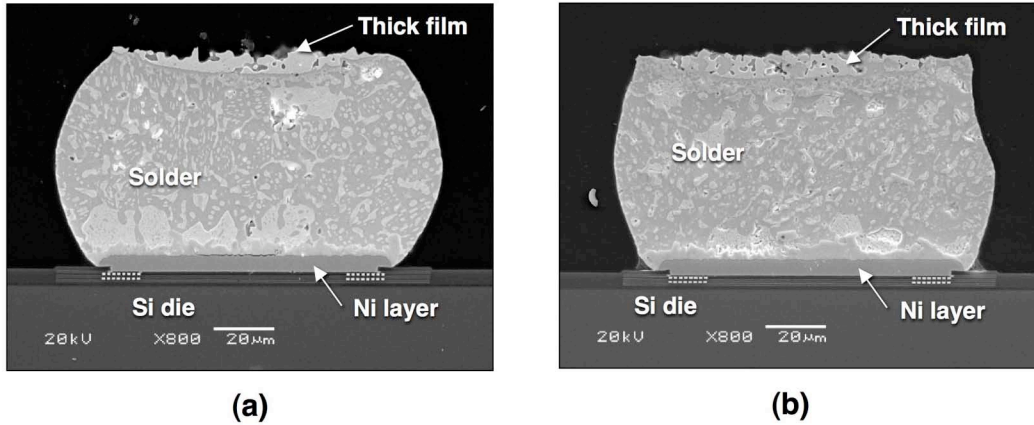
**Fig. 58** Low magnification, SEM (SE) images of the cross sections of two solder joints pull tested in the post-thermal cycled condition (TKN/LTCC failure mode) comparing the two test vehicles: (a) DuPont™, U11, joint T6 and (b) Scrantom, U14, joint T2.

The above observations further delineated by means of the higher magnification images of the same films that are shown in Fig. 59. The DuPont™ thick film exhibits the
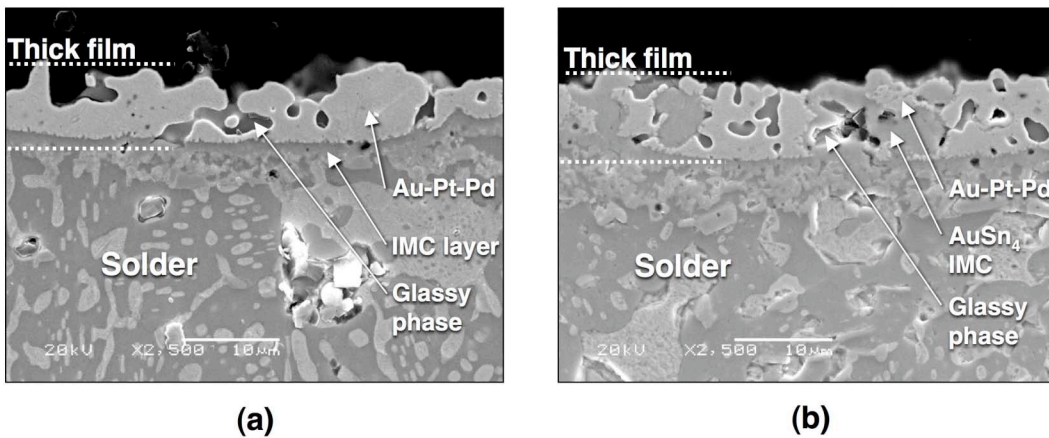


**Fig. 59** High magnification, SEM (SE) images of the cross sections of two solder joints pull tested in the post-thermal cycled condition (TKN/LTCC failure mode) comparing the two test vehicles: (a) DuPont™, U11, joint T6 and (b) Scrantom, U14, joint T2.

previously-mentioned, denser compaction of Au-Pt-Pd and glassy phase particles that created an effective barrier against solder reaching the TKN/LTCC interface (Fig. 59a). This microstructure is in contrast to that of the Scrantom solder joint in Fig. 59b that shows the artifacts of solder infiltration.

A second pair of SEM images were compiled in Fig. 60, which compared the post-thermal cycled DuPont™ and Scrantom solder joint thick film structures. However, in this case, the thick film layers represented the limiting case of "thinnest." The previous observations remained largely unchanged; that is, the thinner DuPont™ layer was still immune to any significant penetration by the solder (Fig. 60a) due a contiguous layer of Au-Pt-Pd and glassy phase particles. The opposite trend was observed in the Scrantom thick film layer (Fig. 60b) where there was extensive solder infiltration by predominantly the Sn component. The Sn was fully converted to $AuSn_4$ IMC by the thermal cycling environment. The glassy phase particles were more widely dispersed in the thick film metal in the latter case.



(a)  (b)
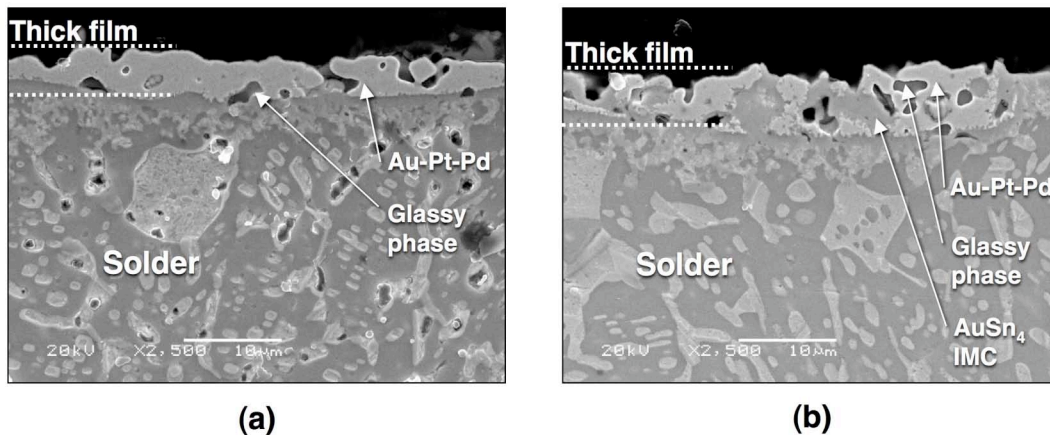
**Fig. 60** High magnification, SEM (SE) images of the cross sections of two solder joints pull tested in the post-thermal cycled condition (TKN/LTCC failure mode) comparing the two test vehicles: (a) DuPont™, U11, B5 and (b) Scrantom, U14, joint B24.

134

A correlation was examined between the pull strength data and the microstructures of the DuPont™ and Scrantom test vehicles solder joints.  First, the die pull strength data are summarized: The die pull test data, which were shown in Fig. 48 showed that, for the as-fabricated condition, the DuPont™ mean strength was slightly less than that of the Scrantom test vehicle; albeit, statistically, the two values were equivalent.  However, after thermal cycling, the DuPont™ pull strengths exhibited a significant drop as compared to the Scrantom case, which showed only a very slight strength loss.  The lower pull strengths exhibited by the DuPont™ test vehicle in either the as-fabricated or post-thermal cycled conditions were accompanied by a greater frequency of TKN/LTCC failure modes (Fig. 49).  The difference of the TKN/LTCC failure mode frequency was, like the pull strength difference, not statistically significant for the as-fabricated condition; but, it was so for the post-thermal cycled pull tests.

Next, the microstructure observations are summarized, beginning with an SEM evaluation of the fracture surfaces (Figs. 51 and 52).  There was a greater presence of the glassy phase at, and minimal solder infiltration to, the TKN/LTCC interface of the DuPont™ solder joints than was observed for the Scrantom solder joint.  This observation was confirmed by metallographic cross sections.  Despite being thinner, overall, the DuPont™ thick film layer was more compact, allowing the Au-Pt-Pd and glassy phase particles to form an effective barrier against molten solder reaching the TKN/LTCC interface.  On the other hand, the Scrantom layer was, overall, thicker, but contained a greater degree of void, many of which, provided access to the TKN/LTCC interface by the Sn component of the molten solder.  Both the DuPont™ and Scrantom solder joints experienced slightly thicker IMC layers at the Sn-Pb/Au-Pt-Pd interface after thermal cycling.  However, in the case of Scrantom thick film having large pores infiltrated with Sn, that Sn was converted to IMC.

There were no distinct differences between the DuPont™ and Scrantom interconnections in terms of either the Sn-Pb (bulk) solder microstructure or in the solder/Si (UBM) interface structures.

The pull strength versus microstructure relationship appeared to contradict the earlier hypotheses. The Scrantom test vehicle exhibited the overall better pull strength performance, yet had a thick film layer with a porosity that permitted significant infiltration of Sn to the TKN/LTCC interface. Based upon the premise that Sn could potentially degrade the adhesion between the thick film layer – specifically, the glassy phase – and the base material, the Scrantom solder joints were expected to be weaker than those of the DuPont™ test vehicle. Therefore, it was concluded that molten Sn, when in close proximity to, or contact with, the TKN/LTCC interface, is not a sufficient condition to cause a loss of the solder joint pull strength. From a more generalized viewpoint, it can also be concluded that the microstructure of the thick film layer – that is, its thickness and degree of porosity do not provide an explicit indication of potential pull strength performance by the subsequent solder joint.

A mechanistic explanation was sought that would explain the difference between DuPont™ and Scrantom pull strengths. A hypothesis was developed for the observed trends, based upon the schematic diagram in Fig. 61. It was assumed that the more contiguous Au-Pt-Pd structure of the DuPont™ thick film layer resulted from a greater degree of sintering that brought-about by the DuPont™ firing process. It can be inferred that the DuPont™ firing process was "hotter" than that performed at Scrantom. A consequence of the hotter firing process was that the glassy phase diffused to a greater degree into the LTCC material below it, leaving less material at the TKN/LTCC interface with which to form the bond. The result was a decrease in the adhesion strength there. Ancillary evidence was observed in the study described in Reference 1 that pull strength was maximized at between two and three firing steps. Additional firing steps, which under the current circumstances would correlate to higher heat input per the DuPont™ process, caused a loss of strength. It can by surmised that the more extensive diffusion of glassy phase was responsible for that effect, as well.
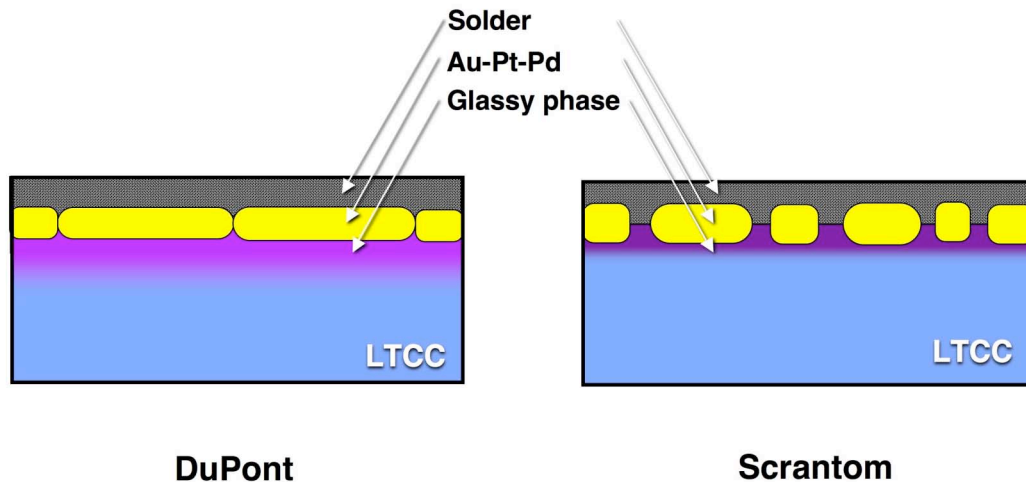
**Fig. 61** Schematic diagrams showing the interface structures of the DuPont™ and Scrantom flip chip solder joints. The greater extent of sintering in the DuPont™ case resulted in a more contiguous Au-Pt-Pd thick film layer.

In summary, a study was performed that examined the pull strength performance of two sub-floors that were equivalent is every respect except that the firing of the printed-and-dried, post-process thick film flip chip pads was performed at two different facilities – Scrantom (current Sandia supplier) and DuPont™ (the industry expert in thick film and LTCC technologies). Both sub-floors were returned to Sandia for the assembly of dice to the bottom side (only). Four of the eight die were pull tested in the as-fabricated condition; the remaining four dice were tested after exposure to the process monitor, thermal cycling condition.

The Scrantom test vehicle had slightly higher mean pull strengths in the as-fabricated condition than were exhibited by the DuPont™ test vehicle. After thermal cycling, the DuPont™ test vehicle exhibited significantly decreased pull strengths while the pull strengths of the Scrantom unit remained largely unchanged. It was observed that the thick film structure of the DuPont™ test vehicle exhibited a thin, yet dense microstructure of sintered Au-Pt-Pd particles glassy phase. On the other hand, the structure of the Scrantom-fired thick film exhibited a greater thickness owing to a greater propensity of voids that were filled by the Sn component of the solder. In all other

aspects, the solder joints of the two test vehicles were similar.  It was concluded that the proximity of solder (Sn) to the TKN/LTCC interface was not a sufficient condition to indicate the potential for low solder joint pull strengths.

Mechanistically, it was hypothesized the lower pull strengths of the DuPont™ module were the result of  more heat input during the post-process firing step.  As a result, the glassy phase diffused to a greater degree to the TKN/LTCC interface, resulting in an absence of the phase at the TKN/LTCC interface that was responsible for the drop in strength, there.

Lastly, three important engineering conclusions were drawn from the study. First of all, there does not appear to be an obvious "discrepancy" in the post-process firing process used by Scrantom.  Secondly, the pull strength data did not exhibit, explicitly, the low pull strength phenomenon.  In fact, the strength values of both units were adequate; albeit, the number of datum was very limited (N = four tests per condition) in both cases. Thus, the range of thick film microstructures represented by the DuPont™ and Scrantom units did not correlate to the low pull strength phenomenon.

# 4.0 Microstructural Analysis

In the previous section, there were distinct differences in the thick film microstructures resulting from the DuPont™ versus Scrantom firing processes. There were also differences in pull strength values between the two test vehicles, which were statistically significant after thermal cycling (Fig. 48). A hypothesis was developed that explained the pull strength trends as a function of the observed microstructures (Figs. 51 – 60); however, that hypothesis appeared to contradict the long-standing premise of degradation to the TKN/LTCC interface with an increased likelihood of its contact with Sn from solders.

It was also pointed out that the *magnitudes* of those strength losses were considerably less than those attributable to the low pull strength phenomenon (i.e., 0.5 – 4.5 lb). Therefore, if a root-cause to the low pull strength phenomenon is to be identified from the thick film microstructure, it is an effect that is far more-subtle than those differences than were observed between the DuPont™ versus Scrantom interconnections.

*4.1 Scanning electron microscopy and energy dispersive x-ray analysis*

A systematic, microstructural study was performed on tested sub-modules, using SEM analysis of the fracture surfaces as well as the cross sections of the interconnections, both pull-tested and those of die that were not pull tested. The study began with the sub-module SF512. The sub-module SF512 was produced at the time that the low pull strength phenomenon first drew attention because this unit was a process monitor for a flight build of sub-modules. This unit also represented the change to the current thick film and dielectric process sequence. The previous sequence had caused cracking of the braze pins.

The pull strength behavior of SF512 is shown graphically in Fig. 62 as a function of individual die sites. The data were plotted separately for the as-fabricated and post-thermal cycled (-55°C/125°C; 20 cycles) conditions. The die sites U01 – U08 are on the top side; U09 – U16 are on the bottom side. The dashed red line is the minimum pull

strength allowed by the acceptance criterion. The sub-module exhibited satisfactory pull strengths in the as-fabricated condition. In fact, the mean pull strength was higher on the bottom side than on the top side of the sub-module. However, after thermal cycling, the pull strength dropped to very low values that were characteristic of the low pull strength phenomenon. There was no longer a strength distinction between the two sides of the test vehicle.
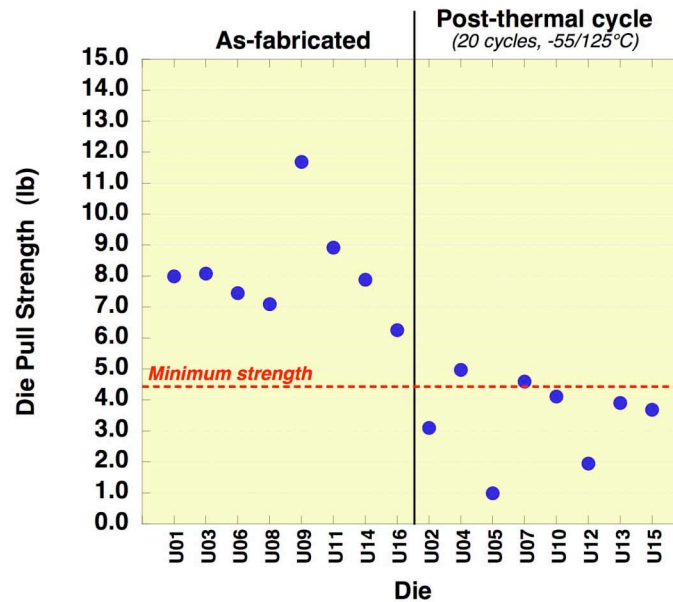


**Fig. 62** Graph of pull strength as a function of die site for the sub-module SF512. The data were divided into segments representing the as-fabricated and post-thermal cycled conditions. The minimum individual die pull strength limit is shown. Sites U01 – U08 are on the top side of the sub-module while sites U09 – U16 are on the bottom side.

The failure mode data were compiled in Fig. 63. In the as-fabricated condition (Fig. 63a), the TKN/LTCC failure mode predominated the results. The higher strengths on the bottom side were accompanied by a greater occurrence of the Si/solder failure mode (with UBM pull-out) as indicated by the red shade. Yet, overall, the number of TKN/LTCC failure sites were high as was the case for sub-modules that were potentially sensitive to the low pull strength phenomenon. The TKN/LTCC failure mode occurred

almost exclusively after thermal cycling, which coincided with the reduced pull strengths. There was also the expected number of LTCC divots accompanying the TKN/LTCC failures after thermal cycling.
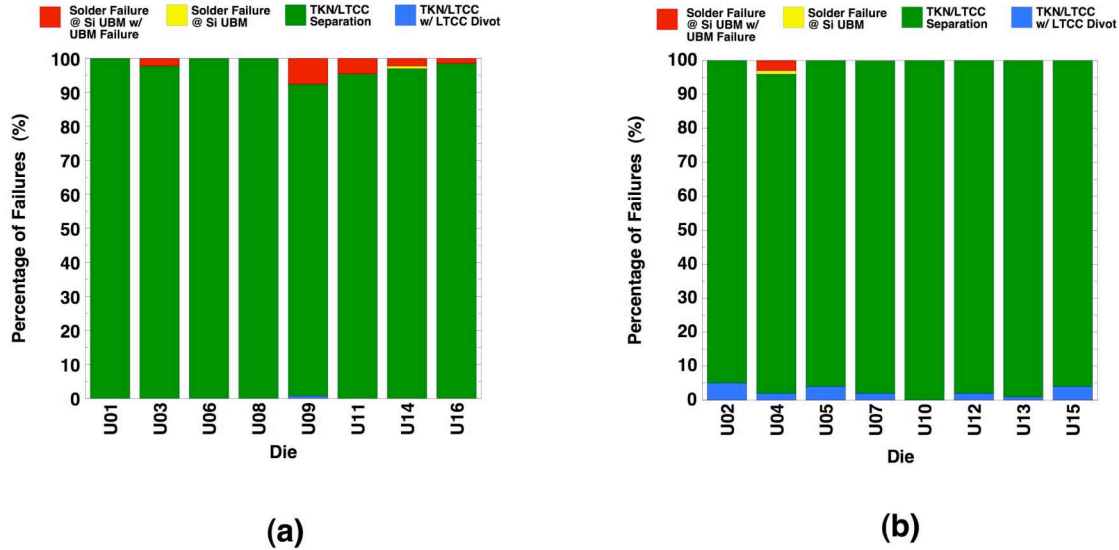


**Fig. 63** Graphs of the failure mode results from sub-module SF512 for: (a) as-fabricated condition and (b) post thermal cycled condition. Each of the four failure modes is designated by color on the bar graphs.

Scanning electron microscopy and energy dispersive x-ray analysis (EDXA) elemental mapping techniques were preformed on several, selected TKN/LTCC fracture surfaces. This approach provided a more detailed elemental spatial distribution of the fracture surface versus the gray tones of SEM images used for Figs. 51 and 52 ; albeit, the analysis is still qualitative. Two representative maps are provided in Fig. 64. In both cases, the recorded failure mode was TKN/LTCC separation. The color legend is as follows: The pink shade around the perimeter is the Sn that had infiltrated these thinner regions of the thick film layer. The yellow regions are comprised of the thick film metal components Au, Pt, and Pd, which were combined together to have the single color of yellow. The red regions are LTCC material (pull-out) comprised of Al and Si that were

combined together to have the same red color.  The blue areas are Pb, which is primarily the glassy phase[8].



**(a)**                                                   **(b)**
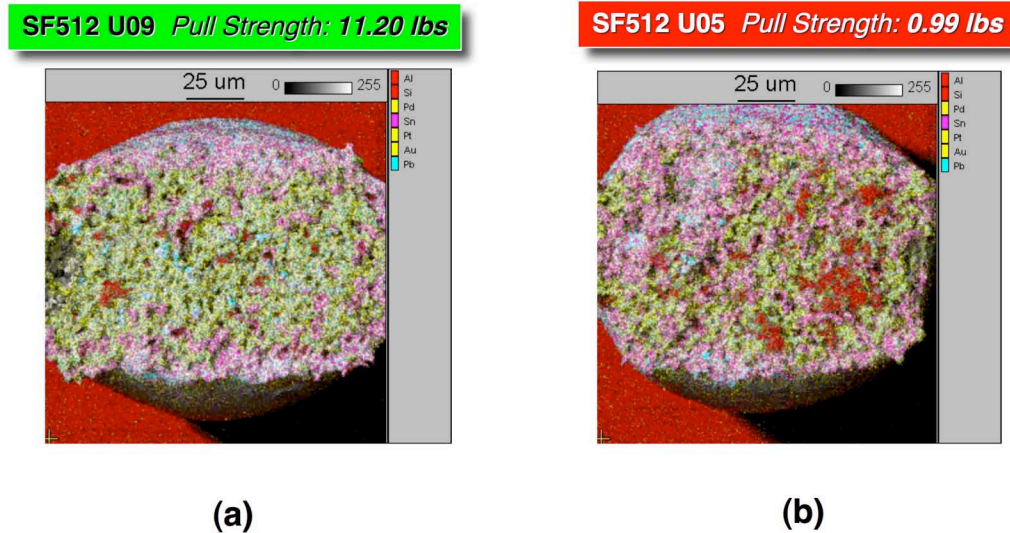
**Fig. 64** SEM/EDXA elemental maps of selected flip chip solder joints from die on the sub-module SF512 having the TKN/LTCC failure mode after pull testing: (a) U09, joint L15, as-fabricated condition, high strength of 11.2 lb and (b) U05, joint R15, post-thermal cycled condition, having a low strength of 0.99lb.  The elements of Au, Pt, and Pd were combined into a single color, yellow, to represent the thick film metal.  The elements Si and Al were combined as red, representing the LTCC material.  Pink is the Sn element and blue is Pb, the latter corresponding primarily to the TKN glassy phase.

The EDXA map in Fig. 64a was taken of the flip chip joint (L15) from the U09 die, which had a high pull strength of 11.20 lb (as-fabricated condition).  The map shows primarily the thick film elements.  There was a small degree of solder infiltration into the center reaches of the thick film (that is, away from the edges) and a few, small LTCC divots (that would not have been observed upon visual inspection).

---

[8] The blue regions representing the element, Pb, were primarily glassy phase because the Pb-rich phase of the Sn-Pb solder was not very prevalent in the voids into which, the molten solder had infiltrated and, as such, would have been exposed at the TKN/LTCC fracture surface.

The SEM/EDXA image in Fig. 64b shows the TKN/LTCC fracture mode surface from the U05 die (joint R15), which exhibited the low pull strength phenomenon (0.99 lb). Although the pull test was performed after thermal cycling, the elevated temperatures of would have caused only a minimal conversion of the Au-Pt-Pd component of the thick film to a $(Au, Pt, Pd)_xSn_y$ IMC via solid-state diffusion. Thus, the increased prominence of the pink in Fig. 64b implies that there is a higher concentration of Sn along the TKN/LTCC interface.

The sub-module SF267 was similarly examined. The die site versus strength profile looked very similar to that of SF512 in Fig. 62. The SEM/EDXA elemental mapping technique was applied to selected solder joints of dice experience either high pull strength or low pull strength for a TKN/LTCC failure mode. Nearly identical results as those shown in Fig. 64, were observed between the fracture surfaces of solder joints for the two pull strength regimes.

(Metallographic cross sections were not performed on any of the dice from the sub-modules SF512 or SF267.)

Because of the low pull strengths that were observed with SF512 and SF267, two additional sub-modules, SF523 and SF541, were assembled with the objective of reproducing the low pull strength phenomenon in order to perform a more detailed, microstructural analysis by metallographic cross sections. Both underfilled and non-underfilled dice were to be so examined. Both sub-modules were thermal cycled (-55°C, 125°C; 20 cycles), that is, pull tests were *not* performed in the as-fabricated condition, in order to further encourage the low pull strength phenomenon. The stereo photographs in Fig. 65 (a, top; b, bottom) shows the purposes of each of the dice on the top side and bottom side, respectively. Two die sites on both top and bottom sides were underfilled per the flight hardware procedures. Assuming that the low pull strength microstructure had, indeed, been reproduced, the cross sections of these joints would determine
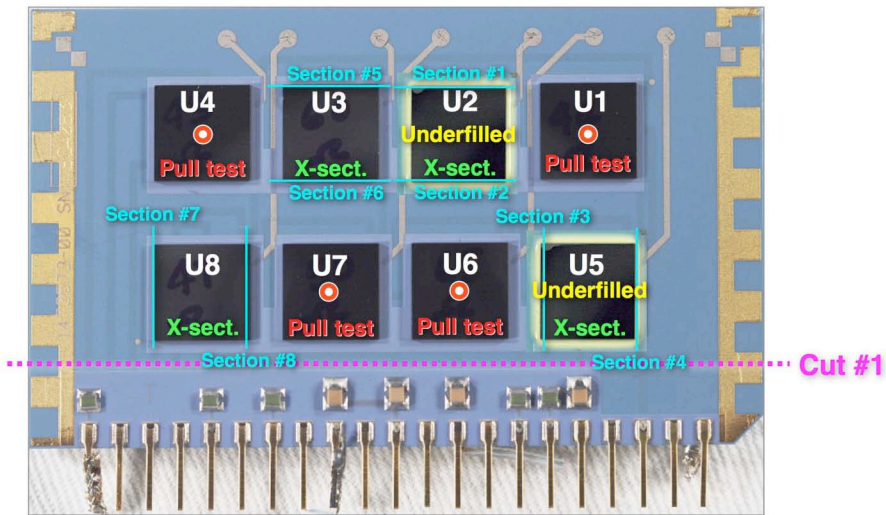
(a)
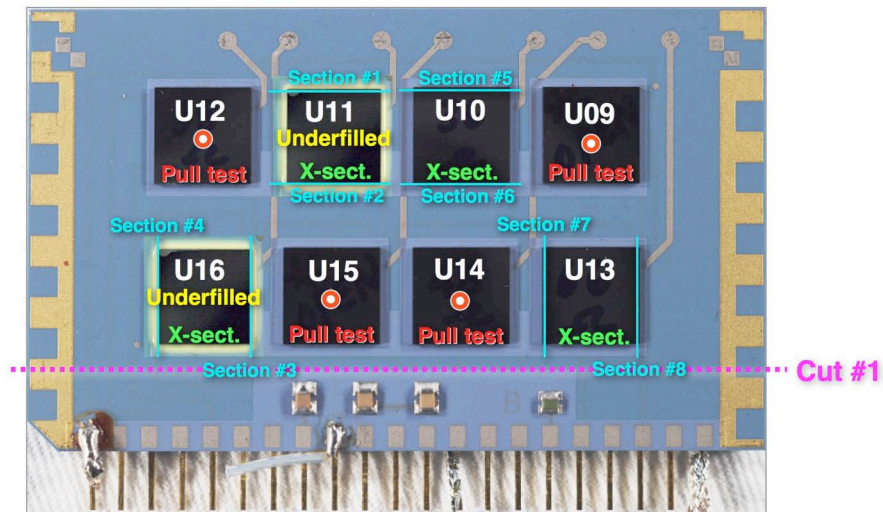


(b)

**Fig. 65** Stereo photographs of the SF523 show tests performed on each of the die sites located on the top side (a) and the bottom side (b) of the unit. These maps represented, as well, the tests performed on the duplicate sub-module, SF541.

whether the underfill could cause an electrical failure of the interconnection by generating a separation at the TKN/LTCC interface. Of six remaining, non-underfilled

dice per side, four were targeted for pull testing and the remaining two joined the underfilled joints for cross section analysis.

Unfortunately, the pull test results of both units *failed* to reproduce the low pull strength phenomenon.  The acceptable strength values were obtained, which are listed below:

- SF523:        Top, 7.1±0.3 lb              Bottom, 6.8±1.4 lb
- SF541:        Top, 7.0±1.4 lb              Bottom, 6.5±1.3 lb

The larger data scatter was caused by the fewer number of test points.  There were no individual die sites of either sub-module that exhibited a pull strength below 5.2 lb.  Also, both sub-modules showed a significant percentage of failures at the Si/solder interface, with and without UBM fracture, which is commensurate with the higher pull strengths. There was also the expected accompaniment of LTCC divots with the TKN/LTCC failure mode per the post-thermal cycled condition.

Nevertheless, the metallographic cross sections were performed on the designated dice of these sub-modules.  Shown in Fig. 66 are low and high magnification SEM images of a representative solder joint from the U10 die (no underfill) of SF523 after thermal cycling.  The two high magnification images (b, d) were taken at edge and center locations, respectively, of the bond pad. In spite of consumption of the thick film and considerable IMC growth, there were no observable cracks at the IMC/LTCC or TKN/LTCC interfaces. Lastly, there were no signs of crack damage in the solder, thick film layer, or in the underlying LTCC material.
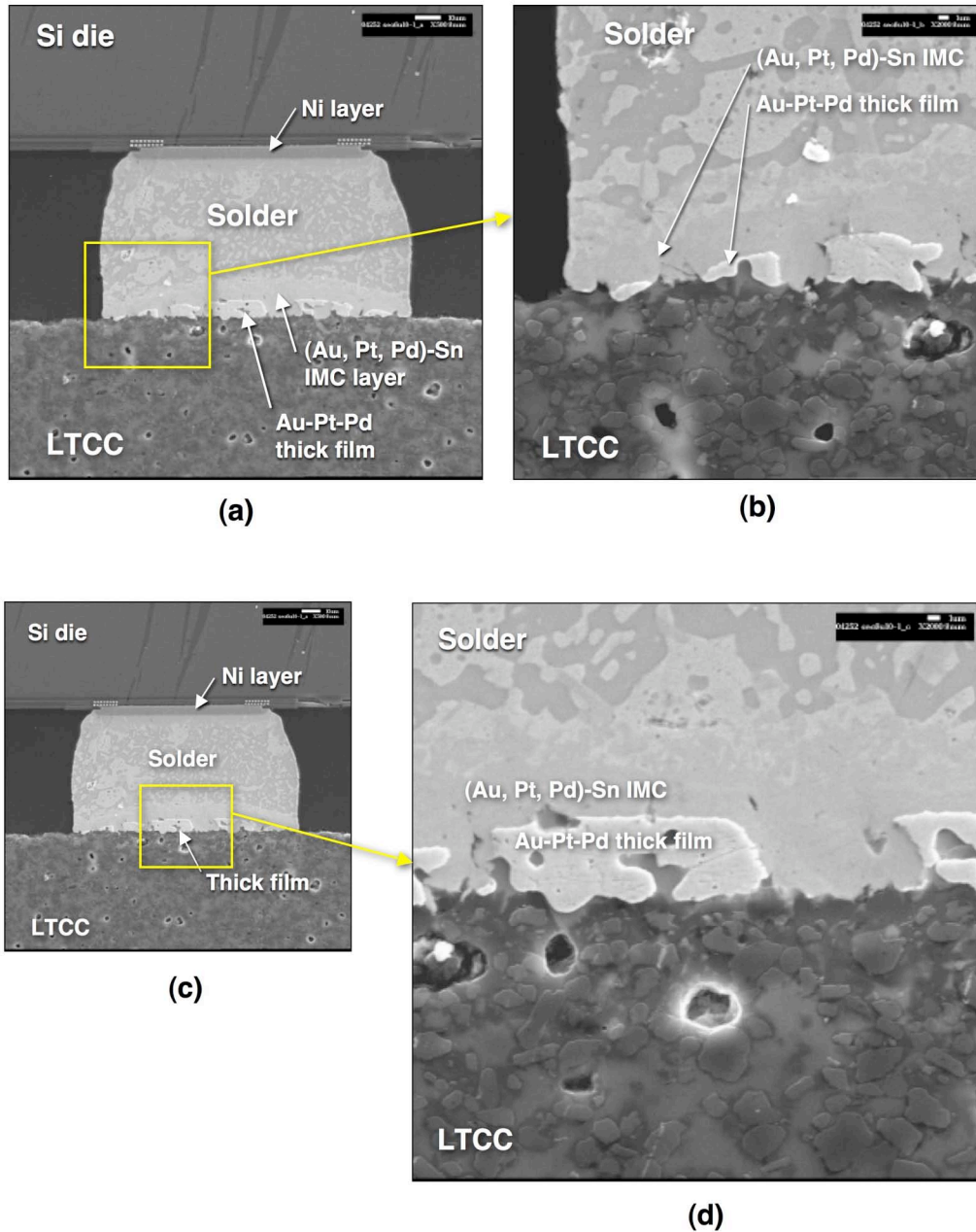
**Fig. 66** (a – d) SEM micrographs showing the microstructure of a representative solder joint, in this case, taken from the die U10 (post-thermal cycle; no underfill) from SF523. Both high magnification images (b, d) confirmed good integrity of the (Au, Pt, Pd)Sn$_4$ IMC/LTCC and TKN/LTCC interfaces.

The same microstructural evaluation was carried out for the non-pull tested dice of SF541. In this case, the cross section was performed on a solder joint from the die

U02, which was underfilled prior to being exposed to the thermal cycling conditions. Low and high magnifications SEM images are shown in Fig. 67 of the solder bump and the interface with the LTCC substrate, respectively. The latter image is comprised of a relatively long bond line between the $(Au, Pt, Pd)_x Sn_y$ IMC and the LTCC. There are no obvious indications of cracking along the interface as shown in Fig. 67b.



(a)

(b)
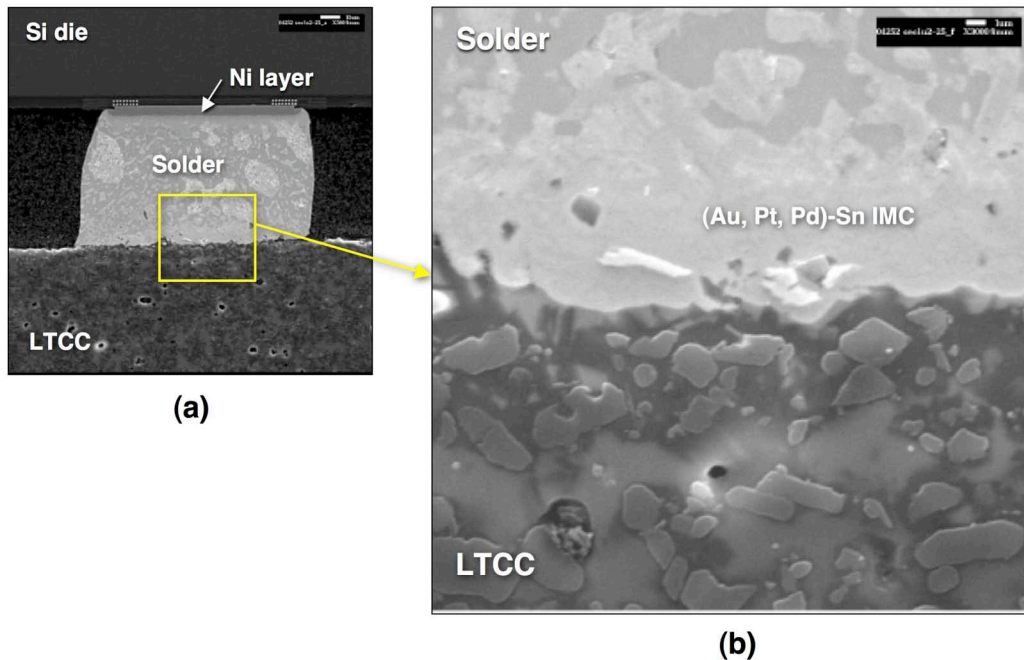
**Fig. 67** SEM micrographs showing the microstructure of a representative solder joint of the die U02 (post-thermal cycle with underfill from sub-module SF541. There were no indications of cracking along the interface between the (Au, Pt, Pd)Sn$_4$ IMC and LTCC substrate.

In summary, the two sub-modules, SF523 and SF541, were built directly following SF512 and SF267 that exhibited the low pull strength phenomenon. The purpose of SF523 and SF541 was to reproduce the low pull strength phenomenon in order to perform a more detailed, microstructural analysis by metallographic cross sections. In this regard, the sub-modules were thermal cycled prior to pull testing and creation of the metallographic cross sections. Both underfilled and non-underfilled dice were so examined. Disappointingly, the low pull strength phenomenon did *not* materialize. The

147

cross sections and SEM images indicated that there was an absence of cracks or separation at the TKN/LTCC interface. There was a considerable quantity of IMC development in the joints[9]. The result was a large expanse of the bond line that was comprised of $(Au, Pt, Pd)_x Sn_y$ IMC bonded to the LTCC substrate interface. Yet, the pull strengths remained high, since there was no cracking or separation along that specific bond line for either the underfilled or non-underfilled dice.

The last observation raised an important point: The presence of the $(Au-Pt-Pd)_x Sn_y$ IMC and, more specifically, the resulting IMC/LTCC interface did not compromise the mechanical integrity of the solder joint. Not only does this observation preclude the IMC as being the source of the low pull strength phenomenon, but it contradicts the long-standing premise that complete dissolution of the thick film layer and resulting formation of an IMC layer, necessarily compromises the mechanical strength of a thick film solder joint. Thus, the subsequently-formed IMC can bond to the thick film glassy phase and to the LTCC substrate constituents (alumina, silica, and its glassy phase).

The follow-up inquiry was whether an IMC that is generated by *solid-state* diffusion processes will also retain good adhesion with the LTCC substrate, or be a possible source of the low pull strength phenomenon. Evidence to this effect was sought from sub-modules that had been exposed to burn-in procedures as well as those that were exposed to accelerated aging for long-term reliability evaluations. In both cases, extensive, solid-state IMC development would have taken place.

First, the sub-module burn-in data will be re-assessed. The sub-module SF088 was assembled with dice, but *without underfill*, and subjected to a burn-in condition of 125°C, 282 hours (air). Thermal cycling (-55/125°C, 20 cycles) was not performed on this sub-module. Dice were selected for either pull testing or microstructure analysis. Shown in Fig. 68 is a plot of the pull strength values for SF088 as a function of die site. Also,

---

[9] The absence of the Pb-rich layer between the IMC layer and the solder, indicated that the IMC created as a consequence of thick film dissolution by the *molten* Sn-Pb solder.

there was included in Fig. 68 the as-fabricated pull strength data from four non-burned in, sub-modules.  There was clearly a loss of strength caused by burn-in.  The dice U05 and U07 had pull strengths that were at the lower acceptability limit for single die values. Overall, the pull strengths of SF088 were satisfactory.  As an average, the bottom side pull strengths were slightly higher versus strength values measured from the top side dice.
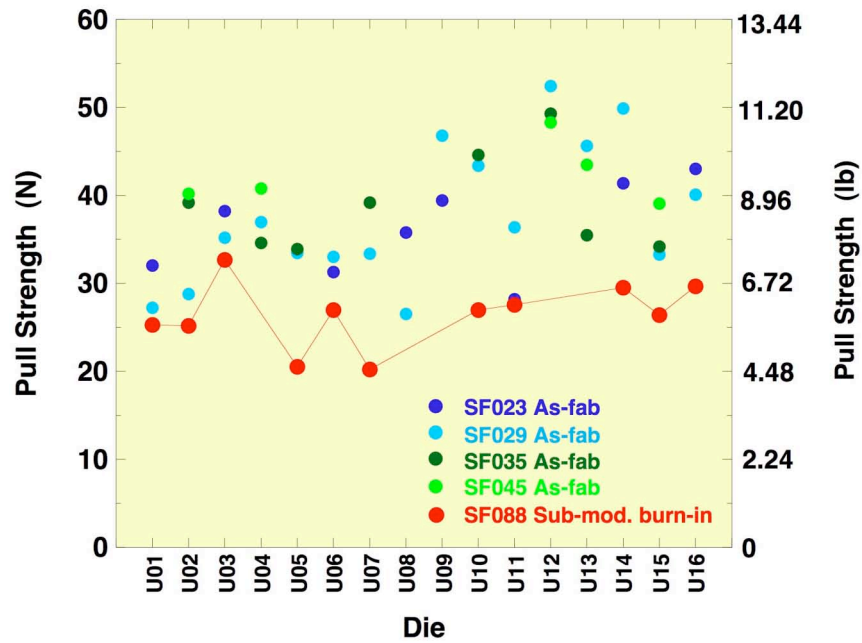


**Fig. 68** Pull strength of dice on SF088 that was subjected to an air burn-in at 125°C for 282 hours.  Comparable data were included from four other sub-modules, SF023, SF029, SF035, and SF045, that were not subjected to a burn-in treatment.

The failure modes were also recorded for the SF088 unit in Fig. 69a.  Similar data were plotted in Fig. 69b representing the SF023 sub-module (no burn-in) for comparison. (The pull strength values, presented in Newtons (N), were also included on the plots.) The lower strengths of SF088 were accompanied by >90% of failures at the TKN/LTCC interface as compared to SF023 (and other sub-modules) that exhibited significant contributions of the solder/Si interface failure modes.
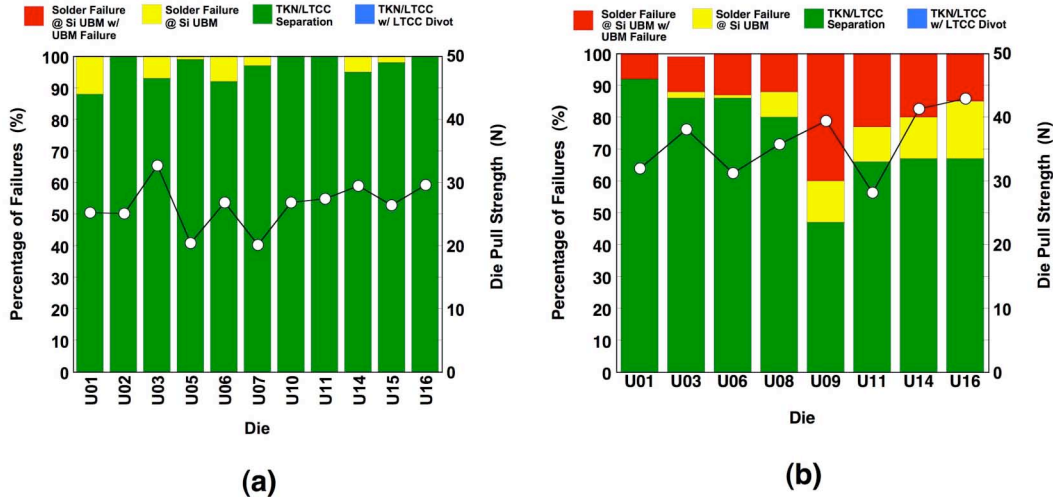
**Fig. 69** Failure modes associated with the pull-tested dice on sub-modules (a) SF088 that was subjected to an air burn-in at 125°C for 282 hours and (b) SF023 that was not exposed to the burn-in treatment. All tests were performed in the as-received condition. The pull strength values were placed over the failure mode bar charts for comparison. (The pull strengths were in the units of Newtons (N); the conversion is 0.224 lb/N.)

Of particular interest in this study were the metallographic cross sections that were taken of the solder joints from dice that were not pull tested on SF088. Shown in Fig. 70 is the solder joint from the non-pull tested U04 die. This solder joint was located towards the center of the row. Nearly all of the thick film layer was consumed by solid-state IMC growth during the burn-in exposure. There were no indications of large-scale cracking along the interface between the $(Au, Pt, Pd)_x Sn_y$ IMC and the LTCC. This point is exemplified in Fig. 71, which shows a high magnification image of the red-box area in Fig. 70. Damage was limited to a few, small, isolated cracks in the glass phase along the interface (red arrow in Fig. 71).
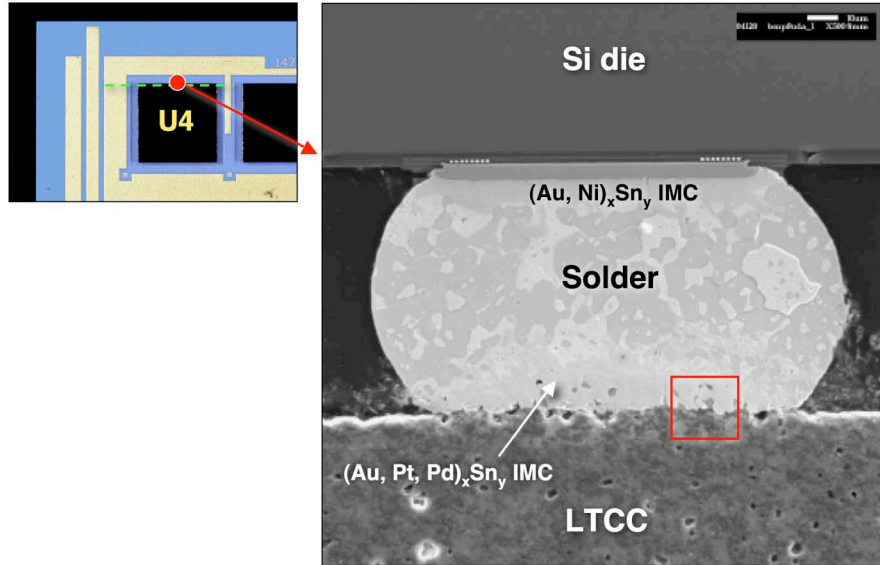
**Fig. 70** Stereo photograph identifying the location of the center-wise solder bump on U04 of the sub-module, SF088, that underwent the burn-in treatment of 125°C, 282 hours. The SEM photograph shows the solder joint in cross section and the location (red box) of the region examined at higher magnification.
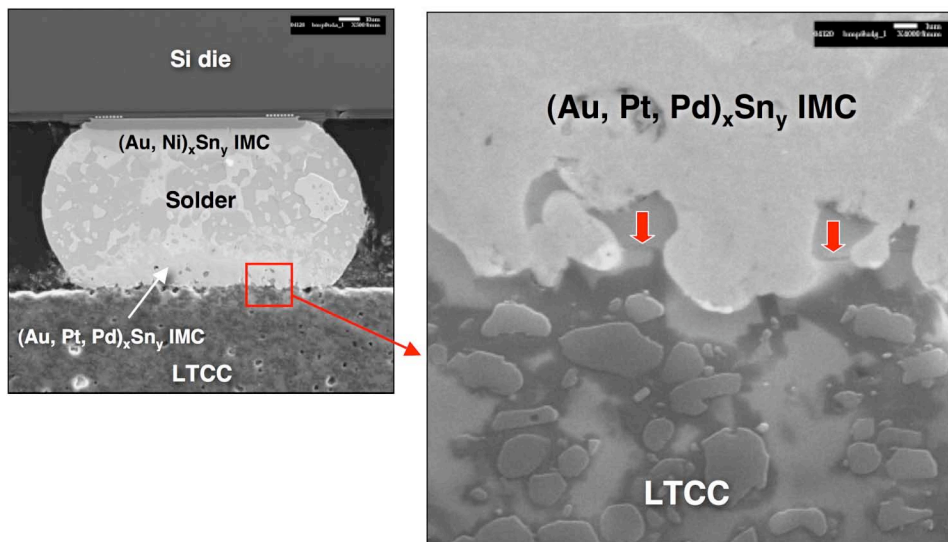


**Fig. 71** Low magnification SEM photograph of the U04 solder joint near the center of the row, and high magnification image of the $(Au, Pt, Pd)_xSn_y$/LTCC interface. The red arrows identify small cracks in the glassy phase that belonged to the thick film layer.

151

More significant crack development was observed at the solder joint of U04 that was located at the end of the row as shown in Fig. 72. The crack opening was widest at the outboard side of the joint. This point is illustrated more clearly by the SEM images in Fig. 73. The crack path followed along the IMC/LTCC interface.
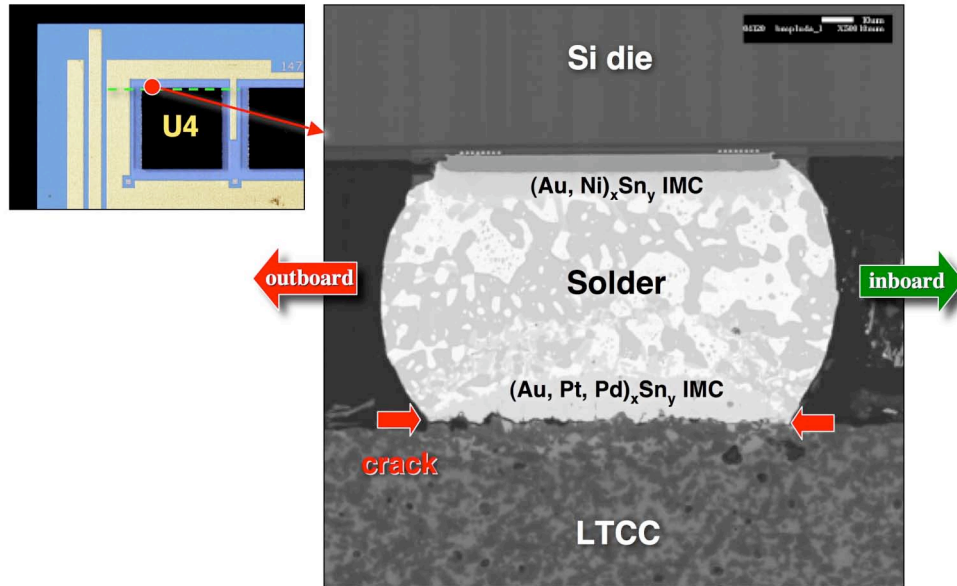


**Fig. 72** Stereo photograph identifying the location of the edge solder bump at the edge of the row on U04 of SF088 that underwent the burn-in treatment of 125°C, 282 hours and the SEM photograph of the solder joint in cross section.

The same pattern of cracking was observed for the solder joints of the U09 die, which was located on the bottom side of the module, using a similar orientation of the cross section. However, the magnitude of the cracks appeared to be reduced along the interfaces of the U09 joints when compared to similar joints on the U04 die.
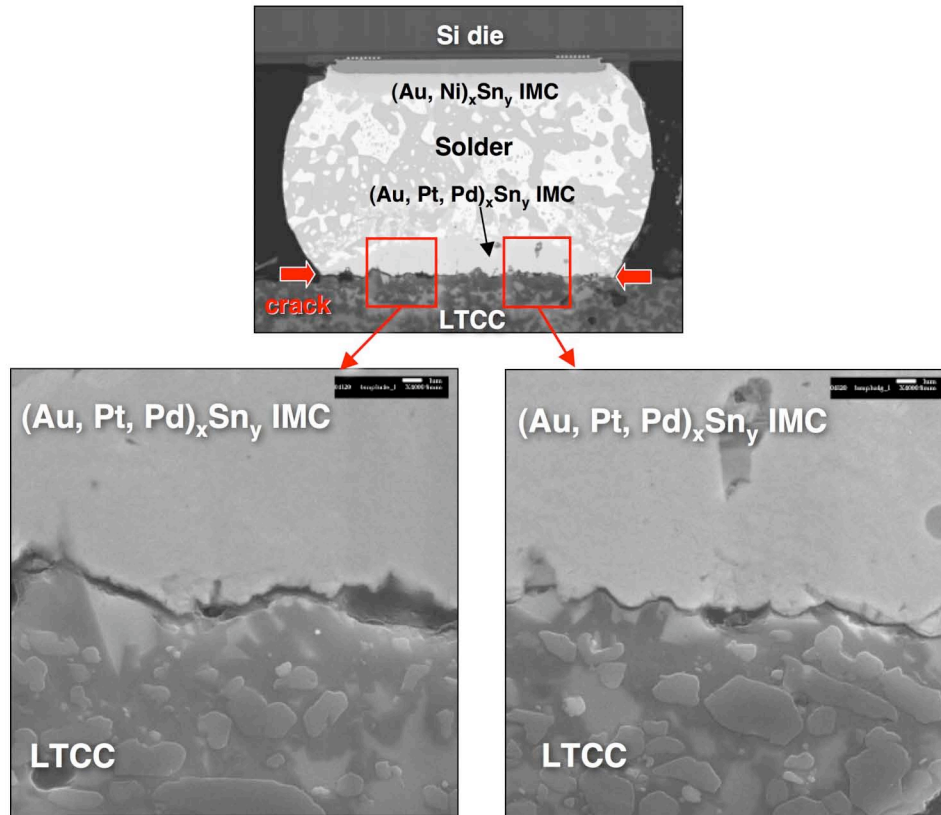
**Fig. 73** Low magnification SEM photograph of the U04 solder joint near the edge of the row, and high magnification images showing cracks along the $(Au, Pt, Pd)_x Sn_y$/LTCC interface.

The top and bottom side dice, U08 and U13, respectively, were cross sectioned in the direction of 90° to the row of solder joints. The intent of examining this orientation was tow-fold. First, the susceptibility of the solder joints to cracking would be assessed in this orientation for which, a dielectric layer covers that edges of the pads. Second, this orientation provides the opportunity to determine the robustness of the connection between the pad – now nearly completely converted to IMC following burn-in – and the conductor trace. As represented in Fig. 74, cracks were not observed at the TKN/LTCC interface or at the pad-to-trace junction. Thus, the cracks investigated in Figs. 72 and 73 were characteristic of the corner joints and, moreover, likely aggravated by the absence of the anchoring function of the dielectric layers over the thick film pads.
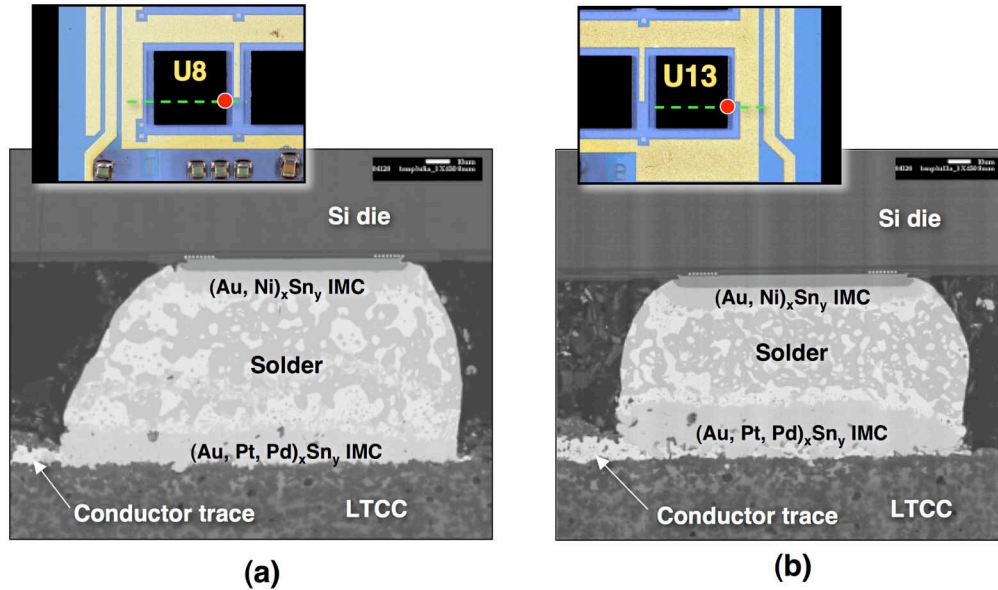
**Fig. 74** Low magnification stereo photographs and SEM images of the cross-die sections of solder joints on the U08 and U13 die from sub-module SF088. These sections provide a view of the junction between the pad and the conductor trace.

Two ancillary observations were made with respect to the SF088 solder joint microstructures. First, it was also noted that the $(Au, Pt, Pd)_x Sn_y$ IMC layer is thinner in the U08 solder joint (Fig. 74a) than is that of the U13 solder joint (Fig. 74b). At the same time, there is more thick film remaining in the latter case than in the former solder joint. This situation developed because the sub-module top side experiences two soldering process cycles. The first soldering cycle attaches the dice to the top side. The second exposure arises from and the soldering cycle used to attach the bottom side dice. Therefore, more of the thick film was dissolved into the Sn-Pb solder on the top side than on the bottom side. Now, under the burn-in conditions, there was more solid-state, IMC layer growth on the bottom side dice solder joints (Fig. 74b) due to the greater quantity of thick film material remaining there. That greater degree of solid-state IMC growth is indicated by the thicker, Pb-layer along the IMC/solder interface.

Secondly, it was noted that the $(Au, Ni)_x Sn_y$ IMC layer that formed at the Ni underbump layer of the Si UBM was slightly thicker on the top side joints than on the bottom side

interconnections.  This discrepancy arose from the fact that more of the thick film layer was dissolved into the solder in the top side solder joints than on the bottom side joints. A higher concentration of Au was available in the top side solder joints, which could then combine with Sn and Ni to form the $(Au, Ni)_x Sn_y$ IMC layer at the Si die side of the interconnections.

In summary, the sub-module SF088 was exposed to the burn-in conditions of 125°C, 282 hours.  The die were not underfilled in order to allow for performing pull strength tests.  The SF088 flip chip solder joints exhibited a reduced strength when compared to non-burn-in units having comparable pedigrees.  But, the strength loss was less than that associated with the low pull strength phenomenon.  Therefore, although it can be concluded that the conversion of the remaining thick film layer to $(Au, Pt, Pd)_x Sn_y$ IMC by its solid-state reaction with the Sn-Pb solder that generated the IMC/LTCC interface, probably contributed to a decreased pull strength.  However, because the magnitude of the latter strength loss less than that observed with the low pull strength phenomenon, the IMC/LTCC interface that formed by solid-state growth, was not a root-cause of the latter phenomenon.  Lastly, this assessment also lent evidence to the fact that development of an IMC/LTCC interface by solid-state diffusion processes does not necessarily predispose the interconnection to poor mechanical integrity or electrical failure.

A follow-on experiment was performed to further evaluate the integrity of the thick film pad/LTCC interface for the flip chip solder joints after sub-module burn-in.  The SF088 dice were not underfilled.  However, the flight assembly process call for underfilling of dice prior to burn-in.  Therefore, the objective of this study was to confirm that the presence of underfill does not cause interconnection failure as a result of the burn-in process.  Of course, with the dice underfilled, it was not possible to perform the pull test; thus, all materials analysis was performed via metallographic cross sections.

Two units, SF220 and SF264 were assembled with dice. The dice were underfilled.  Unit SF264 was subjected to the burn-in conditions of 125°C, 240 hours. The sub-module SF220 was not exposed to the burn-in treatment.  The dice of both sub-modules were cross sectioned according to the map in Fig. 75.   Each cross section included the dice on both the top and bottom side of the sub-module.  The sections #2 and #4 allowed for evaluating the junction between the pad and the trace.
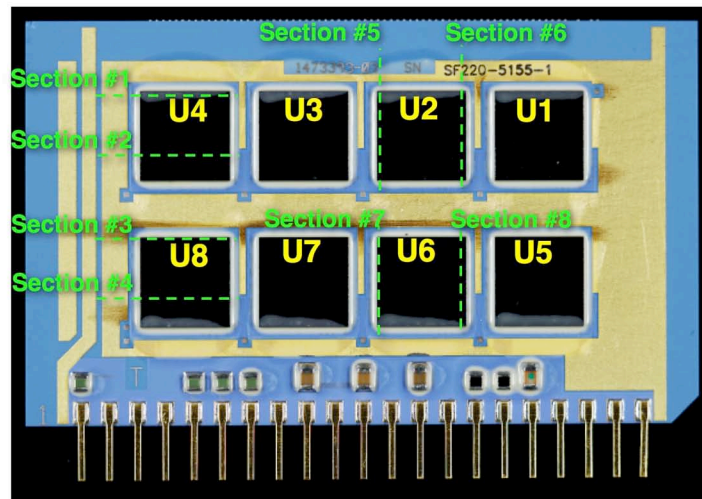


**Fig. 75** Stereo photograph showing the locations of the cross sections made to the dice on sub-module SF220 that was not exposed to the burn-in treatment.  The same locations were evaluated for sub-module SF264, which was exposed to the burn-in conditions of 125°C, 240 hours.

Shown in Figs. 76 and 77 are solder joints from the top and bottom dice, U02 and U13, respectively, of the burned-in sub-module, SF264. There were no indications of cracking at the interface between, what had become a $(Au, Pt, Pd)_x Sn_y$ IMC, and the LTCC substrate.  "Islands" of thick film were observed intermittently along the interface, as exemplified in Fig. 76.  In the case of the solder joint in Fig. 77, the entire thick film layer had been converted to IMC; yet, there were no indications of fracture along the interface.
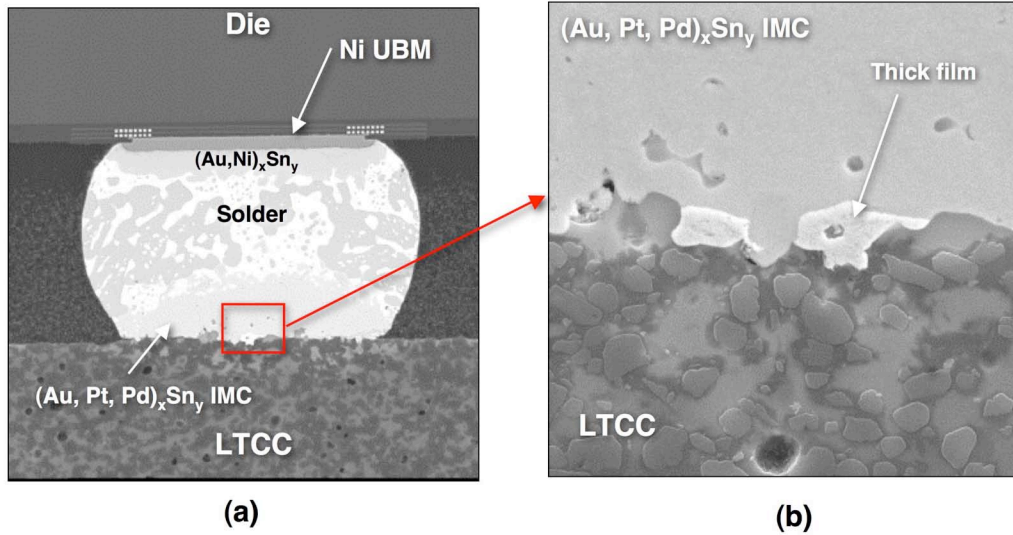
**Fig. 76** SEM photographs of the solder joint on U02 (top side) of the sub-module SF264 that was exposed to the burn-in conditions of 125°C, 240 hours: (a) low magnification view of the joint and (b) high magnification image of the interface between the $(Au, Pt, Pd)_x Sn_y$ IMC and the LTCC substrate.
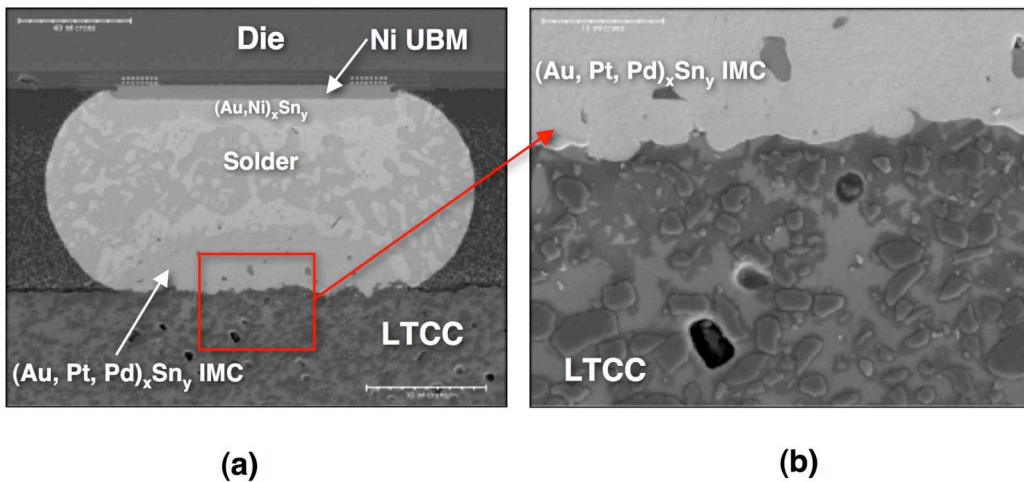


**Fig. 77** SEM photographs of the solder joint on U13 (bottom side) of the sub-module SF264 that was exposed to the burn-in conditions of 125°C, 240 hours: (a) low magnification view of the joint and (b) high magnification image of the interface between the $(Au, Pt, Pd)_x Sn_y$ IMC and the LTCC substrate.

The cross section #4 extended through the solder bump-plus-trace connection on U08 and U13, as well.  The SEM photographs in Fig. 78, which were taken of the U13 die solder joint, which showed that the solid-state IMC growth during burn-in did not cause a loss of interconnectivity between the pad and the trace.  Also, as noted in the previous micrographs, there was no loss of adhesion between the solder bump and the LTCC.



(a)                                        (b)
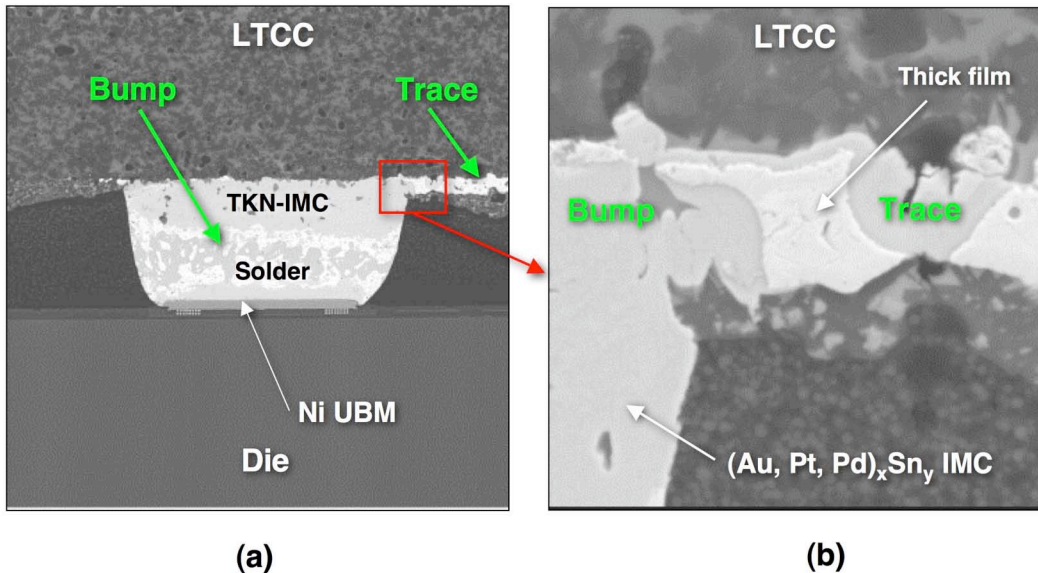
**Fig. 78** SEM photographs of a solder joint on U13 (bottom side) of the sub-module SF264 that was exposed to the burn-in conditions of 125°C, 240 hours: (a) low magnification view of the joint and (b) high magnification image of the junction between the pad and the trace showing good integrity there.

The same cross section analyses were performed on the solder joints of sub-module SF220 that had not been exposed to the burn-in treatment.  The corresponding die solder joints showed the lesser extent of IMC development and a good bond between the Au-Pt-Pd thick film and the LTCC interface.

In summary, a microstructural analysis was made of the solder joints of underfilled dice on sub-module SF264, which experienced burn-in at 125°C for 240 hours.  The sub-module SF220 provided the baseline unit as it was not exposed to the burn-in

conditions.  The burn-in conditions caused nearly complete consumption of the thick film into the $(Au, Pt, Pd)_x Sn_y$ IMC by solid-state reaction with the Sn-Pb solder.  The presence of underfill did not cause an observable crack damage to the interconnection structures.  These results indicated that the $(Au, Pt, Pd)_x Sn_y$ IMC that forms by solid-state growth is not responsible for the low-strength phenomenon and further evidence that the complete conversion of a thick film layer to IMC by solid-state reaction is not a life-limiting benchmark for such soldered thick film interconnections.

The assessment of the burned-in sub-modules has shown that there is satisfactory adhesion between the $(Au, Pt, Pd)_x Sn_y$ IMC and LTCC substrate.  However, burn-in is an isothermal aging process.  It was also necessary to evaluate the robustness of the solder joints and, specifically, the TKN/LTCC and IMC/LTCC interfaces under thermal cycling conditions, which are more apt to generate potentially damaging residual stresses within the interconnection structures.  The purpose of assessing thermal cycling residual stresses vis-à-vis finding the root-cause of the low pull strength phenomenon is that the latter appeared to be particularly accentuated after process monitors were exposed to the thermal cycling acceptance step.

Shown in Fig. 79 are two SEM photographs showing solder bumps on the test vehicle designated FCMSIP005.  This unit was exposed to 2800 thermal cycles of 0°C/100°C with 15 min hold times. The die in Fig. 79a was not underfilled while that in Fig. 79b had received the underfill material.  In terms of large-scale degradation to the interconnections, the image in Fig. 79a illustrated the extensive damage that was observed in these interconnections when underfill was absent.  The thermal mechanical fatigue cracks propagated along the boundary between the coarsened, Sn-rich phase and the remaining Sn-Pb solder. Conversely, there was no fatigue cracks in the underfilled solder joints (Fig. 79b).  In the latter case, there was considerable Sn-Pb solder coarsening, but uniformly throughout the solder volume.  This homogenous coarsening is an effect of only the elevated temperature exposure resulting from the thermal cycling condition.  The localized coarsening of the microstructure in Fig. 79a is a

*strain-enhanced* coarsening effect caused by fatigue deformation to the solder.  The comparison in Fig. 79 illustrates the higher strains (stresses) that are present in the solder joint that undergoes thermal mechanical (temperature cycling) fatigue in the absence of an underfill.



(a)　　　　　　　　　　　　　　　　(b)
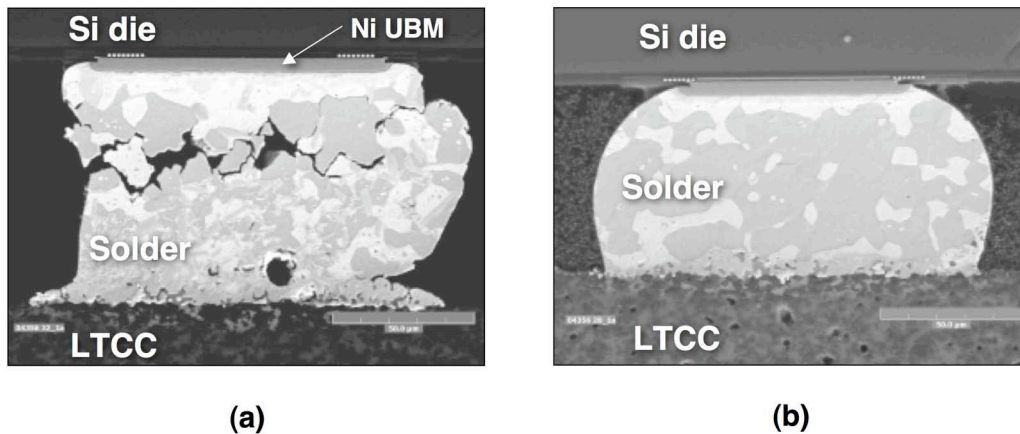
**Fig. 79** SEM photographs of solder joints from the test vehicle FCMSIP005 exposed to 2800 thermal cycles (0°C/100°C, 15 min hold times): (a) die without underfill and (b) die with underfill.

This analysis also has important implications in terms of determining a root-cause to the low pull strength phenomenon. The large number of thermal cycles caused nearly complete conversion of the Au-Pt-Pd thick film to $(Au, Pt, Pd)_x Sn_y$ IMC in both images in Fig. 79.  Yet, there was no cracking or separation at the IMC/LTCC interface of either case, particularly in Fig. 79a, in which the solder microstructure attests to the high degree to fatigue strain that was introduced into the joint.  Thus, these observations indicate that the IMC/LTCC interface is very robust and does not pose as a source of the low pull strength phenomenon. Lastly, there was no damage to the LTCC material immediately adjacent to the interface, which could be a potential contributing factor in poor pull strength performance.

A separate test vehicle, SCA083, was thermal cycled to an intermediate count of 1025 cycles and the *non-underfilled* dice subsequently cross sectioned for observation.

There was no evidence of significant microstructural damage to the solder joints, especially, with respect to the TKN/LTCC or IMC/LTCC interfaces.

Two sub-modules, SCA076 and SCA075 were assembled with dice that were all subsequently underfilled.   Those units were exposed to 7200 and 10800 thermal cycles (0°C/100°C, 15 min hold times), respectively.  Shown in Fig. 80 are SEM photographs that represent the microstructure of the solder interconnections from SCA075 (10800 thermal cycles).  The Au-Pt-Pd thick film has been completely consumed in the solid-state reaction that formed the $(Au, Pt, Pd)_x Sn_y$ IMC layer next to the LTCC substrate, except for a few isolated spots. The high magnification image in Fig. 80b illustrates the excellent integrity of the IMC/LTCC interface (and for that matter, the solder joint as a whole).  There were no indications of cracking or separation along the interface or damage within the LTCC material adjacent to the interface. Similar observations were compiled from cross sections of flip chip solder joints on the sub-module SCA076 that was exposed to 7200 cycles.



(a)                                   (b)
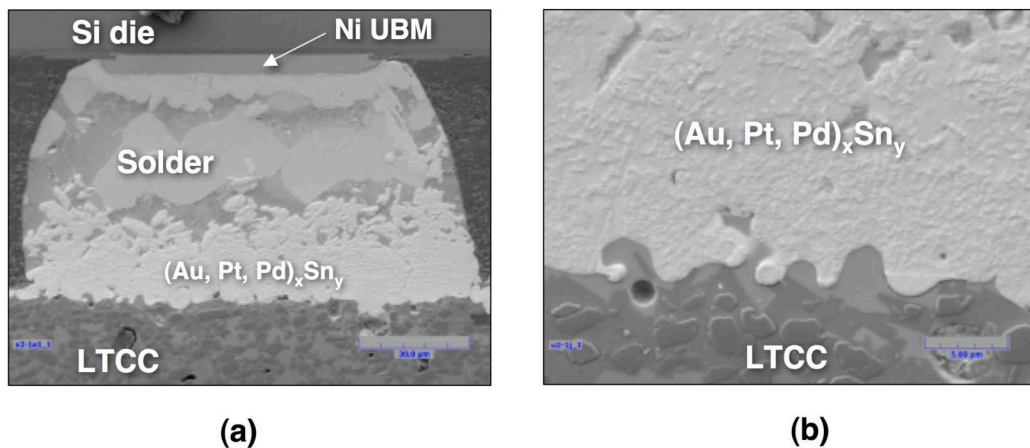
**Fig. 80** (a) Low magnification and (b) high magnification SEM photographs of a representative solder joint from the test vehicle SCA075 exposed to10800 thermal cycles (0°C/100°C, 15 min hold times).  The die were underfilled after assembly.

It is important to further consider the data illustrated by Figs. 79 and 80, as well as the observations made of sub-modules SCA083 and SCA076 with respect to solder and interface strengths. The solder joints of each of these sub-modules demonstrated considerably *longer* accelerated aging lifetimes than would have been predicted by modeling techniques.  It was surmised that this added life was caused by a strengthening mechanism – solder-solution strengthening, precipitation hardening, or a combination of the two mechanisms – through the dissolution of Au, Pt, and Pd thick film elements into the Sn-Pb solder.  In the context of a low pull strength mechanism, the strengthening process would have certainly added stress to the interface between the solder and the LTCC substrate.  The fact that cracks were not observed at the TKN/LTCC interface, which became an IMC/LTCC interface, provided further evidence of its high strength and the *unlikelihood* that this interface, when generated by the solid-state reaction between the solder and Au-Pt-Pd thick film, would be a root-cause of the low pull strength phenomenon.

The above results were considered in the context of process monitor thermal cycles. First, because the solid-state reaction rate kinetics are very slow between the Au-Pt-Pd thick film alloy and Sn-Pb solder, the extent of solid-state IMC reaction is very small during the twenty (20) thermal cycles (-55°C/125°C) when compared to the above cases of isothermal aging (burn-in) and long term thermal cycling[14].  Therefore, the extent of IMC/LTCC interface will also be very minimal.

Secondly, there was a decrease of pull strength that typically followed thermal cycling and was accompanied by an increased frequency of the TKN/LTCC failure mode. Accordingly, the decreased pull strength was not caused by fatigue of the solder in the joint.  Rather, residual stresses that were generated by the thermal cycles and *not* solid-state IMC growth, caused the nominal decrease of solder joint strength.  But, the fact that this strength loss was relatively constant, even when the low pull strength was already observed in the as-fabricated condition, indicates that this thermal cycling "degradation mechanism is separate from that responsible for the low pull strength

phenomenon. Also, the fact that the low pull strength phenomenon was measured in the as-fabricated condition and not further "amplified" by thermal cycling, further confirms that the two consequences of thermal cycling: (a) increased IMC/LTCC interface and (b) a residual stress degradation process were not responsible for the low pull strength phenomenon.

Earlier in this study, it was concluded that the low pull strengths could not be attributed, explicitly, to the TKN/LTCC interface generated by the post-process used to manufacture the *sub-floors*.  The analysis just concluded above, indicated that residual stresses and the conversion of the Au-Pt-Pd thick film to IMC by solid-state aging were not responsible for the low-pull strength phenomenon. By elimination, it appears that *the low pull strength phenomenon is, to a first-order, a consequence to the TKN/LTCC interface upon the formation of the solder joint and then, to a second-order, dependent upon the microstructure of the thick film layer*.

The metallographic cross section analysis continued, examining the TKN/LTCC interface flip chip solder joints from dice that experienced both acceptable and low pull strengths.  The analysis included sub-modules that were in either the as-fabricated or post-thermal cycled condition, since the root-cause of the phenomenon would be present in either case.

This analysis began with the sub-modules SF1155 and SF1168. The SF1155 sub-module was exposed to the process monitor procedures.  The pull tests data from SF1155, which are listed below, were separated into top side and bottom side values:

**SF1155 (test date, 10/03/05):**
- As-fabricated:        Top side: 6.49±0.82 lb;      Bottom side: 5.50±1.88 lb
- Thermal cycled:      Top side: 3.48±0.93 lb;      Bottom side: 2.75±0.91 lb

The as-fabricated pull strengths were very low, and decreased further after thermal cycling.  Higher pull strengths were measured on the top side dice, which reverses the earlier, opposite trend, A second sub-module, SF1168, was assembled in order to verify the poor performance of SF1155.  The results of the as-fabricated pull tests are shown below:

**SF1168 (test date, 10/03/05):**

- As-fabricated:        Top side: 1.87±0.22 lb;      Bottom side: 1.21±0.29 lb

The as-fabricated pull strengths were so poor that the SF1168 sub-module was not exposed to the thermal cycling treatment.  Instead, the remaining dice were subjected to cross section metallographic analysis.

Shown in Fig. 81 are stereo photographs of top side and bottom side of SF1168.  The locations of the cross sections are indicated in the images.



(a)                                                  (b)
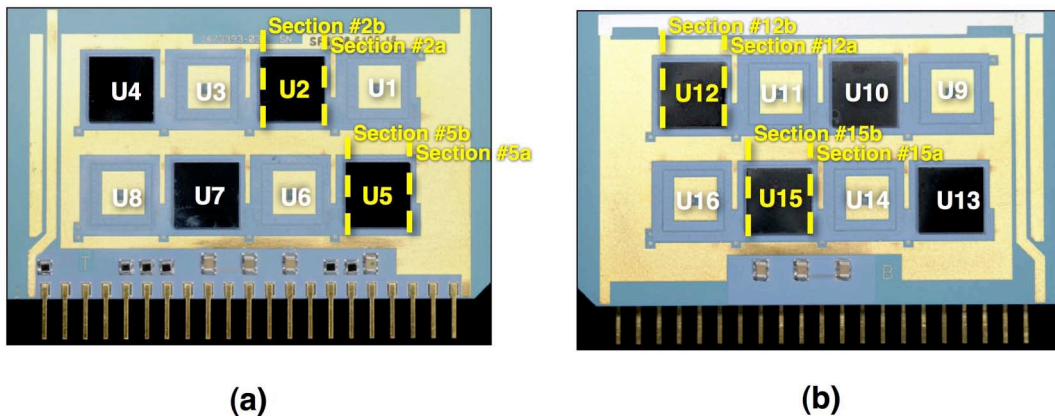
**Fig. 81** Photographs of sub-module SF1168 showing (a) the top side and (b) the bottom side after dice were pull tested in the as-fabricated condition.  The remaining were used for metallographic cross sections, the positions of which, were denoted by the labels and dashed lines.

Each of the individual solder joints was examined per cross section. Shown in Fig. 82a is a low magnification image of a solder bump from section 2, die U02 (top side). A crack is observed all of the way along the TKN/LTCC interface. The high magnification image in Fig. 82b shows that the precise location of the crack is between a reaction layer (in red) and the LTCC substrate. A large number of the solder joints in this cross section, albeit not all of them, exhibited this reaction layer. Also amongst those that exhibited the reaction, not all of them experienced a crack such as that shown in Fig. 82.



(a)                                                    (b)
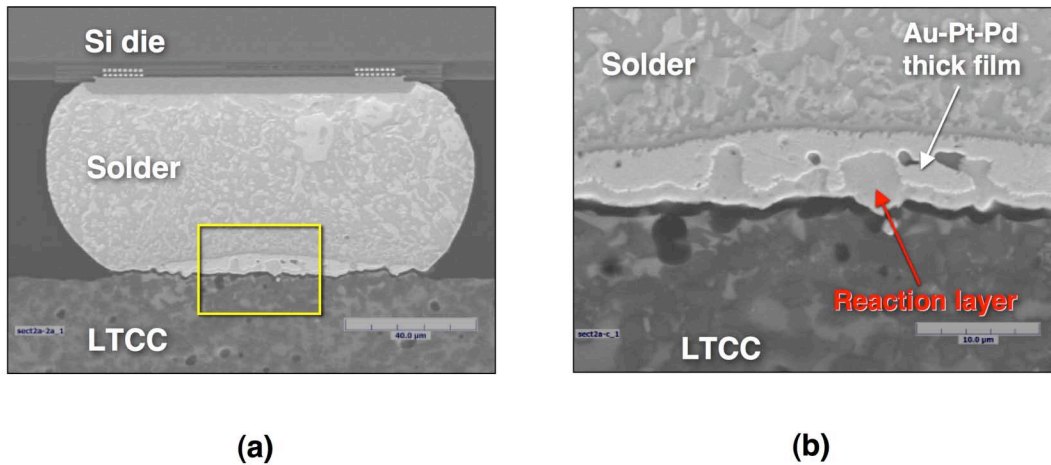
**Fig. 82** (a, b) Low and high magnification, SEM photographs showing a solder joint on U02 (top side, section #2) of sub-module SF1168.

By comparison, shown in Fig. 83 are SEM photographs of a solder joint that did not exhibit the presence of the reaction layer in the cross section view. Also, a crack was absent from the TKN/LTCC interface.

Of course, a direct correlation between the low pull strength and a reaction layer at the TKN/LTCC interface could only be inferred from Figs. 82 and 83 because the dice were not, themselves, pull tested. In order to draw such a correlation, metallographic cross sections were also performed on the pull tested dice. Shown in Fig. 84 is an SEM image of solder joint #24 of die U11 that was from the bottom side of SF1168. This die

was pull tested and the fracture path was at the TKN/LTCC interface.  This die had a very low pull strength of 0.98 lb.  The reaction layer is clearly visible in the higher magnification images.

By comparison, the SEM images in Fig. 85 show the TKN/LTCC fracture of the #2 solder joint on the U01 die from the top side of SF1155.  The pull strength of this die was very good at 7.26 lb.  The reaction layer was not observed at the interface.



(a)                                                    (b)
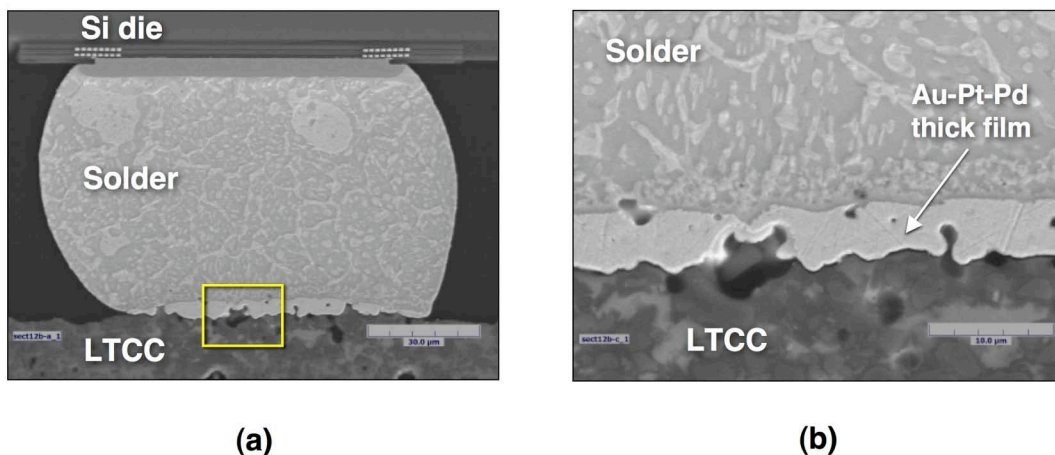
**Fig. 83** (a, b) Low and high magnification, SEM photographs showing a solder joint on U12 (bottom side, section #12) of sub-module SF1168, which did not exhibit the reaction layer between the TKN and LTCC nor crack development there.

The SEM images in Figs. 84 and 85 were examples of a *general* correlation between pull strength and the presence of the reaction layer in all of the cross sections of SF1155 and SF1168.  There were specific instances to the contrary, that is, the solder joints of dice having relatively low pull strengths but for which, the metallographic cross section plane did not show the reaction layer and visa-versa.  These occurrences were attributed to an apparent variability of the reaction layer to be present as a function of location of the cross section plane location in the solder joint as well as solder joint-to-solder joint differences per individual dice.
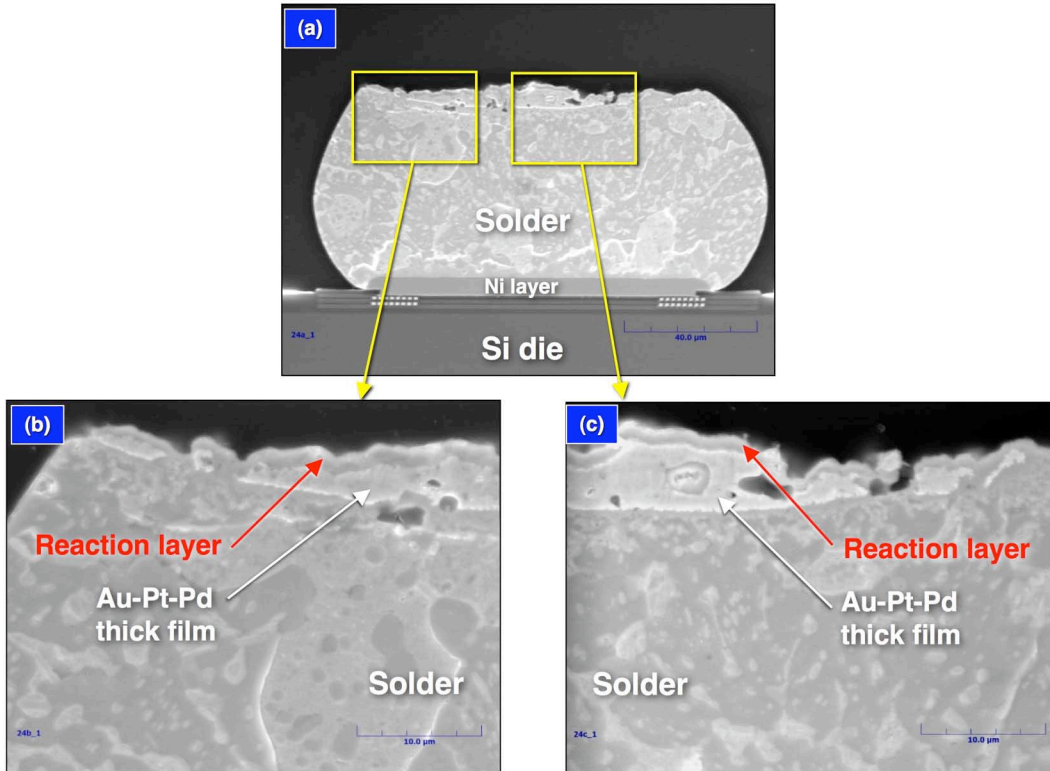
**Fig. 84** (a) Low and high magnification, SEM photograph of solder joint #24, die U11 that was pull tested from bottom side of sub-module SF1168.  The pull strength of the die was 0.98 lb.  (b, c) High magnification images of the TKN/LTCC failure mode, showing the reaction layer that would have be located between the thick film and LTCC substrate.



(a)                                                                (b)
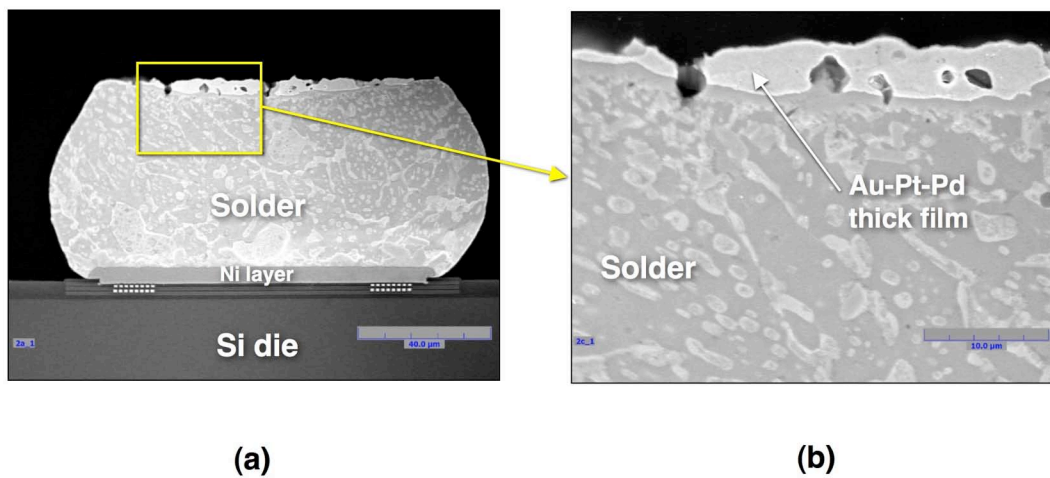
**Fig. 85** (a, b) Low and high magnification, SEM photograph of solder joint #2, die U01 that was pull tested from the top side of sub-module SF1155.  The pull strength was 7.26 lb.

Metallographic cross sections were used to assess the TKN/LTCC interface left on pull-tested solder joints of a second group of sub-modules that exhibited low strength values.  The sub-modules were SF1159, SF1249, SF1419, SF1204, and SF1392.  Their pull strength values are listed below:

**SF1159 (test date, 10/25/05):**

- As-fabricated:     Top side: 5.41±1.13 lb;     Bottom side: 5.64±0.82 lb
- Thermal cycled:     Top side: 0.71±0.34 lb;     Bottom side: 0.86±0.56 lb

**SF1204 (test date, 12/15/05):**

- As-fabricated:     Top side: 2.22±0.98 lb;     Bottom side: 2.63±0.25 lb
- Thermal cycled:     Top side: 0.65±0.21 lb;     Bottom side: 0.40±0.27 lb

**SF1249 (test date, 10/25/05):**

- As-fabricated:     Top side: 8.22±0.51lb;     Bottom side: 7.82±1.27 lb
- Thermal cycled:     Top side: 2.85±1.87 lb;     Bottom side: 3.90±1.53 lb

**SF1392 (test date, 11/18/05):**

- As-fabricated:     Top side: 6.87±1.83 lb;     Bottom side: 4.18±0.68 lb
- Thermal cycled:     Top side: 4.23±0.45 lb;     Bottom side: 0.99±0.27 lb

**SF1419 (test date, 11/18/05):**

- As-fabricated:     Top side: 9.62±0.44 lb;     Bottom side: 8.44±0.10 lb
- Thermal cycled:     Top side: 9.92±2.15 lb;     Bottom side: 9.15±1.17 lb

The worst case, SF1204, is presented in red.  The best pull strength results were obtained from SF1419, which are shown in green.  In terms of the sequence of sub-modules, the pull strength performance initially worsened from SF1159 to SF1204.

(SF1204 exhibited the worst pull strength performance of any sub-module tested within this program.)  Then, an improvement trend was observed.  The sub-modules SF1249 and SF1392 exhibited increased, as-fabricated pull strengths.  Unfortunately, their post-thermal cycled strengths remained low.  Then, there was sub-module SF1419 that exhibited excellent pull strengths for both the as-fabricated and post-thermal cycled conditions.  Lastly, it was also noted that, amongst the five sub-modules above, there was no consistent difference between top side and bottom side pull strengths nor was a trend attributed to the test date.

A comparison was made between the individual die pull strength and the presence of the reaction layer at the TKN/LTCC interface as viewed by the SEM images of the post-pull test solder joint.  The presence of the reaction layer was based upon qualitative observations. Those observations and strength values are listed below:

**SF1159 (test date, 10/25/05):**
- As-fabricated: Top side, U03 (7.03 lb): No reaction layer
  Top side, U08 (4.68 lb): Slight reaction layer
- Thermal cycled: Bottom side, U12 (0.27): Slight reaction layer

**SF1204 (test date, 12/15/05):**
- Thermal cycled: Top side, U02 (0.49 lb): Significant reaction layer

**SF1249 (test date, 10/25/05):**
- As-fabricated: Bottom side, U11 (9.40 lb): No reaction layer
- Thermal cycled: Bottom side, U10 (5.94 lb): No reaction layer
Bottom side, U15 (3.04 lb): No reaction layer

**SF1392 (test date, 11/18/05):**
- As-fabricated: Bottom side, U09 (4.90 lb): Moderate reaction layer

- Thermal cycled:     Bottom side, U10 (10.21 lb): No reaction layer

A similar compilation was made for the sub-modules SF1168 and SF1155.  Those results complimented the data listed above.  As a result of these analyses, it appeared that the reaction layer was present for pull strengths below approximately 3.00 lb.  The layer was absent for pull strengths exceeding approximately 5.00 lb.  Between these two limiting cases, a definitive correlation could not be rendered.

*4.2 Electron probe microanalysis*

Electron probe microanalysis (EPMA) was used to identify the composition of the reaction layer.  Line traces were taken across the interfaces of joints that did not have a crack.  Cracks or "edges" tend to distort the quantitative numbers generated by the EPMA technique, which was already a challenge because the reaction layer was very thin.  Therefore, the EPMA was performed on the non-pull tested solder joints.

In order to facilitate the making of comparisons between the different cases discussed below, the following conditions were imposed on the EPMA trace plots shown in the figures.  The x-axis of was maintained at a total length scale of 20 $\mu$m with intervals of 5 $\mu$m. There were between five and seven traces made across each joint.  Thus, the observations stated below, although referencing a single trace in a figure, were compiled from examining all of the traces of each case.

The spatial resolution of the EPMA trace is ±1 $\mu$m due as determined by the sampling volume from which come the x-rays used for composition measurements.  Therefore, in the case of features (layers, particles, etc.) having spatial dimensions of less than 2 $\mu$m, there is an increased error in the quantitative elemental concentrations.  However, qualitative evaluations can still have significance..

Shown in Fig. 86 is an EPMA trace that was taken across the solder joint from the sub-module SF1168 die.  Recall that SF1168 showed very low pull strengths (Top side: 1.87±0.22 lb; Bottom side: 1.21±0.29 lb) in the as-fabricated condition. However, this particular cross section (die U02, joint #7, trace 4) did *not* exhibit the reaction layer at the TKN/LTCC interface.  Thus, this trace served as the baseline case. The thick film layer is denoted by the 7 – 8 *μ*m wide region of Au, Pt, and Pd signals at 76, 18, and 6 at.%, respectively, between approximately 24 *μ*m and 30*μ*m on the x-axis.
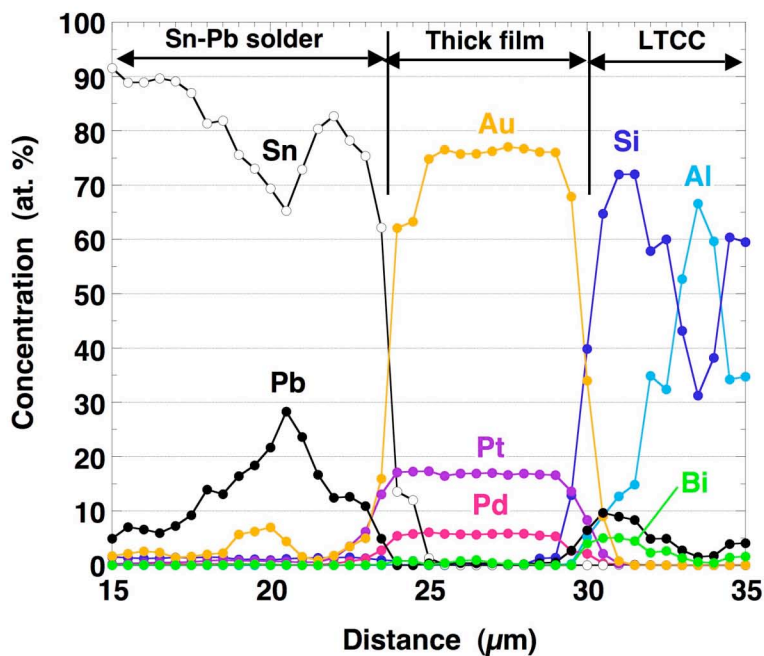


**Fig. 86** EPMA trace across the solder joint from the sub-module SF1168 die, which did *not* show the TKN/LTCC interface reaction layer (U02, joint #7, trace 4).  This trace served as a baseline case.

The LTCC substrate is to the right in the trace, indicated by the Si and Al signals. The Si and Al elemental signals actually indicate the alumina and silicate glass phases of the LTCC material.  The silicate glass phase surrounds the alumina grains.  The solder field is to the left of the Au-Pt-Pd thick film layer as denoted by the Sn and Pb signals.

The Bi and Pb signals exhibited small peaks just within the LTCC material. These peaks likely originated the Bi-O and Pb-O glassy phases of the thick film. The glassy phases diffused to the interface to provide adhesion between the Au-Pt-Pd conductor of the thick film and LTCC substrate. The Pb-bearing glass was also a modifier to the silicate glass in the LTCC substrate; hence, its signal continued at an elevated level further into the LTCC substrate. The Pb peak did *not* originate from the solder.

The EPMA trace in Fig. 87 was taken across a different solder joint of the U02 die from sub-module SF1168. In this case, the TKN/LTCC interface exhibited the reaction layer, which is identified in the figure. The reaction layer had high concentrations of both Sn and Pb. At these levels, the Sn and Pb originated primarily from the molten solder. The
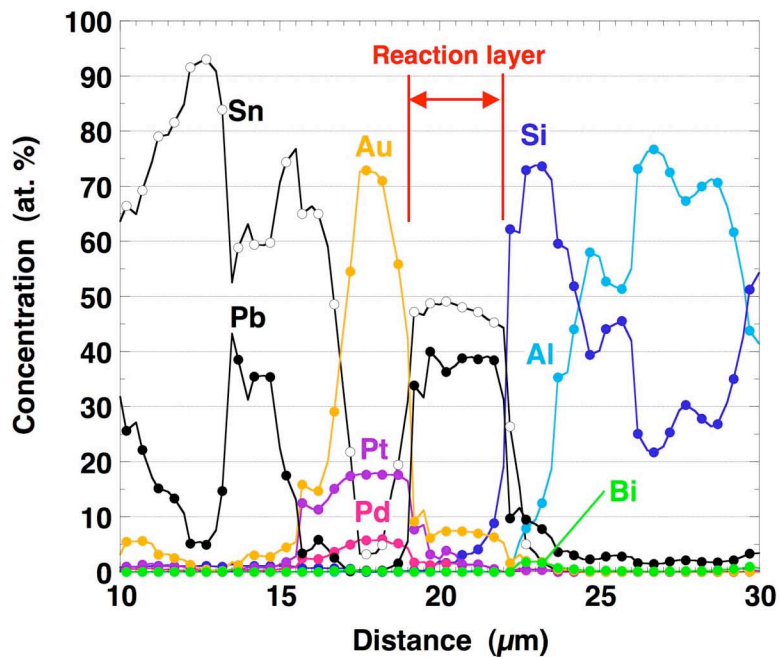


**Fig. 87** EPMA trace across the solder joint from the sub-module SF1168 die, which did show the reaction layer at the TKN/LTCC interface (U02, joint #3, trace #2).

presence of solder constituents is due to the 3-D structure of the porous thick film, which allowed the molten solder to permeate to the interface, in this case, from an out-of-plane

direction. However, the proportion of Sn and Pb did not duplicate that of bulk solder composition.

The EPMA trace in Fig. 87 also showed the reaction layer to be comprised of a significant Au signal and lesser Pd and Pt signals. These presence of these elements may have resulted from dissolution of the thick film by the molten solder as it flowed to the TKN/LTCC interface. The concentrations of Au, Pt, Pd, and Sn were close to stochiometric ratios of $(Au, Pt, Pd)_x Sn_y$ IMC; however, the strong presence of Pb throughout the reaction layer precluded the expressed presence of the IMC.

The Pb peak associated with the Si signal of the LTCC was still present (centered at the $22 - 23\,\mu$m location on the x-axis), albeit, cut off by the newly formed reaction layer. There was very little evidence of the Bi peak. It was noted that the Si signal tapered off into the reaction layer in a considerably more gradual manner than was observed for the TKN/LTCC interface in Fig. 86. This behavior suggested that there was a small degree of interdiffusion between the reaction layer and the Si-based glassy phase already present at the interface.

The EPMA trace in Fig. 87 represented one of the two bounding conditions of the reaction layer chemistry, that condition being where there are comparable signals of Pb an Sn. The other bounding condition is shown in Fig. 88 in which the Sn content of the layer was at a very high value and the Pb concentration was very low. This predominant condition was more like this latter case, that is, the Sn peak dominating the Pb signal. Gold and to lesser degrees, Pt and Pd, were present in the reaction layer, but at concentrations that were too low to confirm the $(Au, Pt, Pd)_x Sn_y$ IMC stochiometry. Bismuth was absent from the layer. There was a significant presence of Si in the layer (similar to Fig. 87). Therefore, the reaction layer was a combination of the solder elements, thick film metal, and glassy phase contributed by the thick film, the LTCC, or both.
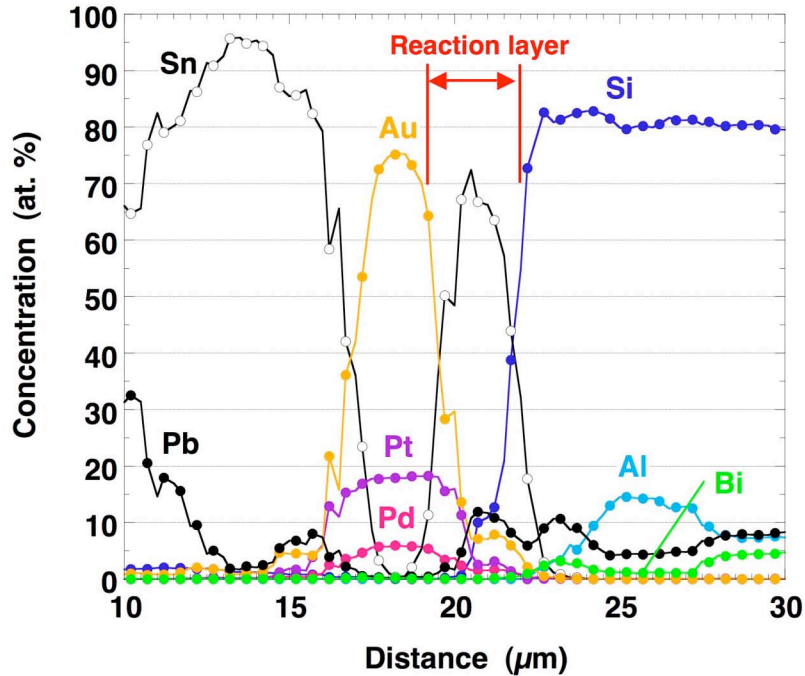
**Fig. 88** EPMA trace across the solder joint from the sub-module SF1168 die, which did show the reaction layer at the TKN/LTCC interface (U02, joint #3, trace #2). In the case, the reaction layer had a far greater concentration of Sn in that layer.

The reaction layer appears to have been created by a reaction between the molten solder – primarily, the Sn component and lesser presence of the Pb component – and the glassy phases present at the TKN/LTCC interface. The correlation between the reaction layer and low pull strength phenomenon would support those findings of earlier investigators that indicated that Sn degraded the adhesion performance of the thick film glassy phase [3 – 8].

However, it was noted earlier that there were solder joints in aged samples (isothermal annealing and extensive thermal cycling) in which the thick film metal was fully consumed by the solid-state reaction between it and the Sn component of the solder, resulting in formation of an IMC. Under this circumstance, Sn would also be in close proximity to the glassy phase layer, albeit, as a component of an IMC. Thus, it became

174

necessary to determine if a reaction layer was associated with the IMC layer or that it (the reaction layer) formed by a process that was separate from the IMC reaction.

The EPMA traces were taken across the interfaces of solder joints on the sub-modules SCA076 and SCA075.  These two sub-modules were exposed to very long-term temperature cycling between 0°C and 100°C for 7200 and 10800 cycles, respectively. In the case of SCA076 solder joints, the thick film was completely consumed in the formation of the $(Au, Pt, Pd)_x Sn_y$ IMC at nearly every location in all of the solder joints. The thick film layers were *completely* consumed for IMC formation of all SCA075 solder joints (post 10800 cycles).  (Because the flip chips on both SCA076 and SCA075 were underfilled, pull tests were not performed on them so that strength values could not be obtained from these sub-modules.)

Shown in Fig. 89 is the EPMA trace taken across the TKN/LTCC interface of a solder joint form SCA076 (7200 thermal cycles).  The thick film was consumed by formation of a $(Au, Pt, Pd)_x Sn_y$ IMC.  The IMC/LTCC interface is characterized by continuously decreasing Sn signal (as well as Au and Pt signals). There was no significant *peak* of Sn (or Pb) at the interface that was characteristic of the reaction layers of Figs. 87 and 88.  (Note: The x-axis scales are the same in all three figures.)  The increasing Al signal and small Si peak are a result of the glassy phase that provides adhesion, which then transitioned into the bulk LTCC material  film because an alumina grain is situated directly at the interface in this trace.

A direct comparison was provided in Fig. 90.  The EPMA trace from SF1168, which was shown in Fig. 88, is reproduced in Fig. 90a.  The Sn signal peak indicates the reaction layer.  Shown in Fig. 90b is the EPMA trace from SCA075 (U04, joint #3, trace #2, 10800 thermal cycles).  Instead of a Sn peak, there is a gradually decreasing Sn signal (and similarly decreasing Au, and Pt signals).  The decreasing Sn signal, together with the increasing Al and Si signals indicated the glassy phase and transition into the LTCC

material.  There are no indications of the reaction layer similar to that in Fig. 90a, which formed as a consequence of solid-state IMC development.
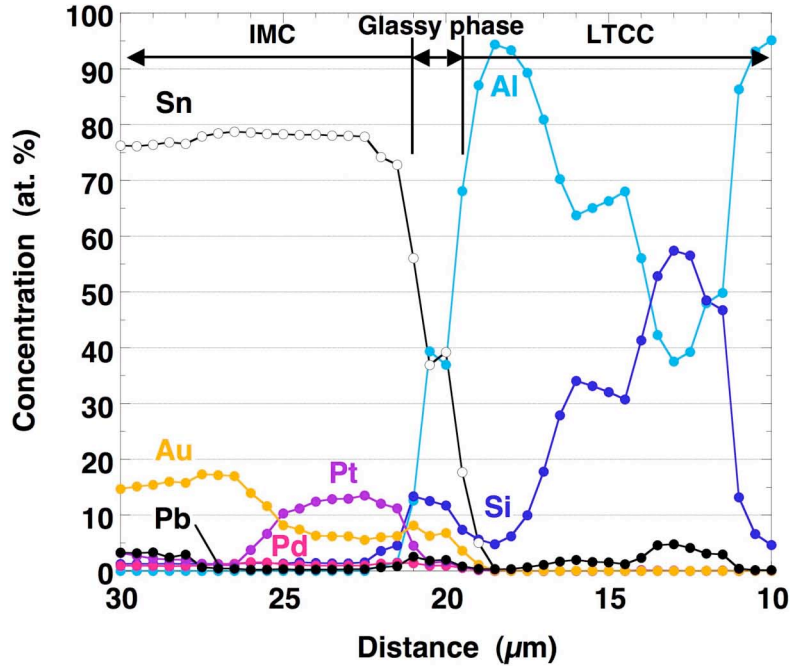


**Fig. 89** EPMA trace across the solder joint of a die from the sub-module SCA076 (joint C; Trace 3), which was exposed to 7200 thermal cycles (0°C/100°C).  The glassy phase is indicated by the small Si peak.

An interim summary is compiled of the microstructural results described above. It was observed that those solder joints associated with die exhibiting the low pull strength phenomenon, were more likely to exhibit a reaction layer at the TKN/LTCC interface. The reaction layer was comprised Sn and Si plus, to lesser extents, Pb, Au, Pt, and Pd. In most cases, the Sn peak was the dominant element; the presence of Si indicated a role had by the glassy phase adhesion layer in the development of the reaction layer. The source of the Sn (and Pb) was the *molten* Sn-Pb solder present during the
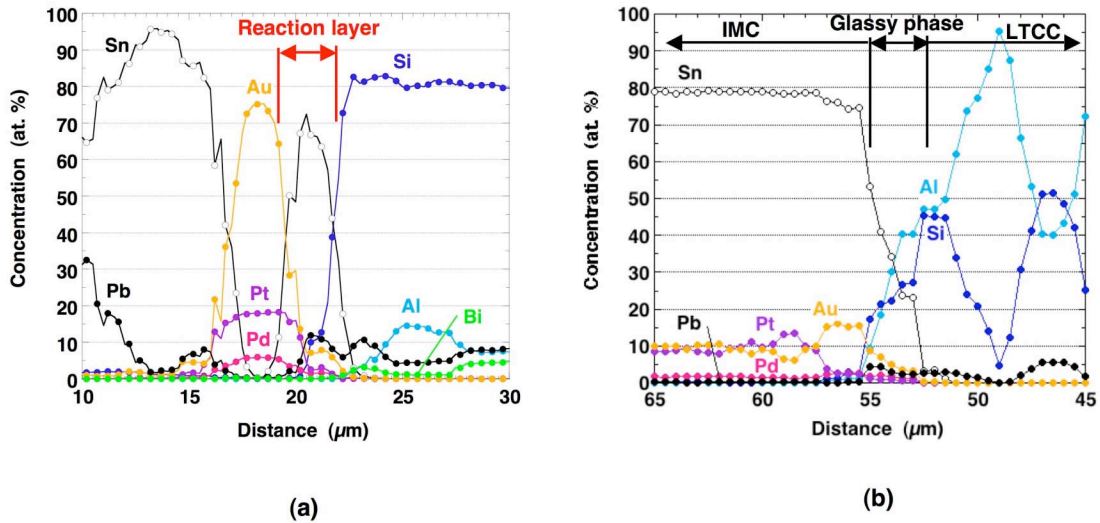
**Fig. 90** (a) EPMA trace across the TKN/LTCC interface of a solder joint of a die from the sub-module SF1168 (joint 3; Trace 3) that exhibited the reaction layer. (b) EPMA trace across the IMC/LTCC interface of a solder joint (Die U04, joint 3; Trace 2) of SCA075 was exposed to 10800 thermal cycles (0°C/100°C). The TKN was fully consumed by solid-state IMC growth.

assembly process. Therefore, this microstructural evidence shows that the root-cause of the low pull strength behavior was degradation to the glassy phase at the TKN/LTCC interface due to contact between the molten solder and the glassy phase (Si) that resulted in the appearance of a newly-formed reaction layer. It was hypothesized earlier that the thick film microstructure had a second-order role in the low pull strength phenomenon. Per the current mechanism, that role was that the thick film microstructure controlled the ability of the molten solder to reach the TKN/LTCC interface and then, to create the reaction layer.

*4.3 Root-cause hypothesis development*

The studies in references [3 – 8] concluded that the degradation mechanism of Sn in terms of thick film strength was that it weakened the bond between the metal component of the thick film and the interface glassy phase. That mechanism does not appear to be the case here because the low strength phenomenon appears to be

caused by a weakening of the interface between the thick film layer and the LTCC substrate due to formation of the reaction layer.

The reaction between Sn and silica glass is well-known – e.g., the "float glass" process. Here, the molten soda lime-silica glass is poured on a bath of molten Sn, allowing the Sn to diffuse into the glass [15]. Although the BDYE solder assembly process certainly does not include temperatures commensurate with those of molten glass, the fact that the Sn is molten increases the potential reaction with the glassy phase of the thick film (and silica component of LTCC). As alluded to in reference [15], the possible consequence of a reaction between the Sn is partial crystallization of the $SiO_2$ glass phase due to valence changes caused by diffusion of Sn ions into material. The crystallization process can lead to an increased brittleness of the glass that leads to the low pull strengths.

As noted above, the analysis also showed that the development of the reaction layer varied within the same solder joint as well as between different interconnections on the same die. This variability was a consequence of subtle differences in the microstructure of the thick film layer, which perhaps were amplified by the layers being very thin. (The term, "microstructure" rather than porosity is used to refer to the role of the thick film layer on the pull strength because, as was demonstrated in the study that compared performances between the DuPont™-fired sub-floor versus Scrantom-fired sub-floor, porosity may not be, explicitly, the controlling factor in the pull strength performance of the solder joints.) The suspect variations of the thick film layer microstructure that controlled contact between the molten solder and glassy phase were not made apparent by microanalysis techniques (SEM, Auger electron spectroscopy, metrology, or EPMA). At a higher level, experiments have further indicated that, whatever those variations may be, they could not be readily controlled by material pedigrees, post-process firing steps, or the soldering assembly process. Thus, the low pull strength phenomenon did not occur consistently across the sub-modules built from the same sub-floor lot, causing

the "process monitor" (pull strength) approach to be ineffective at screening for this phenomenon at the sub-floor (LTCC) lot level.

It did appear that the low pull strength phenomenon occurred with a measure of consistency across the dice on a given sub-module. The consistency improved when dice were further descretized according to top side and bottom side. Therefore, those small variations of thick film microstructure that allowed for, or prevented, the occurrence of the reaction layer responsible for the low pull strength phenomenon, were sensitive to top side versus bottom side cases. But, again, microanalysis could not decipher the source(s) of the difference(s) to the thick film microstructures.

If it is assumed that the LTCC post-process firing conditions remained relatively consistent, particularly for a lot of sub-floors that would have been processed at the same time, then the source of the thick film variations can be narrowed down to the thick film ink printing process. Previous pad height studies ruled out the thick film pad thickness as an explicit factor. Instead, it is proposed, here, that the variations of thick film microstructure occurred by the following scenario: During the printing process, the percentages of deposited metal and glassy phase components was not reproducible. Furthermore, given the somewhat consistent behaviors at the sub-floor top and bottom sides, it is suspected that variations in the thixotropic properties of the ink were responsible for the variations in metal and glassy phase percentage. This inability to reproducibly deposit the same percentages of metal and glassy phase caused variations to the post-fired, thick film pad microstructure. The non-reproducibility of the thick film ink composition was a consequence of the printing of the very thin layers being highly sensitive to variations in the thick film ink thixotropic properties, irrespective of whether those variations of thixotropic properties were controllable or uncontrollable, that is, in the latter case, simply inherent to the ink technology.

# 5.0 Analysis of Process Monitors of Sub-floor Lot #33

A brief synopsis is compiled below, which describes pull strength performance of sub-modules build from sub-floor LTCC lots #29 – #32.

- The process monitors SF1591 and SF1608 for Flight 11, which were built from **lot #29** sub-floors, exhibited excellent strength performance (Fig. 46a).

- However, the sub-modules SF1660 (Flight 12) as well as SF1659 and SF1662 (both Flight 13) built from **lot #30** material exhibited very disappointing pull strength behavior.

- Similar, poor pull strengths were observed for sub-modules built of **lot #31** sub-floor LTCC material (Fig. 47a): SF1731 and SF1751 (Flight 14) as well as SF1726 and SF1742 (Flight 15).

- Then, the pull strength behavior improved for sub-modules built from **lot #32** sub-floors. The process monitors SF1802 (Flight 16) and SF1815 (Flight 17) exhibited excellent pull strength performance as shown in Fig. 47a.

Metallographic cross sections were not performed on sub-module process monitors from these lots #29 - #32. It was not anticipated that the results would differ from those obtained from the previous, extensive cross section efforts.

The next sub-module process monitor was SF1824 for the Flight 18 hardware, which was built from LTCC sub-floor lot #33 material. The pull strength values are shown below:

**SF1824 (test date, 6/7/07):**
- As-fabricated:       Top side: 7.96±0.52 lb;       Bottom side: 8.31±1.88 lb
- Thermal cycled:      Top side: 4.78±1.72 lb;       Bottom side: 6.27±0.67 lb

The SF1824 passed the as-fabricated, pull strength specification, showing higher pull strengths on the bottom side dice than the top side, which was also the prevalent pattern for lots #29 - #31.  There was evidence that the bond pad footprint on two of the four sides of the solder bump rows were smaller on the top side than on the bottom side, which may have accounted for the slightly lower pull strengths there.  However, after thermal cycling, low die pull strengths on the top side caused the overall strength metric to fall below the acceptance level (red).  Again, the same trend was observed, which was for higher pull strengths on the bottom side.

A second sub-module, SF1855 (lot #33) was pull tested as a process monitor.  The pull strength data are listed below:

**SF1855 (test date, 7/20/07):**
- As-fabricated:          Top side: 7.62±0.70 lb;          Bottom side: 8.53±1.88 lb
- Thermal cycled:          Top side: 2.97±0.17 lb;          Bottom side: 3.85±1.41 lb

Obviously, the results were disappointing.  Although the as-fabricated strengths were well above the specification (and still showed a higher value on the bottom side), the strengths rapidly dropped off as a result of thermal cycling (bottom side still stronger than the top side).  In fact, six of the eight strength values were in the 2 – 3 lb range.

It was deemed prudent to, once again, perform metallographic cross sections on the solder joints that experienced the low strengths.  Because all of the dice were tested, the cross sections were made to the pull-tested solder joints.  Shown in Fig. 91 are low and high magnification SEM photographs of a solder joint on die U01 (top side) of SF1855 that was pull tested in the as-fabricated condition.  The pull strength of U01 was 8.39 lb. The failure mode was separation of the TKN/LTCC interface.  It is clear that there is only a spotty presence of thick film material at the interface.  The extent of thick film material remaining was considerably less that was usually observed of top side dice

in the as-fabricated condition.  (See Figs. 9 and 10 amongst others.)  There was some evidence of a reaction layer having formed at the TKN/LTCC interface (not in Fig. 91), but on only one die and, even in that case, to a very limited extent amongst a handful of solder joints.



(a)                                                  (b)

**Fig. 91** (a) Low magnification SEM photograph of a solder joint from the U01 pull-tested die of SF1855 (lot #33).  The die was located on the top side and represented the as-fabricated condition.  (b) High magnification SEM photograph of the solder joint side of, what would have been, the TKN/LTCC interface.

The same observations were made of the solder joints from the U11 die (bottom side) that also tested in the as-fabricated condition.  The SEM photographs appear in Fig. 92. The pull strength of die U11 was also very high at 10.06 lb; its failure mode was separation at the TKN/LTCC interface.  There was slightly more thick film remaining here as compared to U01 because the bottom side solder joints are exposed to only one reflow step.  Nevertheless, the remaining thicknesses were reduced when compared to historical observations.  There was no reaction layer present at the TKN/LTCC interface

**Fig. 92** (a) Low magnification SEM photograph of a solder joint from the U11 pull-tested die of SF1855. The die was located on the bottom side and represented the as-fabricated condition. (b) High magnification SEM photograph of the solder joint side of, what would have been, the TKN/LTCC interface.

This U05 die (top side) was exposed to the process monitor thermal cycle step (20 cycles; -55°C/125°C) prior to pull testing. The pull strength of U05 was a very low 3.24 lb. The failure mode was TKN/LTCC separation. Shown in Fig. 93 are SEM micrographs of two solder joints. In Figs. 93a and 93b, there was substantial development of a reaction layer. A second solder joint in that same cross section, which is depicted by the SEM photographs in Figs. 93c and 93d, exhibited a lesser presence of the reaction layer. These micrographs demonstrated the variability with which the reaction layer appeared in the solder joints of this die. To complete this analysis of SF1855, there was the case of die U12 of SF1855 (bottom side, post thermal cycled) for which the reaction layer was not observed in any of the solder joint cross sections. This die exhibited an acceptable pull strength of 6.32 lb.
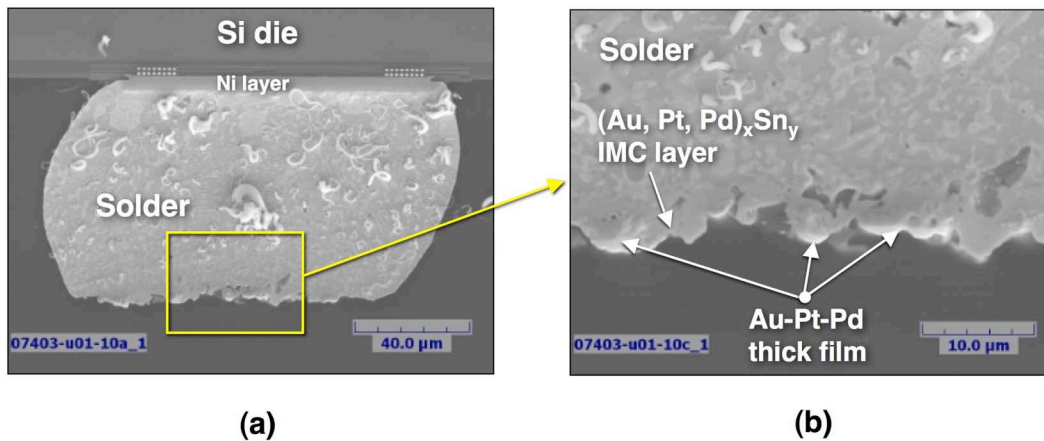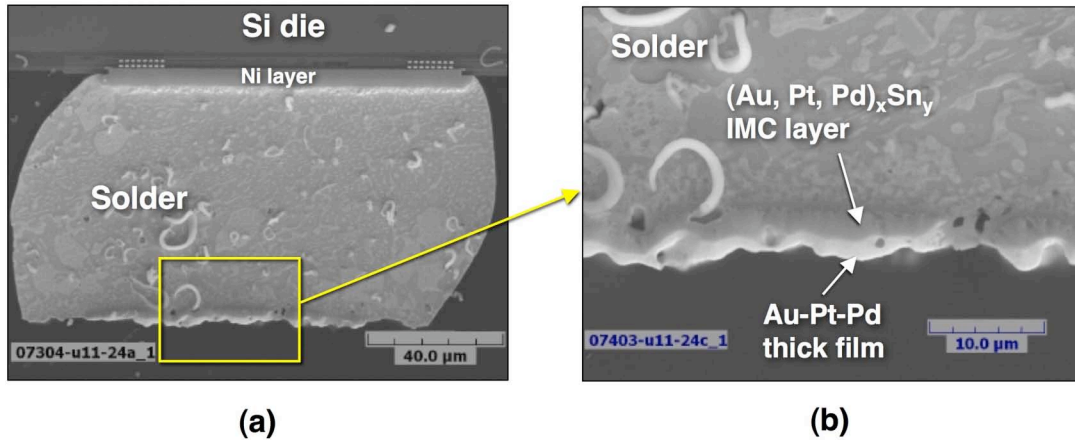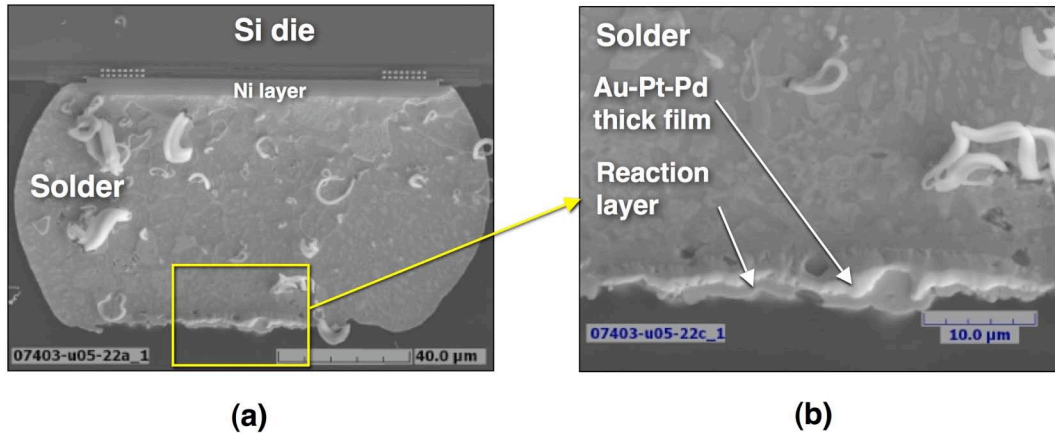
**Fig. 93** (a) Low magnification SEM photograph of the solder joint number 11 from the pull-tested die U05 of SF1855. The die was located on the top side and was tested after thermal cycling (20 cycles; -55°C/125°C) condition. The failure mode was TKN/LTCC separation. (b) High magnification image showing that a significant reaction layer that had developed at the TKN/LTCC interface. (c, d) Low and high magnification SEM photographs of the solder joint number 16 (U05) that shows very limited formation of the reaction layer. The failure mode remained that of TKN/LTCC interface separation.

The data from sub-module SF1855 confirmed the conclusions drawn from the many analyses described above. The die pull strengths correlated with the presence of the reaction layer. The correlation was nominal, which was expected because the pull strengths fell within the "marginal" between the bounding conditions of <3.0 lb (consistent reaction layer) and >5.0 lb (no reaction layer). The more limited extent of the reaction layer that formed in the solder joints of dice on this sub-module required the residual stresses generated by thermal cycling to cause sufficient interface that was revealed by the low pull strengths.

In summary, the analysis of the pull strength performances of sub-modules built from sub-floor lots #29 - #33 further confirmed the earlier correlation between the presence of the reaction layer at the TKN/LTCC and the low pull strength phenomenon. This point was exemplified by the case of SF1855. In this particular case, development of the

184

reaction layer was marginal; hence, the pull strengths fell within the region between the bounding conditions of < 3.0 lb (consistent reaction layer) and > 5.0 lb (no reaction layer).

From an overall manufacturing perspective, the pull strengths of lots #29 - #33 confirmed that, despite the increased scrutiny paid by the supplier to the materials and fabrication processes of the sub-floors, those measures could not provide for a control of the microstructure of the very thin, thick film pads that is required to prevent the low pull strength phenomenon. However, it was noted that, in general, the added scrutiny resulted in a shift in the low pull strengths to occurring primarily after exposure to the thermal cycle conditions. Recall that the thermal cycling exposure is strictly a step within the process monitor evaluation and, moreover, is "for information only." Acceptable, as-fabricated pull strengths, together with the use of an underfill material, would assure the integrity of the dice solder joints for flight units.

# 6.0 Pull Strength and Failure Mode

The low pull strength phenomenon was investigated further by examining more closely the correlation between the strength values and failure mode. It was observed that the TKN/LTCC failure mode and, more specifically, formation of the reaction layer at the TKN/LTCC interface, characterized the low pull strength phenomenon. However, it is necessary to give attention to the role of the solder/Si interface failure mode in the overall pull test performance. The objective of the following discussion was to determine whether the predominance of the TKN/LTCC failure mode was due entirely to a weakening of the TKN/LTCC interface by the reaction layer or that there were other contributing factors in the mechanical behavior of the interconnections.

As noted earlier, because the solder/Si (including UBM fracture) failure mode and TKN/LTCC (including divots) failure mode are mutually exclusive, the following analyses have been based upon the TKN/LTCC mode. *Only the as-fabricated data were analyzed in this manner* because they represented the condition of the interconnections immediately after assembly. In the case of post-thermal cycling, there is the additional complexity of further degradation to the interconnections. (That is not to say that potentially useful information could not originate from a similar analysis of the post-thermal cycled results; it was simply a precaution at this point.)

The data were presented according to the sequence of the sub-floor serial number. When possible, the data were grouped together according to one or more lot numbers of sub-floors in order to illustrate trends based upon build sequence. Although the emphasis of this analysis has been placed on the failure mode, it is important to also consider the magnitudes of the pull strengths. Listed below are the acceptance criteria for the as-fabricated pull strength acceptance criteria:

*As-fabricated:*   [Mean – 95%CI] > **6.75 lbs**

Minimum load of any one die > **4.5 lbs**

[TKN/LTCC + divot] < 25% of *all* joints.

Because in some cases, the data described below are of individual die pull strengths, the criterion of minimum, individual die strength has also been listed, here.

Shown in Fig. 94 is a plot of TKN/LTCC failure mode percentage as a function of pull strength for the two units SN006 and SN008 that were built very early in the program. The percentage of the TKN/LTCC interface failure mode was nearly always less than 50%. Therefore, failure at the Si die side of the soldered interconnection was very prevalent. All pull strengths exceeded the minimum criterion of 4.5 lb. The data did not exhibited a significant correlation between TKN/LTCC failure mode percentage and die pull strength.
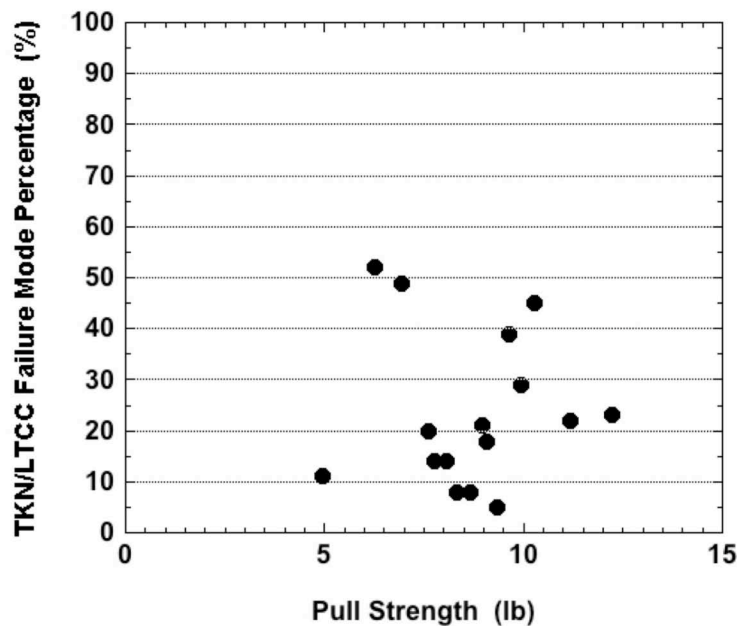


**Fig. 94** TKN/LTCC failure mode percentage as a function of pull strength for the sub-modules SN006 and SN008. The data included only the as-fabricated condition.

The next data set included the sub-modules SF206, SF244, SF247, SF255, SF267, SF274, SF281, and SF284. These units were built from sub-floor lots of less than #4. The failure mode versus pull strength data are shown in Fig. 95; the color code

designates the individual sub-module numbers per the legend at the lower left-hand corner.  All of these sub-modules exhibited excellent die pull strength performance. However, it is also indicated in Fig. 95 that, when compared to Fig. 94, there was an increased predominance of the TKN/LTCC failure mode, in particular, sub-modules SF206 – SF247.  The sub-modules SF255 – 281 exhibited a bi-modal failure mode distribution of low and high percentage groupings of the TKN/LTCC failure mode. The same bi-modal distribution was observed with sub-module SF284, but less strongly so. The two TKN/LTCC failure mode groupings correlated with top and bottom side die locations; the lower percentages of TKN/LTCC failures were associated with the top side dice while the higher percentages of this failure mode occurred with the bottom side dice. Irrespective of the magnitude of the bi-modal distribution, the different failure mode groups did not correlate with individual die pull strengths per Fig. 95.
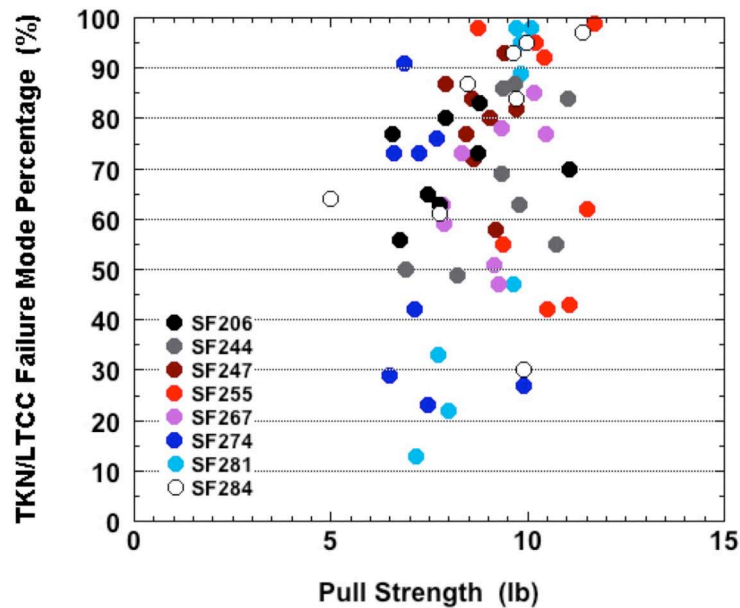
**Fig. 95** TKN/LTCC failure mode percentage as a function of pull strength for the sub-modules SF206, SF244, SF247, SF255, SF267, SF274, SF281, and SF284.   The data represent the as-fabricated condition.

The next group of sub-modules were those with serial numbers SF512, SF539, SF562, SF568, and SF630 representing sub-floor LTCC lots #4 and #5.  The data are shown in

Fig. 96, representing the as-fabricated condition. Although overlapping Fig. 96 with Figs. 95 and 94 would indicate that there very little difference to the pull strength values, the failure modes showed a clear trend towards preference for the TKN/LTCC separation. This point was particularly true for the sub-modules SF512 and SF539 with greater than 90% of failures had this mode. The data for sub-modules SF568 and SF630 were clustered in the range of 75 – 85%. The sub-module SF562 exhibited the bi-modal distribution between the bounding cases of >90% and 75 – 85%. As previously observed, the pull strengths of these sub-modules did not exhibit a correlation with the TKN/LTCC failure mode percentage.



**Fig. 96** TKN/LTCC failure mode percentage as a function of pull strength for the sub-modules SF512, SF539, SF562, SF568, and SF630 representing the as-fabricated condition.

Shown in Fig. 97 are the data for sub-modules SF1159 (lot #14), SF1204 (lot #15), SF1249 (lot #16), SF1392 (lot #18), and SF1419 (lot #19). These data exhibited very mixed results. There was the case of SF1159 that showed nearly 100% TKN/LTCC failures and pull strengths that approached the individual die minimum criterion. The sub-module SF1204 exhibited 100% TKN/LTCC failure mode and pull strength values

that were below the minimum 4.5 lb for *all* dice.  The sub-modules SF1249 and SF1419 exhibited excellent pull strength values, but with vastly different failure mode behaviors. The unit SF1249 exhibited TKN/LTCC failure mode percentages that were all >90%. On the other hand, SF1419 showed this failure mode within the range of 5 – 70%.  The sub-module, SF1392, exhibited a failure mode/pull strength trend that was a combination of the latter two cases; the result was a wide spread of both pull strengths (some below the criterion) and TKN/LTCC mode percentages.  Although a strict correlation still could not be drawn between pull strength and failure mode, a developing trend was that individual die strengths less than 4.5 lb were accompanied by the 100% TKN/LTCC failure mode. The pull strength behavior of these sub-modules marked the appearance of the low pull strength phenomenon.



**Fig. 97** TKN/LTCC failure mode percentage as a function of pull strength for the sub-modules SF1159, SF1204, SF1249, SF1392, and SF1419 representing the as-fabricated condition.

The next group of sub-modules that were evaluated included the units SF1465, SF1471, SF1475, and SF1476. All of the units were from the lot #20 build of sub-floors. The

failure mode and pull strength data are shown in Fig. 98. The pull strengths were distributed over a very wide range of values, more so than any of the previous sub-module data. The sub-module, SF1471, exhibited the widest range of strengths from approximately 6 lb to as high as almost 14 lb. The TKN/LTCC failure mode percentages also exhibit a greater range of values, not only between sub-modules but also between individual dice within each sub-module; the latter trend was most pronounced in the SF147x units. The trend emerged from the data in Fig. 98 of increasing TKN/LTCC failure mode percentage with decreasing pull strength.
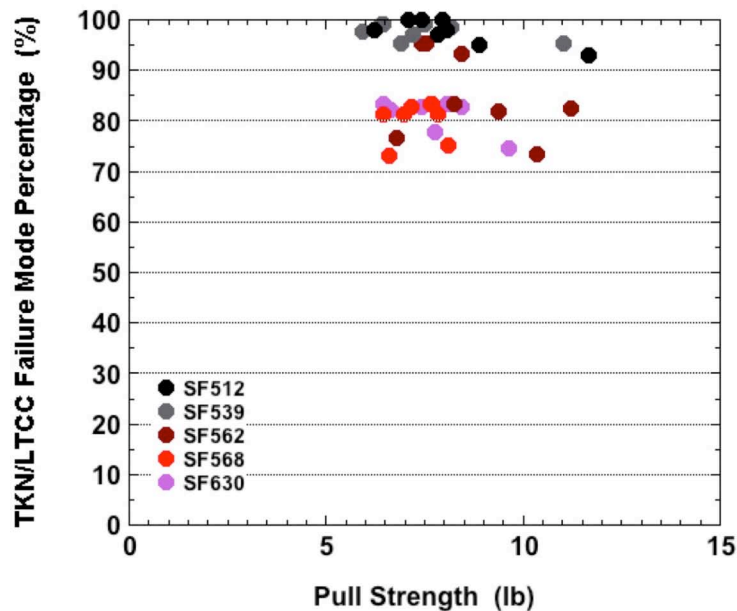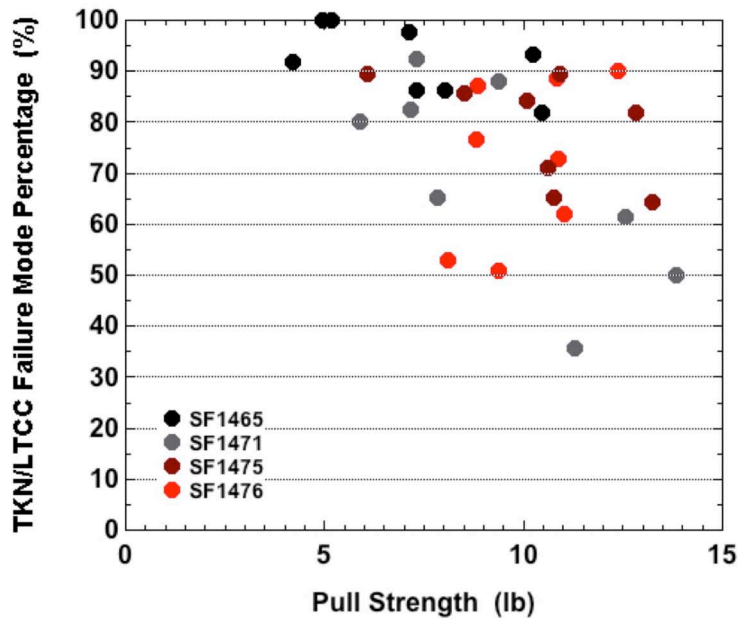


**Fig. 98** TKN/LTCC failure mode percentage as a function of pull strength for the sub-modules SF1465, SF1471, SF1475, and SF1476 representing the as-fabricated condition.

The next set of data, which are shown in Fig. 99, were taken from the sub-modules SF1525, SF1545, SF1571, and SF1577. All of these units represented lot #21 sub-floors. Like the lot #20 data (Fig. 98), there was a very wide range of pull strengths. In fact, all but SF1577 had one or more die pull strengths that were below the acceptance criterion. On the other hand, unlike the lot #20 results, the TKN/LTCC failure mode percentages were within a very narrow range; the majority of datum were > 95%. As a

result of the latter behavior, a correlation could not be developed between pull strength and TKN/LTCC failure mode percentage.
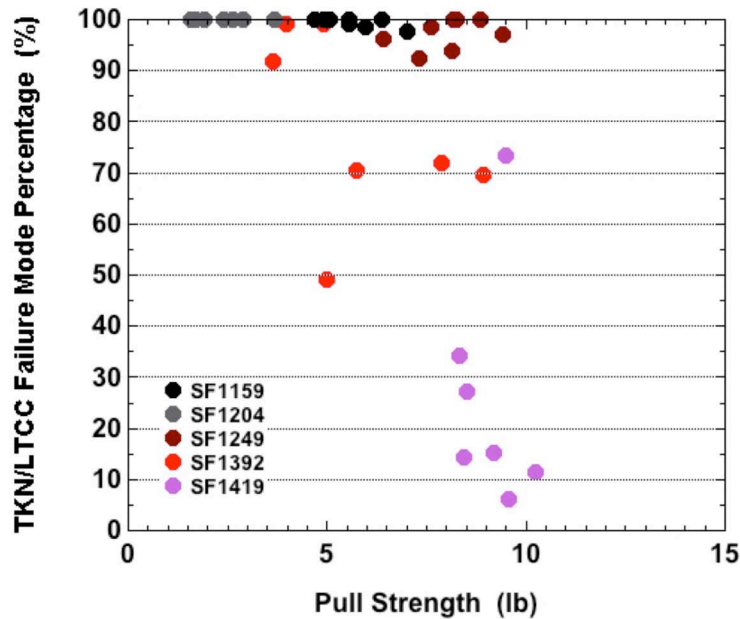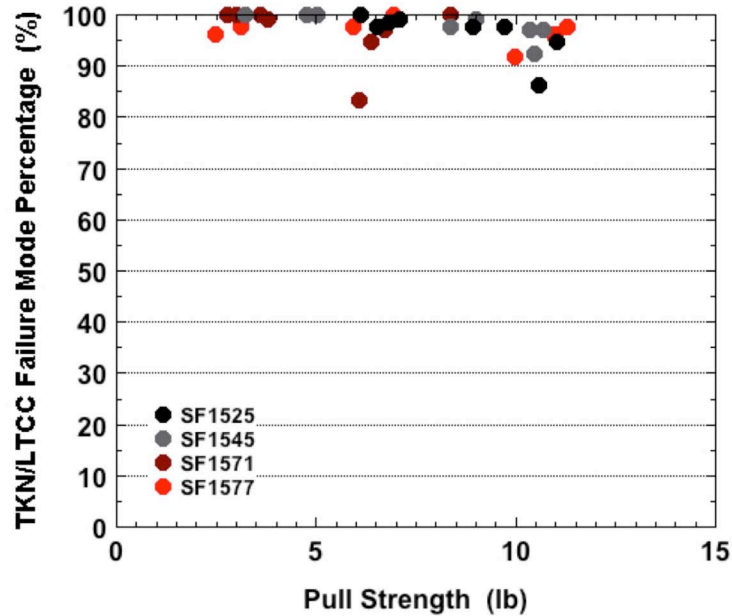


**Fig. 99** TKN/LTCC failure mode percentage as a function of pull strength for the sub-modules SF1525, SF1545, SF1571, and SF1577 representing the as-fabricated condition.

The next sub-floors were from lot #29.  Prior to the manufacturing of lot #29, a precursor lot designated S-Lot29-X was made with X=1, 2, 3, or 4, identifying the four sub-modules that were provided for pull testing.  As described in detail earlier, the sub-floors X=1 and X=2 were made improperly.  The process was corrected and the latter two units, S-Lot29-3 and -4, were considered to be "acceptable."  Therefore, the pull strength and failure mode data obtained from these sub-modules, as well as the data from sub-modules SF1591, SF1594, SF1599, SF1608, and SF1610 were plotted together in Fig. 100.
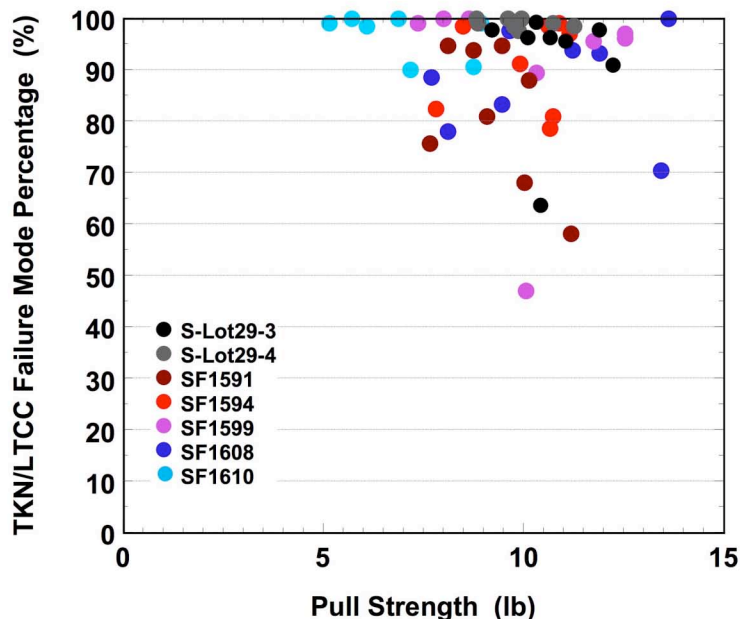
**Fig. 100** TKN/LTCC failure mode percentage as a function of pull strength for the sub-modules S-Lot29-X (X=3 and 4) representing a build of sub-floors that were the precursor to lot #29 and SF1591, SF1594, SF1599, SF1608, and SF1610. All data pertain to the as-fabricated condition.

The data showed a narrowing of the range of pull strengths. More, importantly, the pull strengths shifted to higher values so all of the latter exceeded the lower acceptance limit is 4.5 lb. There was a wider range of the failure mode percentages. However, there was not a significant, quantitative correlation that could be drawn between the pull strength and the TKN/LTCC failure mode percentage.

The failure mode versus pull strength data are shown in Fig. 101 for the combination of sub-modules representing lot #30 (SF1659, SF1660, and SF1662) and lot #31 (SF1726, SF1731, SF1742, and SF1751). The low pull strength phenomenon occurred to SF1662 (lot #30). The TKN/LTCC failure mode was dominant (>95%). The pull strengths for the other lot #30 sub-modules and those of lot #31 were generally very good. The TKN/LTCC separation predominated the failure modes, although to a lesser extent with the solder/Si failure mode in some cases exceeding 20%. Excluding the case of

SF1662, within the batch of acceptable pull strengths, there was no correlation between pull strength and TKN/LTCC failure mode percentage.



**Fig. 101** TKN/LTCC failure mode percentage as a function of pull strength for the sub-modules from lots #30 (SF1659, SF1660, and SF1662) and #31 (SF1726, SF1731, SF1742, and SF1751). All data pertain to the as-fabricated condition.

The last data set that was part of the failure mode versus pull strength analysis was drawn from the sub-modules of lots #32 (SF1802 and SF1815) and lot #33 (SF1824 and SF1855). All four sub-modules, as process monitors, passed the acceptance criteria in the as-fabricated condition. The plot of TKN/LTCC failure mode versus pull strength is shown in Fig. 102. The pull strengths of the SF1802 and SF1815 belonging to lot #32 were very high; the values for the lot #33 units were slightly lower, but still considered to be very good. Overall, the pull strengths were held within a tighter range of values when compared to previous data. The predominant failure mode was separation at the TKN/LTCC interface: >70% for SF1802 and SF1815 and >90% for SF1824 and SF1855. Thus, the slightly lower pull strengths of the lot #33 sub-modules were accompanied by a generally higher percentage of the TKN/LTCC failure mode so that a correlation could be established between the two metrics in this data set.
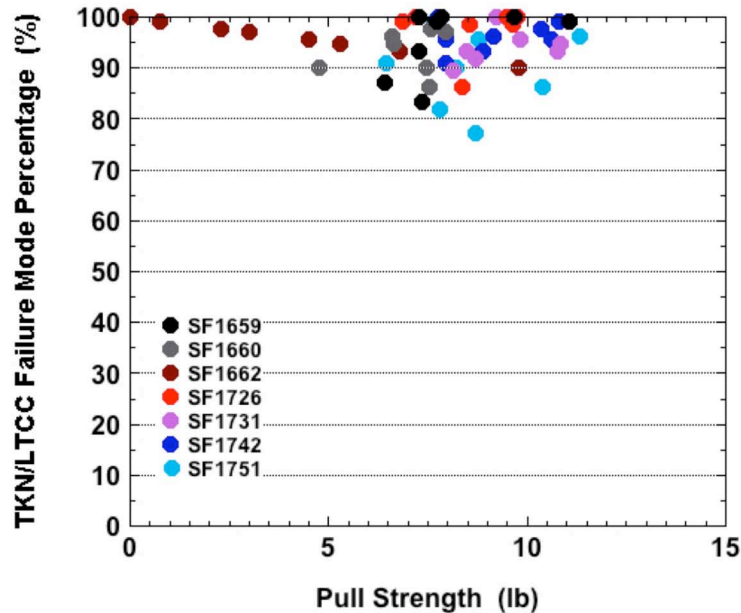
**194**
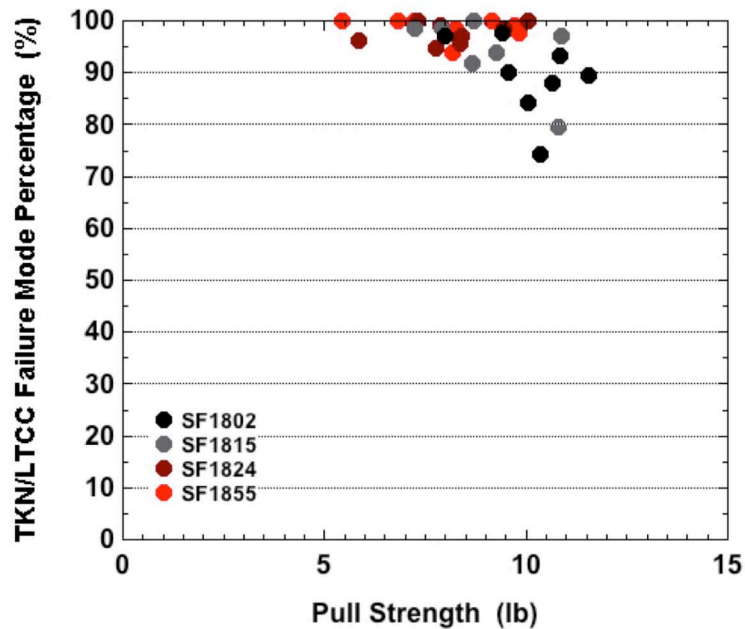
**Fig. 102** TKN/LTCC failure mode percentage as a function of pull strength for the sub-modules from lots #32 (SF1802 and SF1815) and #33 (SF1824 and SF1855). All data pertain to the as-fabricated condition.

It was noted earlier that this pull strength versus failure mode analysis was based upon the as-fabricated condition. The sub-modules SF1824 and SF1855 exhibited low post-thermal cycle pull strengths that were indicative of the low pull strength phenomenon. These two sub-modules experienced lower pull strengths when compared to the other two units as well as generally higher percentages of the TKN/LTCC failure mode (>92%). It is perhaps the combination of these two trends in the as-fabricated condition, that is, pull strengths nearing 5 lb and a TKN/LTCC failure mode percentage of >92% that indicates the low pull strength phenomenon after thermal cycling. A cross section failure analysis was performed on SF1855. The evaluation revealed that the very thin, thick film layer, which increased the likelihood of Sn reaching the glassy phase interface and forming the reaction layer.

A summary is compiled of the failure mode versus pull strength analyses that were described above. First of all, progressing through the build history of sub-floors that is represented by the sequence of graphs in Figs. 94 – 102 showed the general trend of an increasing predominance of the TKN/LTCC failure mode, beginning with the SF5XX sub-modules.  Therefore, the TKN/LTCC failure mode became associated with both low and high pull strengths.

Secondly, the predominance of the TKN/LTCC failure mode over an increasingly wider pull strength range necessarily implied, first of all, that the strength of the solder remained high (for the reasons of solid-solution strengthening and precipitation hardening that were discussed at the beginning of this report).  Secondly, there was a decrease in the occurrence of the solder/Si failure modes.  Recalling with the aid of Fig. 1b, the materials and interfaces are *in series* so that the weaker "element" determines the overall pull strength value.  Thus, the predominance of the TKN/LTCC failure mode at the high-end pull strength values implied that the solder/Si interface structure had a higher intrinsic strength than did the TKN/LTCC interface. A further determination of the source of the improved solder/Si interface strength – whether it was the underbump metallurgy (UBM) attachment to the silicon or the solder/UBM (Ni) interface – required additional analyses that were not performed in this study.

## 7.0 Mitigation and Alternative Bond Pad Approaches

Previously, sub-modules suspected of having been exposed to an $N_2$-10%$H_2$ atmosphere were then subjected to air annealing treatment (250°C, 260 hours) in order to heal damage to the TKN/LTCC interface caused by the purported reduction of Bi-O glassy phase (and perhaps also Pb-O) located there.  A strong correlation was never demonstrated between the $N_2$-10%$H_2$ exposure and low pull strength phenomenon (or any degree of reduced pull strength for that matter).

However, it was observed that the healing treatment improved some of the pull strength values. The strength improvements were quite variable.  In one of three cases, the improvement was substantial; in the remaining two cases, it was only modest, at best. Since it could not be concluded that the $N_2$-10%$H_2$ exposure reduced pull strength, it was not possible to also conclude that, in fact, the healing treatment actually re-oxidized the Bi-O glassy phase.

An alternative scenario is proposed to explain the strength improvement.  The exposed surfaces of the thick film layer – exposed on top and the walls of pores – would have had the Pd component oxidized during the healing treatment.  The Pd-O that formed on the exposed surface would have been burnished away prior to flip chip soldering, resulting in excellent solderability for the interconnection as a whole.  However, the walls of interior pores would have been out-of-reach of the burnishing process.  Thus, those surfaces would have lost a degree of solderability, resulting in a more limited penetration by the molten solder towards the TKN/LTCC interface and, consequently, a reduced likelihood of pull strength degradation.  Therefore, per this scenario, an air-annealing step may provide the means to prevent the low pull strength behavior. Further investigation would be necessary in order to optimize the time and temperature parameters[10].

---

[10] A countering argument to this scenario can be made, based upon the assumption that the multiple, post-processing firing steps, which are performed in air at temperatures in the range of 800 – 900 °C, would have fully oxidized the surfaces of the internal pores.  The firing temperatures certainly exceeded

The alternative technology proposed to eliminate the low pull strength phenomenon is to replace the thick film layer with physical vapor deposited (PVD), thin film pads. In the historic multi-chip module (MCM) terminology, the use of thin film conductors was described as multi-chip module, deposited or MCM-D. Denser metal layers and well-controlled thicknesses are provided by evaporation or sputtering thin film techniques. Larger-sized features (e.g., the pads of the passive devices) can be defined by the use of shadow masks. For smaller features such as those of the BDYE flip chip bond pads, lift-off techniques can be implemented that are based upon photoresist definition steps. Thin film pads are currently being actively studied for the next-generation of MCM product.

---

the 250°C healing treatment temperature; however, the latter treatment used a 260 hour duration, which exceeded even the cumulative time from all of the post-process firing steps (0.25 hours x 14 steps after pad formation = 3.5 hours).

# 8.0 Summary

1. The construction of the BDYE detector requires the assembly of sixteen Si processor dice on a low-temperature, co-fired ceramic (LTCC) substrate – eight on the top side and eight on the bottom side. The attachment is by mean of 63Sn-37Pb (wt.%) flip chip solder interconnections in a double-reflow soldering process (in nitrogen).

2. The LTCC conductor bond pad is a single print, 71Au-26Pt-3Pd thick film layer applied in series of post-process, print-dry-fire steps. The very fine interconnection pitch is realized by reducing the pad thickness to approximately one-third of that of traditional single print, thick film technology.

3. The quality metric of the flip chip solder joints is the strength measured by pulling the die from the LTCC substrate at a rate of 10 mm/min. As part of the process monitor test methodology, the pull strengths were measured in both the as-fabricated condition (four dice per each of the top and bottom sides) and after thermal cycling (-55/125°C; 15 min hold times; 20 cycles) for the remaining eight dice. Acceptance criteria were established for both conditions.

4. During the course of the program, extremely low pull strengths were observed intermittently for the dice of some process monitors; this occurrence was referred to as the *low pull strength phenomenon*. The low pull strengths, which were observed for both the as-fabricated and post-thermal cycled conditions, were accompanied by an inordinately high occurrence of the TKN/LTCC interface failure mode.

5. A statistically significant correlation could not made between pull strength and the following materials and/or processes: (1) thick film ink or LTCC materials; (2) pad height (thickness) within the BDYE process window; (3) the dice soldering assembly process; or (4) the pull test procedure. There was a difference between top side versus bottom side pull strengths; however, the trend was not consistent on a sub-floor lot-to-lot basis.

6. Auger electron spectroscopy (AES) technique did not detect composition differences of surface or near-surface region between the top side and bottom sides of the sub-floors *prior to* the Au-Pt-Pd post-processing steps. The AES analysis detected small concentrations of Ca and K at the surface and near-surface volumes LTCC material *after* the post-processing steps, which differed slightly between the top side and bottom side surfaces. It was not readily apparent as to the role of Ca- and K-based compounds on the pull strength performance of the flip chip solder joints.

7. The inadvertent use of a $N_2 - 10\%H_2$ gas atmosphere to attach pins to the LTCC sub-floor was examined as a possible cause of the low pull strength phenomenon. Historical sub-module pull strength data could not provide a clear correlation between the exposure and pull strength due to the intrinsic variability of the pull strength property. The low pull strengths could not be consistently reproduced by knowingly subjecting sub-floors to a $N_2 - 10\%H_2$ gas atmosphere. A "healing" treatment (250°C, 260 hours, air) provided a small improvement to low pull strength sub-modules, but not to the degree or consistency needed to meet acceptance limits. There was no direct evidence that the healing treatment repaired the purported damage caused by the $N_2 - 10\%H_2$ gas atmosphere.

8. Improved materials and process control were implemented for sub-floor lots #29 - #31; yet, the low pull strength phenomenon was still observed. Grit blasting the LTCC surface prior to post-processing was implemented on a consistent basis beginning with lot #32. While the as-fabricated pull strengths were not changed, higher strengths were observed for the post-thermal cycled condition. (However, subsequent lot #33 data confirmed that grit blasting did not eliminate the low pull strength phenomenon.)

9. A study compared the die pull strengths (as-fabricated and post-thermal cycled) between sub-modules that were post-processed at Scrantom versus DuPont™. The

Scrantom unit exhibited slightly higher, as-fabricated pull strengths and significantly higher, post-thermal cycle pull strengths when compared to the DuPont™ processed unit.  All pull strengths exceeded the low pull strength phenomenon  There was not an obvious "discrepancy" in the Scrantom post-process firing process. The fact that the Scrantom unit had more porous layer demonstrated that porosity and consequently, the proximity of molten Sn-Pb solder to the TKN/LTCC interface, was not a sufficient predictor of the low pull strength phenomenon.

10. Pull strength and microstructural analyses was made of the solder joints on sub-modules exposed to the burn-in conditions of 125°C and 240 – 282 hours, which resulted in a nearly complete conversion of thick film to the $(Au, Pt, Pd)_x Sn_y$ IMC. Only a moderate strength loss was observed, indicating that IMC formation and, in particular, development of an IMC/LTCC interface, were not responsible for the low-strength phenomenon.  These joints withstood underfill stresses, as well.

11. Long-term, thermal cycling, which combined the effects of solid-state IMC growth and fatigue stresses in the joints, as well as stresses generated by the presence of an underfill material, did not cause the low-pull strength phenomenon nor were they the source of obvious damage to the interconnections.  The general strength loss due to thermal cycling was by a mechanism/process that was separate from that responsible for the low pull strength phenomenon.

12. Metallographic cross sections revealed the presence of a *reaction layer* at the interface between the thick film layer and the LTCC substrate.  The following microstructure/mechanical properties relationship was compiled: (a) the reaction layer was present for pull strengths below approximately 3.00 lb; (b) the layer was absent for pull strengths exceeding approximately 5.00 lb; and (c) a clear correlation could not be obtained between these two limiting cases.

13. The reaction layer was comprised Sn, Pb, Au, Pt, and Si, but not at concentrations that were indicative of an IMC. The source of Sn was the *molten* Sn-Pb solder present during the assembly process. The root-cause of the low pull strength behavior was a degradation of the TKN/LTCC interface, specifically, the glassy phase layer, caused by a reaction layer between it and Sn of the molten solder. Crystallization of the glassy phase layer by Sn is the suspected mechanism. The thick film microstructure had a second-order effect by controlling the ability of the molten solder to reach the interface *and* susceptibility of that interface glassy phase to degradation.

14. Because of the thin layers, the printing process was too sensitive to minor variations in the ink thixotropy to reproducibly deposit the same percentages of glassy phase and metal phase. Variations of thick film layer composition caused subtle changes to the thick film microstructure that made the subsequent solder joint susceptibility to the low pull strength phenomenon.

15. The pull strength data confirmed that the low pull strength phenomenon occurred, most consistently only at the level of dice on the given side (top or bottom) of a sub-module. Therefore, the "process monitor" approach would be unable to screen for this phenomenon at the sub-floor (LTCC) lot level.

16. The overall trend observed through the build history of the sub-modules was for an increased occurrence of the TKN/LTCC failure mode. The source of this trend was an increase in the strength of the solder/Si interface. The strength of the bulk solder remained higher than that of either interface. The low pull strength phenomenon was accompanied by a nearly 100% TKN/LTCC failure mode.

17. Although the air annealing treatment could provide some strength improvement, it did not do so with a magnitude that would always mitigate the low pull strength

phenomenon.  An alternative means to prevent this problem is the use of thin film

PVD conductors (MCM-D technology).

# 9.0 References

[1] P. Vianco, G. Uribe, and G. Zender, "Pull Strength Evaluation of Sn-Pb Solder Joints Made to Au-Pt-Pd and Au Thick Film Structure on Low-Temperature Co-Fired Ceramic – Final Report for the MC4652 Crypto-Coded Switch (W80)," *Sandia Report* **SAND2006-2451** (Sandia National Laboratories, Albuquerque, NM 2006).

[2] T. Hitch, "Adhesion, Phase Morphology, and Bondability of Reactively-Bonded and Frit-Bonded Gold and Silver Thick-Film Conductors," *J. Electronic Materials* 3 (1974) pp. 553 – 577.

[3] A. Milgram, "Influence of Metallic Diffusion on the Adhesion of Screen Printed Silver Films," *Metall. Trans.* 1 (1970) pp. 695 – 700.

[4] W. Crossland and L. Hailes, "Thick Film Conductor Adhesion Reliability," *Solid State Tech.* 14 (1971) pp. 42 – 47.

[5] T. Hitch and K. Bube, "Basic Adhesion Mechanisms in Thick and Thin Films," RCA Laboratories for Naval Air Systems Command, *PRRL -77-CR-2* (1976).

[6] R. Perecherla, and R. Buchanan, "Adhesion Failure Modes in Copper Thick Film Conductors," *Inter. J. of Microcircuits and Elect. Pack.* 18 (1995) pp. 29 – 40.

[7] C. Peckinpaugh, and R. Tuggle, "Thick Film Adhesion – Evaluation and Improvement," *Proc. ISHM Symp.* (1968) pp. 3.3.1 – 3.3.13.

[8] R. Schuster, "Conductor Adhesion Degradation After Prolonged Exposure to Solder Paste Before Reflow," *Inter. J. of Hybrid Microel.* 4 (1981) pp. 182 – 189.

[9] P. Vianco, meeting notes, BDYE project, dtd. December 19, 2005.

[10] *DuPont Microcircuit Materials – DuPont Green Tape™ Materials System Design and Layout Guidelines* (2003) E.I. du Pont de Nemours and Company, Inc., Wilmington DE.

[11] V. Chernogorenko and K. Lynchak, "Production of Bismuth Powder by the Reduction of bismuth Oxide with a Mixture of Molecular and Atomic Hydrogen," *Powder Metall. and Metal Ceramics* 12 (1973) pp. 360 – 362.

[12] A. Witkowska, J. Rybicki, and A. Di Cicco, "EXAFS Analysis of Bismuth Atom Neighborhood in Reduced Bismuth Silicate Glass," *Phys. and Chem. Of Glasses* 43C (2002) pp. 124 – 127.

[13] A. Witkowska, J. Rybicki, and J. Bosko, "A Molecular Dynamics Study of Lead-Bismuth-Silicate Glasses," *IEEE Trans. on Dielectrics and Elect. Insul.* 8 (2001) pp. 385 – 389.

[14] P. Vianco, J. Stephens, and J. Rejent, "Intermetallic Compound Layer Development During the Solid State Thermal Aging of 63Sn-37Pb Solder/Au-Pt-Pd Thick Film Couples," *IEEE Trans. On Components, Packaging, and Manufacturing Technology Part A* 20 (1997), p. 478.

[15] S. Takeda, R. Akiyama, and H. Hosono, "Effect of Oxygen Diffusion from the Atmosphere on Sn Depth Profile of Float Glass at Temperatures Above Tg," Asahi Glass Company, Ltd., R&D Library, Vol. 52, paper 3, (2002).

## Distribution ("E" = electronic, only)

| | | | |
|---|---|---|---|
| 1(E) | MS0352 | K. Ewsuk | 01715 |
| 1(E) | MS0892 | L. Rohwer | 01715 |
| 1 | MS0888 | A.C. Kilgo | 01822 |
| 1 | MS0888 | G.L. Zender | 01822 |
| 3 | MS0889 | P.T. Vianco | 01824 |
| 1 | MS0889 | J.A. Rejent | 01824 |
| 1 | MS0889 | J.M. Grazier | 01824 |
| 1(E) | MS0889 | J.S. Custer | 01824 |
| 1(E) | MS0889 | R. Tandon | 01825 |
| 1(E) | MS0889 | J. Glass | 01825 |
| 1 | MS0959 | F.R. Uribe | 02452 |
| 1(E) | MS0959 | B. Wroblewski | 02452 |
| 1(E) | MX0959 | D. Blair | 02452 |
| 1(E) | MS0406 | G. Thayer | 05711 |
| 2 | MS0971 | V. Chavez-Soto | 05733 |
| 1 | MS0982 | K. Lamppa | 05765 |
| 2 | MS0982 | C.A. Reber | 05765 |
| 1(E) | MS0899 | Technical Library | 09536 |